Quaternary Science Reviews 346 (2024) 109021

Contents lists available at ScienceDirect

Quaternary Science Reviews

journal homepage: www.elsevier.com/locate/quascirev

A detailed record of large explosive eruptions from Japan between ~120 and 50 ka preserved at Lake Suigetsu

Sophie O. Vineberg [a,*], Paul G. Albert [b], Danielle McLean [a], Takehiko Suzuki [c], Richard A. Staff [a,d,e], Keitaro Yamada [f,g], Ikuko Kitaba [f,h], Junko Kitagawa [i,j], Christina J. Manning [k], Hannah M. Buckland [b], Gwydion Jones [b], Fumikatsu Nishizawa [l], SG14 Project Members [1], Takeshi Nakagawa [f], Victoria C. Smith [a]

[a] Research Laboratory for Archaeology and the History of Art, School of Archaeology, University of Oxford, Oxford, OX1 3TG, UK
[b] Department of Geography, Swansea University, Swansea, SA2 8PP, UK
[c] Department of Geography, Tokyo Metropolitan University, Tokyo, 192-0397, Japan
[d] Scottish Universities Environmental Research Centre, University of Glasgow, East Kilbride, G75 0QF, UK
[e] The British Museum, London, WC1B 3DG, UK
[f] Research Centre for Palaeoclimatology, Ritsumeikan University, Kusatsu, Shiga, 525-8577, Japan
[g] Institute for Geothermal Sciences, Kyoto University, Kyoto, 606-8224, Japan
[h] Research Center for Inland Seas, Kobe University, Kobe, 657-8501, Japan
[i] Varve Museum, Wakasa, Fukui, 919-1331, Japan
[j] Fukui Prefectural Satoyama-Satoumi Research Institute, Wakasa, Fukui, 919-1331, Japan
[k] Centre for Dynamic Earth and the Solar System, Department of Earth Sciences, Royal Holloway, University of London, Egham, Surrey, TW20 0EX, UK
[l] Kanagawa Prefectural Museum of Natural History, Odawara, 250–0031, Japan

ARTICLE INFO

Keywords:
Ash fall
Cryptotephra
Lake Suigetsu
Tephrochronology
Glass chemistry

ABSTRACT

We present the findings of a detailed non-visible (cryptotephra) tephra investigation of the Lake Suigetsu (Japan) sedimentary sequence spanning ~120 to 50 ka. Thirty-nine new cryptotephra and two visible tephra horizons are identified during this interval interspersed between visible tephra layers associated with large-magnitude eruptions and regional event markers (e.g., Aso-4, K-Tz, Ata). The newly identified volcanic deposits are geochemically analysed using major (EMP) and trace (LA-ICP-MS) element glass analyses, and the chemical fingerprints are used to trace these deposits to subduction related volcanoes located along the three main Japanese islands (Kyushu, Honshu and Hokkaido), as well as nearby intraplate volcanoes. Our findings provide geochemical, chronological and ash-fall constraints on the activity at multiple volcanic centres; in particular, the Kirishima volcanic complex in the southern volcanic region of Kyushu. Furthermore, the Lake Suigetsu cryptotephra record reveals distal ash-fall from two notable large magnitude (≥M6.0) eruptions, the Plinian Sambe Kisuki (SK) eruption and the caldera-forming Toya eruption, both of which are important widespread tephrostratigraphic markers suitable for linking regional terrestrial and marine sequences. Using the Lake Suigetsu age-depth model, they are dated to 100.4 ± 3.1 ka (±1σ) and 108.1 ± 3.9 ka (±1σ), respectively. Finally, our investigation reveals numerous eruption deposits which have not yet been identified in near-vent sequences, indicating eruption under-recording. This research re-affirms Lake Suigetsu as the single most comprehensive ash-fall record of East Asian explosive volcanism over the past 150 kyr, and contributes significantly to our understanding of the timing and ash dispersals of pre-historic eruptions.

1. Introduction

Large explosive eruptions have caused significant and incredibly widespread environmental and societal effects in history (Oppenheimer, 2003) and are therefore of substantial scientific interest/importance (e.g., Tambora 1815CE and Krakatau 1883 CE eruptions). Although

* Corresponding author.
E-mail address: sophie.vineberg@st-annes.ox.ac.uk (S.O. Vineberg).
[1] www.suigetsu.org.

https://doi.org/10.1016/j.quascirev.2024.109021
Received 6 September 2024; Received in revised form 16 October 2024; Accepted 20 October 2024
Available online 15 November 2024

historical records and the high-resolution polar ice cores have provided detailed eruption archives for the last couple of millennia (e.g., Sigl et al., 2015), knowledge of eruptions further back in time (e.g., across the last glacial to interglacial cycle) are not particularly well constrained. A statistical re-analysis of the LaMEVE (Large Magnitude Explosive Eruptions; Crosweller et al., 2012) database suggested that almost 89% of medium-large sized (Volcanic Explosivity Index [VEI] or Magnitude [M] ≥4) eruptions are currently missing from the eruption record at ~100 ka (Kiyosugi et al., 2015). Detailed eruption histories across such timescales are essential for the development of robust hazard and risk assessments, providing insight into the frequency and behaviour of large events (e.g., caldera forming eruptions) and their return intervals (e.g., Uesawa et al., 2022).

The East Asian Pacific region is home to over 30% of the global population (Cook et al., 2010) and has one of the greatest population densities living within 100 km of an active volcano (Brown et al., 2015). Japan alone has over 130 active volcanic centres, many of which have produced several of the largest magnitude volcanic eruptions in the last 200 kyr (Newhall et al., 2018; Machida and Arai, 2003). Sixteen Japanese volcanoes are considered candidates to produce a large eruption (VEI/M ≥ 7) in future millennia (Newhall et al., 2018). However, reconstructing the past eruption histories of these centres has proved difficult using near-vent (proximal) eruption records alone. This is partly due to the burial, destruction and subsequent erosion of eruption deposits around the productive volcanoes, and that Japan has a high degree of urbanisation, strong seasonality and dense vegetation in less developed areas. Distal sedimentary archives such as lacustrine and marine sediment cores can overcome such preservation and accessibility issues and may even capture separate medium-sized events (e.g., VEI/M ≥ 4) more clearly than their proximal counterparts (Chen et al., 2019; McLean et al., 2018; Wulf et al., 2018; Tomlinson et al., 2014).

The Lake Suigetsu sedimentary record (central Japan; location shown in Fig. 1) provides a key tephro-stratotype of explosive volcanism for Japan spanning the last 150 kyr. To date, seventy-six visible and non-visible (cryptotephra) deposits have been identified and geochemically characterised in the sediments (Albert et al., 2018, 2019a, 2024; McLean et al., 2016, 2018, 2020a, 2020b; Smith et al., 2011a, 2013). Whilst many of the tephra layers have been correlated to arc volcanoes located on Honshu and Kyushu (e.g., Albert et al., 2018; Albert et al., 2019a; Smith et al., 2013), several layers also originate from Japanese centres located >500 km north of Lake Suigetsu (e.g., Hokkaido), as well as the more distal intraplate volcanoes such as Ulleungdo in South Korea and Changbaishan on the border of China and North Korea (Albert et al., 2018, 2019a; McLean et al., 2016, 2018; Smith et al., 2011a). Investigations of cryptotephras within the Lake Suigetsu sediments have also been completed for the Holocene and Late Pleistocene (0–20 ka and

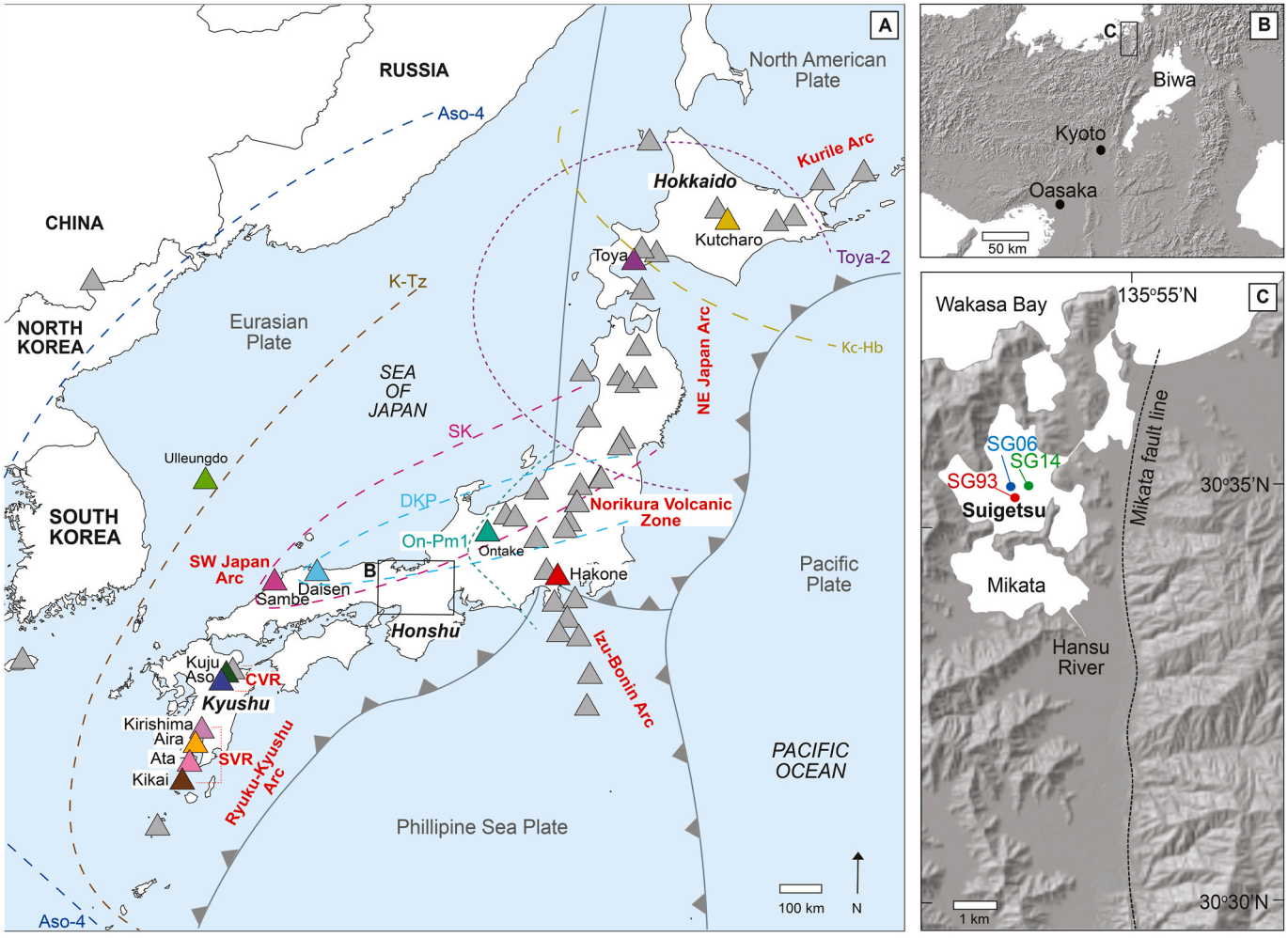

Fig. 1. **(A)** Volcanoes (triangles) that have been active in and around Japan in the Quaternary. The volcanoes that are mentioned in the text and likely sources of the tephra in Lake Suigetsu in this period are coloured. The dashed lines denote the ash dispersal boundaries for various widespread tephra layers (as labelled), which are from (Machida, 2002). The red labels are the volcanic arcs: SVR = Southern Volcanic Region; CVR = Central Volcanic Region; SWJA = SW Japan Arc; NVZ = Norikura Volcanic Zone; NEJA = NE Japan Arc. **(B)** Proximity of Lake Suigetsu to Lake Biwa and major Japanese cities. **(C)** Location of Lake Suigetsu as part of the five Mikata Lakes, adjacent to Wakasa Bay. The positions of all three coring campaigns are marked (B and C modified after Nakagawa et al., 2005).

30–50 ka) and reveal volcanic deposits from an additional eight volcanic centres indicating that there are four times as many cryptotephra deposits preserved relative to visible tephra layers (Albert et al., 2024; McLean et al., 2018). The identification of these tephra within the well dated Lake Suigetsu sequence (Bronk Ramsey et al., 2012) provides tight age constraints for past eruptions and enabled the integration of regional tephrostratigraphies, as well as facilitating the first direct link to the Greenland ice cores (i.e., the B-Tm tephra, 946 CE; Oppenheimer et al., 2017; McLean et al., 2016; Sun et al., 2014).

To further refine the Late Quaternary tephrostratigraphic framework for the East Asian/Pacific region, we investigate the unexplored cryptotephra record preserved in the ca. 20 m of the Lake Suigetsu sediments (SG14 core) dated between ~120 and 50 ka (Bronk Ramsey et al., 2012; Schlolaut et al., 2012, 2018). The high-resolution sediments of Lake Suigetsu offer unprecedented insight into the timing, frequency and dispersal of ash-fall events dispersed over this now heavily populated region of East Asia.

2. Study site

Lake Suigetsu is the largest of the of the 'Mikata Five Lakes' (4.3 km^2) and is in a small tectonic basin situated on the western side of the Mikata fault (Fig. 1C). These lakes are situated on central Honshu Island (35°35′0″N, 135°53′0″E, 0 m above present sea level), adjacent to Wakasa Bay on the Sea of Japan coast (Fig. 1). The principal tributary, the Hasu River, enters on the southeast edge of Lake Mikata which adjoins Suigetsu through a narrow channel (Fig. 1C). The low energy environment and deep-water column (34 m) hinder disturbance to the deposited sediments. This unique hydrological configuration means that the sedimentary environment is highly stable and dominated by fine-grained deposition as coarser material settles out upstream in Lake Mikata (Nakagawa et al., 2021). Lake Suigetsu is situated 150 km from the nearest active volcano (Ontake, Fig. 1A) and thus, is not inundated with locally sourced volcanic glass, which would hinder the identification of low-concentrated cryptotephra from more distant volcanic sources.

3. Eruption histories of volcanoes in and around Japan between ~120 and 50 ka

Volcanism in Japan occurs via subduction along the Ryuku-Kyushu Arc, SW Japan Arc (SWJA), the NE Japan Arc (NEJA) and the Kurile Arc (Fig. 1). Intraplate volcanism is also relevant in this region with volcanoes located in South Korea (Halla on Jeju island located off the south coast of South Korea and Ulleungdo located in the Sea of Japan) and on the North Korea/China border (Changbaishan) (Fig. 1A; Brenna et al., 2012). Many of these centres have been highly productive during the Late Quaternary (Fig. 2), several of which have produced some of the largest known caldera-forming eruptions (VEI/M ≥ 7; see Machida and Arai, 2003). An overview of the known eruption histories from these volcanic centres likely to be identified in Lake Suigetsu in the ~120–50 ka timeframe are provided in Table 1 and are discussed in brief in the following sections. All ages reported from the literature in this section are quoted ±2σ.

3.1. The Central Volcanic Region (CVR) associated with the Ryuku-Kyushu Arc

The CVR is located in northeast Kyushu and notably includes the Aso caldera and the Kuju volcanic complex (Fig. 1A). Aso has been highly productive during the Late Quaternary with numerous Plinian eruptions of ≥M4 (Table 1). The present caldera is one of the largest on Earth and is a product of at least four M6-8 eruptions (Machida and Arai, 2003; Miyabuchi, 2009). The Aso-4 eruption is the most recent caldera-forming event and is dated to 86.4 ± 1.1 ka ($^{40}Ar/^{39}Ar$; Albert et al., 2019a), and resides within sediments associated with Marine Isotpe Stage (MIS) 5b (Aoki, 2008). It provides a key widespread tephrostratigraphic marker and is frequently identified in distal records

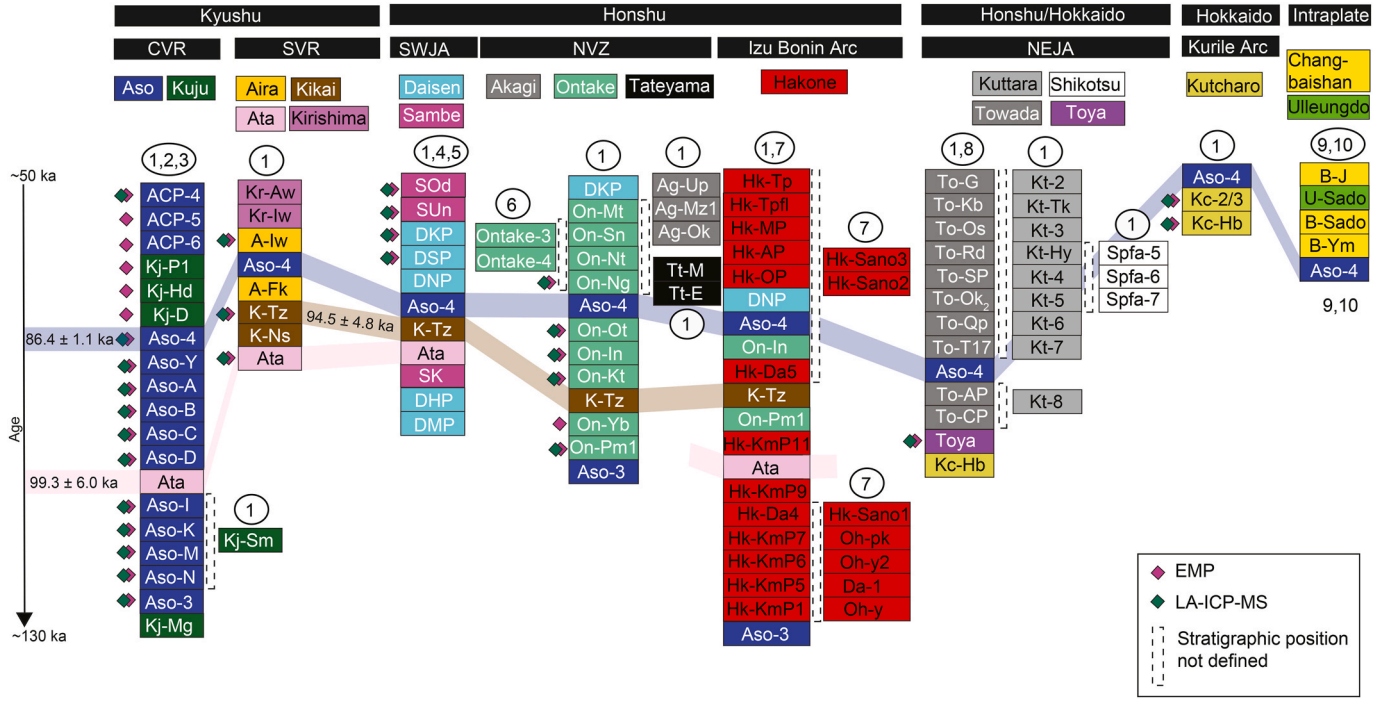

Fig. 2. Relative stratigraphic order of known eruptions (~130–50 ka), based largely on the proximal stratigraphies, in and around Japan. The key widespread marker layers that link several of the stratigraphies include the Ata (from Aira volcano), K-Tz (Kikai) and Aso-4 (Aso) tephras. The ages of Ata and K-Tz are modelled ages based on their position the Lake Suigetsu sediments (Smith et al., 2013; Albert et al., 2019a), and Aso-4 has been directly dated via $^{40}Ar/^{39}Ar$ (Albert et al., 2019a). References: 1. Machida and Arai (2003); 2. Albert et al. (2019a); 3. Kamata et al. (1998)Kamata et al. (1998); 4. Albert et al. (2018); 5. Nagaoka et al. (2001); 6. Hayakawa (1985); 7. Kobayashi and Koyama (1996); 8. Matsu'ura et al. (2014). Medial marine records: 9. Ikehara et al. (2004); 10. Lim et al. (2013).

across East Asia (Figs. 2 and 3). The proximal stratigraphies from outcrops close to the caldera indicate that there were a series of post-caldera Plinian fall eruptions from central cones following the Aso-4 eruption, which span ~60–50 ka (Miyabuchi, 2009). ACP4 is the most widely traced of these eruptions with a visible ash layer identified in Lake Suigetsu, SG06-3912 (49,974 ± 33 cal. BP; Albert et al., 2019a). The pre-Aso-4 deposits are buried under the tephra from the caldera generating eruption (Fig. 2; Table 1) and the number of eruptions are still unclear. At least four eruptions (several with multiple phases) are observed beyond the caldera walls, two units (Aso-Y and Aso-ABCD; SG06-5287) occur above the widespread Ata marker tephra, while multiple units are recognised between Ata and the Aso-3 (caldera-forming) eruption deposits (Table 1; Fig. 2; Hoshizumi et al., 2022; Albert et al., 2019a).

The Kuju volcanic complex lies North of Aso and consists of over twenty small stratovolcanoes and lava domes (Kawanabe et al., 1997), and has produced some widely dispersed tephras (Machida and Arai, 2003). Kuju activity at ~55–53 ka includes three deposits: Kj-D, Kj-P1 and Kj-Hd (Fig. 2). Both the Kj-Hd (Handa) ignimbrite and Kj-P1 Plinian fall deposits are considered to have erupted contemporaneously (Okuno et al., 2017)

and have been identified distally in Lake Suigetsu (SG06-4141; Albert et al., 2019a). Older Kuju deposits that have been reported: Kj-Sm at 110 ± 4.0 ka (Fig. 2) and Miyagi (Kj-Mg), which is beneath Aso-3 and considered to be > 150 ka (Hayakawa, 2023; Kaneko et al., 2015; Machida and Arai, 2003). Glass compositions of the CVR tephras are well established; most notably for the eruptions from Aso. Glasses from Aso erupted between 135 and 50 ka range from trachy-dacite through to rhyolites, and plot on a distinctive K_2O evolutionary trend relative to those erupted from many other Japanese volcanic centres, including Kuju (Fig. 2; McLean et al., 2020a; Albert et al., 2019a; Kimura et al., 2015; Machida and Arai, 2003). In contrast, glasses from Kuju are rhyolitic and cannot be discriminated from those erupted from volcanoes in the SWJA using major or trace element compositions (Matsu'ura et al., 2021). Geochemical data are available for four of the Kuju deposits that are listed in Fig. 2.

3.2. *The southern volcanic region (SVR) associated with the Ryuku-Kyushu Arc*

The SVR is located on southern Kyushu and includes the Ata, Kikai and Ata calderas, and the Kirishima volcanic complex furthest north (Fig. 1A). The submerged Ata caldera beneath Kagoshima Bay was partly created during the M7.5 Ata eruption which generated 350 km^3 of tephra (Machida and Arai, 2003) and is found across Kyushu and Honshu beneath the Aso-4 deposit (Figs. 2 and 3). Kikai caldera is the

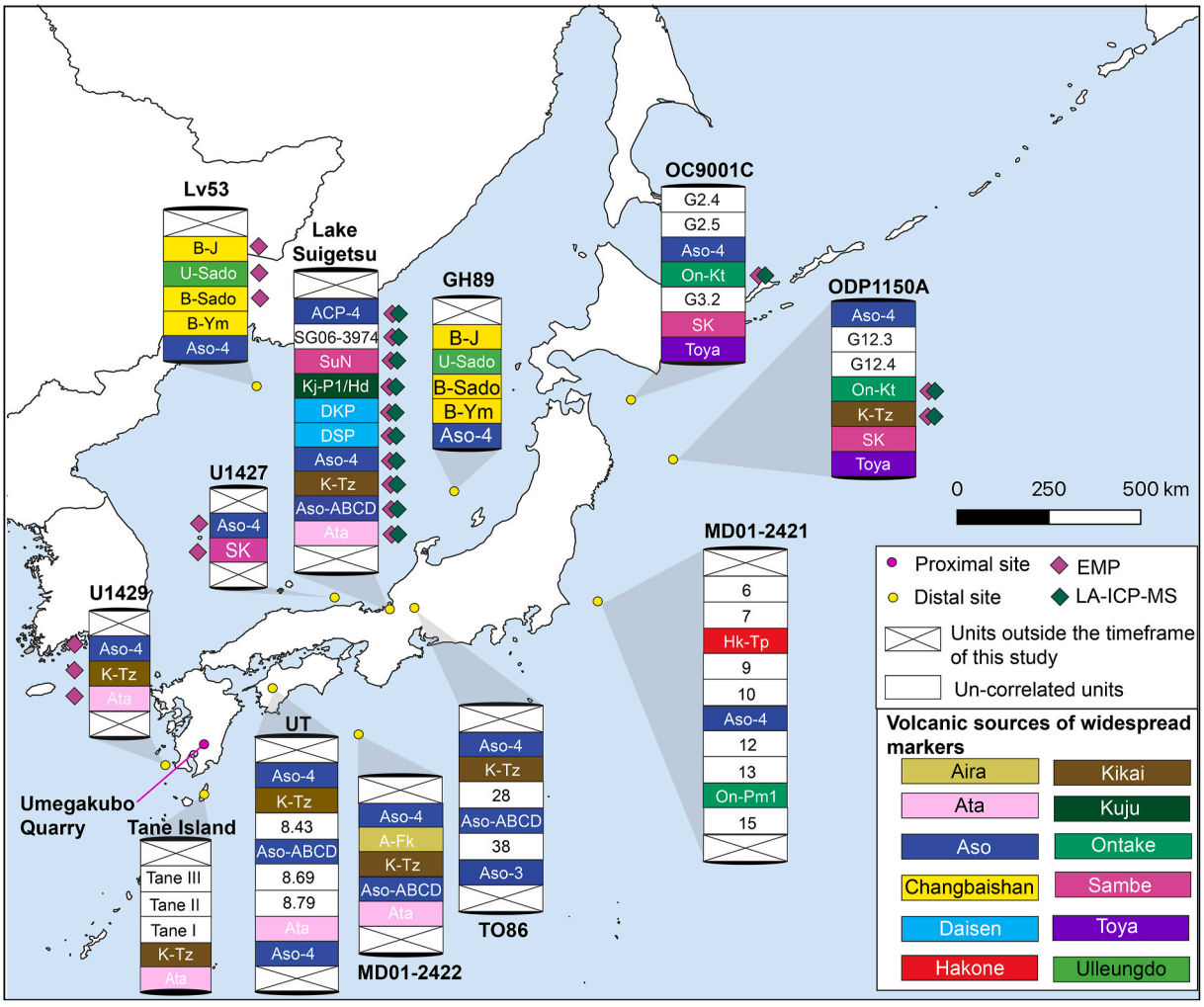

Fig. 3. Sedimentary records that contain identified and correlated tephras in the ~120–50 ka interval. The terrestrial records include Lake Suigetsu (SG06/SG14; Smith et al., 2013; Albert et al., 2018, 2019a) and Lake Biwa (TO86; Nagahashi et al., 2004); and the marine records include: OC9001C and ODP1150A (Matsu'ura and Komatsubara, 2024); GH89 (Ikehara et al., 2004; Lim et al., 2013); MD012422 (Matsu'ura et al., 2021); Lv-53 (Derkachev et al., 2019); UT (Tsuji et al., 2018); U1427 and U1429 (Sagawa et al., 2018). The purple and green diamonds show which deposits have been characterised via EMP, or LA-ICP-MS in previous studies and can be used for comparison in this study.

product of two large magnitude eruptions occurring in the last ca. 100 kyr: the Kikai Akahoya (K-Ah), which is one of the largest Holocene eruptions (M7.3), and the older M7.2 Kikai Tozurahara (K-Tz; Table 1) eruption. Further Kikai eruptions are documented between the Ata and K-Tz deposits, the Kikai Nagase (K-Ns; Fig. 2; Machida and Arai, 2003) as well as the younger post-K-Tz Tane tephras (Fig. 2; Okuno and Kobayashi, 1994).

Aira has been active since 100 ka (Nagaoka et al., 2001) and the caldera was generated during the enormous M7.9 Aira Tanzawa (AT) eruption that produced a widespread tephra. The AT tephra is ~35.1 cm thick in the Lake Suigetsu sediments (the thickest tephra recorded at the site) and has been assigned an age of 30,078 ± 96 cal. BP based on the Lake Suigetsu age-depth model (Smith et al., 2013). Prior to the AT tephra, two Aira deposits, the older Fukuyama eruption (A-Fk) and the younger Iwato eruption (A-Iw), are identified in proximal exposures interspaced by the Aso-4 tephra (Fig. 2). The Kirishima complex comprises multiple small stratovolcanoes and pyroclastic cones that are known to have been active over the last 60 kyr, including the Iwaokoshi (Kr-Iw) and Awaokoshi (Kr-Aw) tephras (Nagaoka and Okuno, 2011). Of the SVR units in this timeframe, only the Ata and K-Tz tephras are particularly widespread and found in marine and terrestrial sediments around Kyushu and southern and central Honshu (Figs. 2 and 3). They have been identified in Lake Suigetsu with modelled ages of 99.3 ± 6.0 ka and 94.5 ± 4.8 ka, respectively (Albert et al., 2019a; Smith et al., 2013).

Previous Lake Suigetsu tephra investigations have identified eighteen SVR crypto-/tephra deposits (Albert et al., 2019a, 2024; McLean et al., 2018, 2020a; Smith et al., 2013). Geochemical characterisation of these units and proximal units around the volcanoes has generated detailed compositional fingerprints for the centres within the SVR (e.g., Albert et al., 2019a). Glasses erupted from Kirishima are compositionally distinct from other SVR glasses, plotting along a well-defined SiO_2 vs. K_2O trend and containing higher Th contents (Albert et al., 2024). Glasses erupted from Ata, Aira and Kikai share similar major element compositions (Albert et al., 2019a), but trace element concentrations are useful for discrimination. Glasses erupted from Aira have lower Y and Zr and extend to higher Th than those from Kikai and Ata, and Nb contents can distinguish products from Kikai and Ata (Albert et al., 2019a).

3.3. SW Japan arc (SWJA)

The SWJA relates to back arc volcanism in SW Honshu and includes the stratovolcanoes of Daisen and Sambe (Fig. 1). The explosively erupted products are well documented, yet inconsistencies exist in the volcanic histories, and the frequency of recorded events decreases further back in time (Albert et al., 2018). There were at least eight eruptions between 125 and 60 ka, three of which have been identified in Lake Suigetsu (Table 1); the most widespread are the 59.6 ka Daisen Kurayoshi Pumice (DKP; Albert et al., 2018; Machida and Arai, 2003) and the ca. 100 ka Sambe Kisuki (SK; Machida and Arai, 2003; Kimura et al., 1999).

The proximal deposits of Daisen and Sambe are often heavily weathered and altered (e.g., Furusawa, 2008) and consequently, only limited reliable volcanic glass data are available to characterise the tephras (e.g., Albert et al., 2018; Kimura et al., 2015). The SWJA glasses are characterised by lower Y contents at given Th contents relative to other Japanese centres (Albert et al., 2018). Geochemically distinguishing the two volcanoes is possible, as Sambe tephras typically exhibit higher CaO at a given SiO_2 content and are more depleted in Zr relative to those from Daisen (Albert et al., 2018). Notably, glasses do show partial overlap at major and trace element levels with those erupted at Kuju (Albert et al., 2019a).

3.4. Izu Bonin Arc

The Izu Bonin Arc lies on the eastern margin of the Philippine plate and extends south from Hakone volcano into the Pacific Ocean (Fig. 1). Volcanic centres along the Izu Bonin Arc are typically stratovolcanoes, with few experiencing caldera forming eruptions (Machida, 1999). Only Hakone was active in the interval relevant to this study (Fig. 2).

Despite the number of volcanic systems located along the Izu-Bonin Arc (sixteen centres; Tatsumi et al., 2016), only limited geochemical glass data exists for the Kawagodaira, Niijima, Kozushima and Hakone volcanoes (see: Albert et al., 2019a, 2024; Suzuki et al., 2016; McLean et al., 2018). Quaternary explosive volcanism at the Izu-Bonin Arc is typically rhyolitic (Tamura and Tatsumi, 2002) and is predominantly represented by low-K tholeiites (<1 wt% K_2O) that are highly depleted in Th (Bryant et al., 2003). The Hakone glasses can be distinguished from other tholeiitic deposits from other arc settings as they have lower Al_2O_3 and higher FeO contents, and are extremely low in Th (<2 ppm) and Rb (<30 ppm; Albert et al., 2019a). Although more than twenty eruptions occurred from Hakone pre-50 ka, none of the glasses in these units have been subjected to detailed geochemical characterisation (Fig. 2).

3.5. Norikura Volcanic Zone (NVZ)

The NVZ is located at the southern edge of the NE Japan arc (NEJA) in central Honshu and includes several stratovolcanoes such as Haruna, Akagi, Asama, Tateyama and Ontake (Fig. 1). These are known to have produced several large explosive ≤ M6 eruptions (Albert et al., 2019a) but only deposits from the Akagi, Ontake and Tateyama have been reported prior to 50 ka (Fig. 2; Machida and Arai, 2003). The largest known eruption is the ca. 95 ka Ontake Daiichi (On-Pm1) that occurs in MIS 5c (Machida and Arai, 2003). At least ten eruptions occurred at Ontake between 95 ka and 60 ka (Table 1; Machida and Arai, 2003), and several widespread key markers (K-Tz and Aso-4) have been identified between some of these Ontake derived units (Fig. 2). Notably, several Ontake tephras have been recognised in marine sediments of the western Pacific Ocean (Fig. 3). Akagi stratovolcano, located to the northwest of Ontake, also produced a series of large Plinian eruptions during the Pleistocene, and three are identified between the Aso-4 and DKP marker layers (Fig. 2; Machida and Arai, 2003).

Major element compositions of the Ontake glasses are like other Japanese centres, but they can be distinguished based on Th and Zr content (Albert et al., 2019a). Matsu'ura and Komatsubara (2024) geochemically characterised five units relevant to this study and indicate that Hf and Zr abundances are lower in the Ontake units below the K-Tz marker layer (Fig. 2). There are no published detailed geochemical data for the three Akagi and two Tateyama eruption deposits that occurred between Aso-4 and the DKP (Fig. 2).

3.6. NE Japan arc (NEJA)

A series of Late Quaternary calderas are situated along the NEJA (Fig. 1), which include Towada (northern Honshu), Kuttara, Shikotsu, and Toya (Hokkaido), and have produced at least twenty-three known explosive volcanic eruptions between 100 and 50 ka (Fig. 2; Machida and Arai, 2003). One of the largest Late Quaternary eruptions to occur along the NEJA is associated with the formation of the Toya caldera (tephra volume 170 km^3, with a radial dispersal). The age of the Toya tephra remains poorly constrained using radiometric methods; for instance, U-Pb and U/Th dating of zircons has yielded an age of 108 ± 19 ka (Ito, 2014); similarly, single aliquot regeneration–red thermal luminescence (SAR–RTL) dating yielded ages of between 104 ± 30 and 118 ± 30 ka (Ganzawa and Ike, 2011). The Toya tephra is also chrono-stratigraphically constrained by its position in MIS5d sediments dated at around 105–115 ka (Machida and Arai, 2003; Matsu'ura et al., 2014).

The restricted Y, Rb and Th contents of glasses erupted from the NEJA are useful for discerning them from those from other Japanese arcs (Albert et al., 2019a). However, there are no geochemical data for

Kuttara glasses. Glasses erupted from Towada, Shikotsu and Toya can be distinguished from each other by their CaO content (Albert et al., 2019a). Despite the number of NEJA deposits preserved in the proximal realm in the timeframe relevant to this study, geochemical data are only available for the Toya tephra (Fig. 2).

3.7. Kurile Arc

The Kurile Arc extends from northern Hokkaido to Kamchatka (Russia) and includes three Quaternary calderas (Akan, Mashu and Kutcharo) that form a cluster in eastern Hokkaido (Fig. 1). The Kutcharo caldera was formed by a series of major eruptions between 340 and 30 ka, including two large explosive eruptions (M6.4 and M7.2), Kutcharo-2/3 (Kc-2/3) and Kutcharo-Hb (Kc-Hb), which are both preserved beneath the widespread Aso-4 deposit (Fig. 2). Reported activity at both Akan and Mashu are much younger and thus not relevant to the timeframe of this study (Machida and Arai, 2003).

Glasses erupted from Kutcharo volcano are calc-alkaline and rhyolitic and can be discriminated from other Japanese volcanic centres using SiO_2 vs. K_2O plots owing to relatively low K_2O content (~1.5 wt%) at a given SiO_2 content (Albert et al., 2019a). Most of the trace elements in the Kutcharo glasses are similar to Kikai, with the exception of lower Y content (Albert et al., 2019a). Major and trace element glass compositions are available for both the Kc-Hb and Kc-2/3 units (Fig. 2) and, whilst both show a degree of overlap, the younger Kc-2/3 glasses span a broader major element compositional range than the older Kc-Hb glasses (Albert et al., 2019a).

3.8. Intra-plate

The intra-plate volcanoes that have dispersed ash across Japan in the past include Changbaishan and Ulleungdo (Fig. 1; Kimura et al., 2015; Machida and Arai, 2003; McLean et al., 2016, 2018, 202a; , Smith et al., 2011a, 2013). Jeju (Halla), an island off the south coast of South Korea is known to have had explosive eruptions (Brenna et al., 2015), but the deposits have not been identified in distal records. The complete eruptive histories of these volcanoes are not well constrained due to poor exposure and inaccessibility.

The alkaline tephra deposits from Ulleungdo and Changbaishan can be easily discriminated from other intraplate sources (e.g., Jeju volcano; Brenna et al., 2015) and from Japanese glasses by the absence of Nb and Ta depletions and more enriched Zr compositions (McLean et al., 2016, 2020b). Ulleungdo derived glasses are phonolite-trachytes and contain lower SiO_2 and higher Al_2O_3 and K_2O compared to other regional volcanic centres (McLean et al., 2016, 2020b). No geochemical data has been reported for the pre-50 ka Changbaishan or Ulleungdo eruption deposits sampled near the volcanoes; however, some major element glass data are available for deposits preserved in marine cores that are thought to come from these volcanoes (Fig. 3; Chun et al., 2007; Derkachev et al., 2019).

Three >50 ka Changbaishan tephras have been identified in marine records across the Sea of Japan: Baegdusan-Yamato Basin (B-Ym; ca. 85.8 ka), Baegdusan-Sado-Oki (B-Sado; ca. 67.6 ka), and Baegdusan-Japan Basin (B-J; ca. 50.6 ka) (Fig. 3; Ikehara et al., 2004; Lim et al., 2013). Similarly, the Ulleungdo derived U-Sado, also known as the SKP-II layer (Chun et al., 2007), has been reported in marine records and has an age of ~60.5 ka based on stratigraphy (Ikehara, 2015; Lim et al., 2013).

4. Materials and methods

4.1. Cryptotephra extraction techniques

To identify the cryptotephras preserved in the sediments spanning ~120–50 ka, the master SG14 core was contiguously sub-sampled at ca. 5 cm (low) resolution from 38.83 to 59.79 m composite depth (CD). Positions of elevated shard concentrations in the low-resolution samples were resampled at 1 cm (high) resolution, which were used to refine the stratigraphic positions of the cryptotephra peaks.

All samples were dried, weighed, and then wet sieved and the >25 μm fraction (alongside blanks to test for any laboratory contamination) were processed using the heavy liquid floatation method outlined by Turney (1998) and Blockley et al. (2005). This stepped floatation method is shown to reliably concentrate the glass shards in the Lake Suigetsu sediments so that cryptotephra peaks can be resolved (e.g., McLean et al., 2022). The extraction residues, i.e. those with the same density as glass, were mounted on slides using Canada Balsam. The glass shards in the sample were counted using a light microscope to quantify the number of shards per gram of dried sediment (shards/gram). Morphological features of the shards were also recorded as in McLean et al. (2018). Where background shard concentrations were high, particularly in the sediments above visible tephra layers, differences in the morphological features and colour of the shards were also used to help identify the stratigraphic position of new primary ash-falls, for instance SG14-5099 and SG14-5367. Samples taken above visible tephra layers (e.g., following the 2.8 cm thick K-Tz tephra) have high shard concentrations due to subsequent (re-)mobilisation of the shards within the catchment (referred to as background). These samples were processed as outlined above and then spiked with a known quantity of *Lycopodium* pollen spores after the sample had been sieved and floated. Each *Lycopodium* tablet has a particular spore count (9666 spores per tablet from batch 3862). The tephra and *Lycopodium* solution was mounted on microscopic slides, and both were counted, and the concentration of glass shards was estimated using the following equation (Payne and Gehrels, 2010): number of glass shards counted/(number of *Lycopodium* spores counted/total number of *Lycopodium* spores added to the sample). The resulting counts are expressed as shards/gram using weights of the dry samples that were taken before sample processing, but were capped at 20,000 s/g as the accuracy of counting spiked samples is undetermined.

4.2. Reference tephra samples

To assess the volcanic sources of the newly recognised Lake Suigetsu cryptotephra deposits, the glasses were geochemically characterised and compared to the published Japanese volcanic glass datasets (e.g., Matsu'ura and Komatsubara, 2024; Albert et al., 2018, 2019a, 2024; McLean et al., 2016, 2018, 2020a; Suzuki et al., 2016; Kimura et al., 2015; Smith et al., 2011a, 2013). Additionally, new major and trace element glass data were obtained for the following temporally relevant eruptions: Kirishima (Kr-Iw and Kr-Aw) and Sambe (SK). These eruption deposits were sampled close to the volcanoes where the stratigraphy is clear; locations are reported in Supplementary Material and the glass compositions are reported in Table 4.

4.3. Glass compositions

Individual glass shards were manually picked using a syringe mounted on a micromanipulator (outlined in Lane et al., 2014), and subsequently mounted on to Struers.

SpeciFix 20 epoxy resin stubs. Samples with shard concentrations >10,000 shards/gram samples were directly pipetted onto stubs. The shards were then covered with a thin film of resin and placed in an oven at 50 °C for 4.5 h to cure. The surfaces of the stubs were manually sectioned using silicon carbide papers to expose the shards on a flat surface, polished with diamonds, and then carbon coated.

Major element compositions of individual glass shards were analysed using a JEOL JXA-8200 wavelength dispersive electron microprobe (WDS-EMP) equipped with 5 spectrometers located in the School of Archaeology, University of Oxford, UK. An accelerating voltage of 15 kV, 6 nA current, and a defocussed 10 μm beam were used. Peak counting times were 12 s for Na, 30 s for other major elements except for

Mn, Cl and P, which were collected for 50 s. A suite of mineral standards was used to calibrate the microprobe, and the MPI-DING references glasses (Jochum et al., 2006) were run as secondary standards during each analytical session. All data analyses presented in figures and tables have been normalised to 100% for comparative purposes and to account for variable hydration (Shane et al., 2008) with raw datainluded in the Supplementary Material. Analyses with analytical totals <94% were discarded as they are not thought to be representative of the true melt composition.

The trace element compositions of individual glass shards were determined using an Agilent 8900 triple quadrupole LA-ICP-MS (laser ablation inductively coupled plasma mass spectrometry; ICP-QQQ) coupled to a Resonetics 193 nm ArF excimer laser-ablation device in the Department of Earth Sciences, Royal Holloway, University of London. A range of crater sizes was used (20 and 25 μm), depending on the area of the sectioned glass. The laser energy density on the target was 3.0 Jcm^{-2}, the repetition rate was 5 Hz. Ablation of the samples lasted 40 s on the sample, followed by 40 s during which there was no ablation, and this gas blank is used to subtract the background signal. The MPI-DING reference glasses were used to monitor analytical accuracy (Jochum et al., 2006). Typically, blocks of eight glass shards and one MPI-DING reference glass were bracketed by the NIST612 glass adopted as the calibration standard. The internal standard applied was ^{29}Si (determined by EMP-WDS analysis). LA-ICP-MS data reduction was performed in Microsoft Excel, as described in Tomlinson et al. (2010). Accuracies of LA-ICP-MS analyses were monitored using MPI-DING reference glasses, ATHO-G and StHs6/80-G, and accuracies were typically ≤5% for many elements measured (see Supplementary Material).

Error bars on plots represent reproducibility, calculated as ± 2 standard deviations of replicate analyses of MPI-DING StHs6/80-G glasses. Error bars on the trace element plots are typically smaller than the symbols. All raw major and trace element data and the secondary standards run alongside are included in the Supplementary Material.

4.4. The Lake Suigetsu core and its chronology

Lake Suigetsu was drilled in 2006 (~250 m from an earlier [SG93] borehole; Fig. 1C) as part of the 'Lake Suigetsu Varved Sediment Project' with the aim of obtaining a complete 'master' sedimentary sequence by recovering overlapping cores from four parallel boreholes (Nakagawa et al., 2012). This ca. 73.2 m sequence, termed SG06, has an incredibly precise chronology for the last 50 kyr as it is the longest continuously varved record from the Quaternary (Schlolaut et al., 2012, 2018). Moreover, ~800 macrofossils from the core have been radiocarbon dated (Bronk Ramsey et al., 2012, 2020; Staff et al., 2011). These chronological data have been incorporated into the international consensus radiocarbon calibration curve (i.e., IntCal13 and IntCal20; Reimer et al., 2013, 2020). In 2014 another coring campaign was undertaken (~320 m east of the SG06 boreholes; Fig. 1C) from four additional boreholes, which have been integrated to form the composite SG14 master sequence. This sequence spans ~98 m (~25 m deeper than SG06) and reaches a thick basal gravel. The SG14 sequence has been precisely tied to the SG06 composite core (correlation model October 28, 2019) using 361 marker layers that include visible tephras. These correlations allow the high-precision SG06 chronology (Bronk Ramsey et al., 2020) to be transferred to the SG14 core. The SG14 composite core sequence was used for this cryptotephra investigation.

SG06 event-free depth(s) (EFD; version Feb 13, 2017) were used within the age model, which excludes instantaneous deposits >5 mm in thickness, i.e., event layers (Staff et al., 2011; Schlolaut et al., 2012). The software package developed to handle the correlation of parallel core sections, 'LevelFinder' (version 7.7.1, http://polsyems.rits-palaeo.com), was used to linearly interpolate between the common marker layers to determine a composite depth (CD) or EFD for the cryptotephra layers. Down to the limit of radiocarbon dating (circa 52 cal ka BP). For the deeper section of the stratigraphy examined in the present study, this chronology was extrapolated using a 'P_Sequence' deposition model within the Bayesian software package, OxCal (Bronk Ramsey, 2008), additionally including a single $^{40}Ar/^{39}Ar$-derived age of 86.4 ± 0.6 ka (±1σ) for the Aso-4 tephra, at a CD in SG14 of 4922.8 cm (Albert et al., 2019a; see below). The SG age model-derived ages for the tephra identified in this section of the SG core are reported in Table 2 and the ±1σ uncertainties are quoted throughout.

5. Results

5.1. Tephrostratigraphy

This detailed cryptotephra study identified a further forty-one eruption deposits in the 20 m of Lake Suigetsu sediments spanning ~120 to 50 ka. These deposits are in addition to the nine visible tephras that were previously reported across this interval (Table 2; Smith et al., 2013; Albert et al., 2018, 2019a). The newly identified crypto-/tephras are labelled herein using a SG14 prefix followed by the composite depth of the base of the tephra, rounded to the nearest integer (in cm; version February 28, 2019), in the 2014 core (Table 2). This labelling convention has been used for all the crypto-/tephras in Lake Suigetsu, including the visible tephra layers reported in SG06. Two new visible tephras are identified, SG14-4582 and SG14-5577, which are a 0.1 cm-thick fine-grained orange-brown ash, and a 0.8 cm thick fine-grained white ash, respectively. The details of all the visible tephra and cryptotephra identified are summarised in Table 2.

The glass shards show considerable variance in terms of their physical characteristics (see Supplementary Material). Shard concentrations for all the cryptotephra identified peak above 200 shards/gram, with most exceeding 1500 shards/gram (Fig. 4, Table 2). Nineteen of these deposits exceed 20,000 shards/gram. The high background shard concentration observed between the SG14-5367 cryptotephra and the SG06-5353 (Ata) tephra are associated with the previously reported SG06-5385 tephra; however, the glasses are too weathered for geochemical analyses and have been discounted as representing an additional primary tephra deposit within the Lake Suigetsu record (see Smith et al., 2013; Albert et al., 2019a).

5.2. Glass geochemical compositions

Major element and trace glass compositions of the forty-one SG14 deposits are presented in Table 3.

The glass compositions of the newly identified crypto-/tephras are generally homogenous, except for the following deposits which span broad compositional ranges: SG14-4002, SG14-4010, SG14-4187 and SG14-4860 (Fig. 5). The glass compositions of the deposits are predominantly rhyolitic residing on either a calc-alkaline or high-K calc-alkaline evolutionary trend (Fig. 5). Trachy-andesite and trachy-dacite tephra deposits are also observed along the High-K calc-alkaline evolutionary series (Fig. 5). The SG14-5033, SG14-5597 and SG14-5851 deposits all show a distinctive Low-K tholeiitic affinity, whilst the SG14-4223 is unique in displaying a shoshonitic affinity, residing on the phonolite-trachyte boundary (Fig. 5A).

Trace element data were obtained for all deposits apart from three, SG14-4010, SG14-5182, and SG14-5520, as the vesicularity and microlite inclusions precluded analyses (Table 3). Similarly to the major element compositional data, individual cryptotephras typically demonstrate relatively homogenous compositions. The phono-trachytic tephra, SG14-4223, displays the highest levels of incompatible trace element enrichment and the most heterogeneity (Fig. 6).

6. Discussion

6.1. Provenance of the SG14 tephra layers erupted ~120 - 50 ka

The major and trace element glass compositions permit thirty-eight

Table 1
Key East Asian eruption deposits reported in proximal and medial locations in the ~120–50 ka timeframe that are most likely to be preserved in the Lake Suigetsu sediments. Those in bold are widespread marker layers (Machida and Arai, 2003), and those previously identified in Lake Suigetsu sediments as visible tephras (layers noted by their SG labels; (Albert et al., 2018, 2019a; Smith et al., 2013).[a]

Region	Volcano	Eruption	Tephra	SG label	Magnitude	Tephra volume	Dispersal	Age	
					(M)	(km3)		(cal. yrs BP/ka)	(Ref.)
Kyushu (Central Volcanic Region; CVZ)									
	Aso	ACP-4	ACP-4	SG06-3912	4.6	0.43	E	49,974 ± 331	1
		ACP-5	ACP-5	–	4.2	0.15	NE	>ACP-4	–
		ACP-6	ACP-6	–	4.3	0.21	E	~60	2
		Aso-4	**Aso-4**	**SG06–4963**	**7.8**	**600**	**-**	**86.4 ± 1.11***	**1**
		Aso-Y	Aso-Y	–	4	0.1	E?	>Aso-4	–
		Aso-ABCD	Aso-ABCD	SG06-5287	5	1	–	~96	3
		Aso-IK	Aso-IK	–	5	1	ENE	>100 < 123	1
		Aso-MN	Aso-MN	–	5	1	ENE	>Aso-IK	–
		Aso-3	**Aso-3**	**-**	**7.5**	**150**	**ENE**	**~123–135**	**4, 5**
	Kuju	Pumice 1/Handa	Kj-P1/Hd	SG06-4141	5.3	2	E	54.4 ± 1.6	6
		Kuju-D	Kj-D	–	–	–	–	>Kj-P1/Hd	–
		Miyagi	Kj-Mj	–	–	–	S	>Kj-P1; >Aso-3	–
Kyushu (Southern Volcanic Region; SVR)									
	Aira	Iwato	A-Iw	–	6	9.5	E	~55	7
		Fukuyama	A-Fk	–	–	–	EN	90	4
	Ata	**Ata**	**Ata**	**SG06–5353**	**7.5**	**350**	**NE**	**99.3 ± 6.0**	**1**
	Kikai	Tozurahara	K-Tz	SG06-5181	7.2	150	NE (radial)	94.5 ± 4.8	1
		Nagase	K-Ns	–	–	–	–	>K-Tz	4
	Kirishima	Awaokoshi	Kr-Aw	–	–	–	ENE	<Kr-Aw	–
		Iwaokoshi	Kr-Iw	–	–	–	ENE	40–45	4
Honshu (South West Japan Arc; SWJA)									
	Daisen	**Kurayoshi Pumice**	**DKP**	**SG06–4281**	**6.5**	**32**	**E**	**59.6 ± 5.5**	**6**
		Sekigane Pumice	DSP	SG06-4318	4.9	0.85	E	61.1 ± 5.8	6
		DNP	DNP	–	6.9	80	E	~80	4
		DHP	DHP	–	–	–	E	>DNP	–
		DMP	DMP	–	–	–	W	~125	3
	Sambe	Oda Pumice Flow	SoD	–	–	–	–	~53 ka	4
		Unan Pumice Fall	SuN	SG06-4124	6.1	13	–	53.8 ± 1.2	1
		Kisuki	**SK**	**-**	**6.3**	**20**	**NE**	**~100**	**4, 9**
Honshu (Norikura Volcanic Zone; NVZ)									
		Nagawa	On-Ng	–	–	–	NE	~83	4
		Ina	On-In	–	6	10	E	~93	4
		Katamachi	On-kt	–	–	–	NNE	~94	4
		Daiichi Pumice	O-Pm1	–	6.7	50	E	~95	4
Honshu/Hokkaido (Northeast Japan Arc; NEJA)									
	Toya	**Toya**	**Toya**	**-**	**7.2**	**170**	**Radial**	**112–115 (MIS5d)/108**	4,10
Hokkaido (Kurile Arc)									
	Kutcharo	Kc-2/3	Kc-2/3	–	6.4	25	N-NNEW	~85	8
		Kc-Hb/4	**Kc-Hb**	**-**	**7.2**	**175**	**W**	**120**	**11**
Intra-plate									
	Changbaisan	Baegdusan–Japan Basin tephra	B-J	–	–	–	–	50.67	12
		Baegdusan–Sado-oki tephra	B-Sado	–	–	–	–	67.68	13
		Baegdusan–Yamato Basin tephra	B-Ym	–	–	–	–	85.88	13
	Ulleungdo	Ulleung–Sado-oki tephra	U-Sado	–	–	–	–	61.18	13

[a] Dispersal and tephra volume estimates are from Machida and Arai (2003) and the LaMEVE database (Crosweller et al., 2012; and references therein). The magnitude (M) of each eruption has been calculated using the published tephra volumes and the equation of Pyle (2000), assuming a magma density of 2300 kg/m^3 and tephra density of 1000 kg/m^3. * indicates ^{40}Ar/^{39}Ar age. Eruption age references as follows: 1 Albert et al. (2019a); 2 Miyabuchi et al. (2011); 3 Hayakawa (2023); 4 Machida and Arai (2003); 5 Kaneko et al. (2015); 6 Albert et al. (2018); 7 Ikehara et al (2006); 8 Smith et al. (2013); 9 Kimura et al. (1999); 10 Ito (2014); 11 Hasegawa et al. (2016); 12 Ikehara et al. (2004); 13 Lim et al. (2013).

deposits to be attributed to their volcanic arcs, and thirty-four of these to specific volcanoes (Figs. 5 and 6; Table 4). In summary, these deposits are from seven different Japanese volcanic arc settings (from the three main islands of Japan), and from intraplate sources (Fig. 5). Due to the number of deposits identified in this study, they have been grouped based on chemical affinities with volcanic sources and regions as listed below and in Table 2.

1) Kyushu Southern Volcanic Region (SVR): Kirishima (5); Aira (1); Ata (2) and Kikai (1)
2) Kysushu Central Volcanic Region (CVR): Aso (11) and Kuju (3)
3) SW Japan Arc (SWJA): Sambe (1) and Daisen (2)
4) Izu-Bonin Arc: Hakone (3)
5) Norikura Volcanic Zone (NVZ): Ontake (2)
6) NE Japan Arc (NEJA): Toya (1)
7) Kurile Arc: Kutcharo (1)
8) Intraplate: Ulleungdo (1)

There are another 7 eruption deposits that could not be reliably correlated to a particular arc or source volcano (Table 2).

6.1.1. *Kyushu (SVR and CVR)*

6.1.1.1. Kirishima. Five cryptotephras have compositions consistent with published and newly analysed deposits from the Kirishima volcanic complex: SG14-4002, SG14-4010, SG14-4053, SG14-4263 and SG14-4496. The SG14-4002 glasses span the broadest compositional ranges in both major and trace elements and extend to lower SiO_2 and Th contents (Fig. 7A–C). The younger two Kirishima deposits (SG14-4010 and SG14-4002) have higher Nb at a given Th contents and can be easily distinguished from older glasses (SG14-4263 and SG14-4496; Fig. 7C) indicating that they may have derived from different vents within the

Table 2
Summary of the tephra layers (visible and cryptotephra) within the ~120–50 ka sediments of Lake Suigetsu (SG06/SG14 cores).[a]

Tephra (SG14 Label)	v/c	v = thickness (cm)/ c = shards/ gram	Average shard length	Glass shard morphology	Position in the SG14 master core (cm)	SG14 CD (cm) (ver. Feb 28, 2019)	SG06 CD (cm) (ver. Feb 28, 2019)	Modelled age (cal BP) (±1s)	Correlation based on glass geochemistry (region, tephra, volcano)		M	Source to Suigetsu (km)
SG14-3911	C	24,890	50–100	F, MV	E−40 (44.5–45.5)	3911.1	3941.9	49.1 ± 0.2	CVR	Aso	–	525 SW
SG06–39741,2	**V**	**0.3**	**-**	**-**	**E-40 (75.4–75.7)**	**3941.8***	**3974.1***	**49.6 ± 0.2**	**SWJA**	**Unknown, Daisen**	–	225 W
SG14-4002	C	300	70	MV, MI	E−41 (32.3–33.5)	4002.4	4040.8	50.5 ± 0.5	SVR	Kirishima	–	620 SW
SG14-4010	C	11,520	60	C, MI	E−41 (39.5–40.5)	4009.5	4047.8	50.7 ± 0.6	SVR	Kirishima	–	620 SW
SG14-4032	C	8325	50	C, F	F-41 (9.0–10.0)	4031.7	4068.6	51.5 ± 1.0	CVR	Aso	–	525 SW
SG14-4050	C	4950	70	B, C, MI	F-41 (27.0–28.0)	4049.7	4086.8	52.2 ± 1.2	CVR	Kuju	–	500 SW
SG14-4053	C	650	60	MI, V	F-41 (30.0–31.0)	4052.7	4089.7	52.3 ± 1.2	SVR	Kirishima	–	620 SW
SG06–41241,2	**V**	**0.2**	**-**	**-**	**F-41 (67.5–67.7)**	**4089.9***	**4124.0***	**53.7 ± 1.5**	**SWJA**	**SuN, Sambe**	**-**	**225 W**
SG06–41411,2	**V**	**1.4**	**-**	**-**	**E-42 (31.9–33.3)**	**4105.7***	**4141.2***	**54.3 ± 1.6**	**CVR**	**Kj-P1/Hd, Kuju**	**5.3**	**500 SW**
SG14-4135	C	>20,000	80	V	F-42 (30.9–31.9)	4135.4	4173.5	55.6 ± 1.8	CVR	Aso	–	525 SW
SG14-4150	C	7290	70	C, V	F-42 (44.9–46.2)	4149.6	4188.2	56.2 ± 1.8	CVR	Kuju	–	500 SW
SG14-4159	C	19,510	70	B, C, MV	G-11 (22.4–23.4)	4158.7	4198.1	56.6 ± 1.9	CVR	Aso	–	620 SW
SG14-4187	C	>20,000	50	PU	G-11 (51.0–52.0)	4187.3	4224.4	57.6 ± 2.0	–	–	–	–
SG14-4223	C	5775	80	B, V	G-11 (87.0–88.0)	4223.3	4259.7	59.0 ± 2.1	Intra-plate	Ulleungdo	–	500 NW
SG06–42811,2	**V**	**0.3**	**-**	**-**	**F-43 (19.9–20.2)**	**4246.3***	**4281.1***	**59.9 ± 2.2**	**SWJA**	**DKP, Daisen**	**6.5**	**225 W**
SG14-4263	C	1083	50	MI, MV	F-43 (36.2–37.2)	4262.8	4294.8	60.4 ± 2.2	SVR	Kirishima	–	620 SW
SG06–43181,2	**V**	**1.7**	**-**	**-**	**F-43 (51.3–53.0)**	**4279.1***	**4318.4***	**61.3 ± 2.3**	**SWJA**	**DSP, Daisen**	**4.9**	**225 W**
SG14-4307	C	2788	40–100	F, MV	E−44 (34.2–35.2)	4306.6	4343.8	62.3 ± 2.3	SVR	Kikai	–	750 SW
SG14-4352	C	5883	70–100	PU	F-44 (25.8–26.8)	4351.9	4388.6	64.1 ± 2.4	CVR	Aso	–	525 SW
SG14-4471	C	1333	40–100	B, MV, MI	F-45 (41.9–42.9)	4470.6	4509.0	68.7 ± 2.5	CVR	Aso	–	–
SG14-4496	C	30,717	50–100	C, V	F-45 (66.9–67.9)	4495.6	4533.1	69.7 ± 2.5	SVR	Kirishima	–	620 SW
SG14-4531	C	>20,000	70	C, MV	E−46 (46.5–48.0)	4531.0	4578.4	71.4 ± 2.4	–	–	–	–
SG14-4582	V	0.1	60	PU	F-46 (45.8–45.9)	4582.1*	4627.6*	73.4 ± 2.4	–	–	–	–
SG14-4598	C	18,650	70	C, MV	F-46 (61.4–62.4)	4598.1	4640.9	73.9 ± 2.4	SVR	Aira	–	–
SG14-4689	C	9360	70	PU	F-47 (49.5–50.5)	4688.6	4716.8	76.9 ± 2.2	SWJA	–	–	–
SG14-4748	C	30,600	120	MI, PU	E−48 (63.0–64.0)	4748.1	4777.2	79.3 ± 2.0	SWJA	DNP, Daisen	–	225 W
SG14-4837	C	>20,000	120	B, MI	E−49 (49.6–50.6)	4837.0	4871.9	83.0 ± 1.5	NVZ	On-Ng, Ontake	–	225 E
SG14-4860	C	>20,000	>100	C, V	E−49 (72.6–73.6)	4860.0	4898.9	84.1 ± 1.3	NVZ	Ontake	–	225 E
SG06–49631,2	**V**	**3.5**	**-**	**-**	**G-12 (57.2–60.7)**	**4922.8***	**4962.4***	**86.4 ± 0.6**	**CVR**	**Aso-4, Aso**	**7.7**	**525 SW**
SG14-5033	C	25,650	60	MI, MV	F-50 (90.0–91.0)	5033	5072.7	89.8 ± 1.6	Izu-Bonin Arc	Hakone	–	300 E
SG14-5071	C	49,225	60	C, F	F-51 (25.8–26.8)	5070.9	5113.1	91.2 ± 1.8	CVR	Aso	–	525 SW
SG14-5099	C	67,850	50–70	MI, V	F-51 (53.4–54.4)	5098.5	5138.5	92.1 ± 2.0	CVR	Aso	–	525 SW
SG06–51811,2	**V**	**0.2**	**-**	**-**	**E-52 (55.3–55.5)**	**5142.2***	**5180.3***	**93.4 ± 2.2**	**SVR**	**K-Tz, Kikai**	**7.2**	**750 SW**
SG14-5183	C	>20,000 S	60–100	C, V	F-52 (37.4–38.4)	5182.0	5219.0	94.7 ± 2.4	–	–	–	–
SG14-5221	C	>20,000	80	C	F-52 (76.4–77.4)	5221.0	5257.0	96.0 ± 2.6	CVR	Aso	–	525 SW

(*continued on next page*)

Table 2 (*continued*)

Tephra (SG14 Label)	v/c	v = thickness (cm)/ c = shards/ gram	Average shard length	Glass shard morphology	Position in the SG14 master core (cm)	SG14 CD (cm) (ver. Feb 28, 2019)	SG06 CD (cm) (ver. Feb 28, 2019)	Modelled age (cal BP) (±1s)	Correlation based on glass geochemistry (region, tephra, volcano)		M	Source to Suigetsu (km)
SG06–52871,2	**V**	**3.5**	**-**	**-**	**E-53 (52.5–56.0)**	**5252.1***	**5286.6***	**96.8 ± 2.7**	**CVR**	**Aso-ABCD, Aso**	**5.9**	**525 SW**
SG06–53531,2	**V**	**1.5**	**-**	**-**	**G-14 (61.0–62.5)**	**5319.9***	**5354.2***	**99.0 ± 2.9**	**SVR**	**Ata, Ata**	**7.5**	**650 SW**
SG14-5367	C	>20,000 S	70	C, F, V	E−54 (68.9–69.9)	5366.9	5398.1	100.4 ± 3.1	SWJA	SK, Sambe	6.3	300 W
SG14-5406	C	11,100	>100	PU	G-15 (43.3–44.3)	5405.5	5447.1	102.1 ± 3.3	CVR	Kuju	–	500 SW
SG14-5469	C	2217	70	C, V	E−55 (67.0–68.9)	5469.0	5515.8	104.4 ± 3.6	SVR	Ata	–	650 SW
SG14-5520	C	1600	80	C	F-55 (57.2–58.2)	5519.8	5565.6	106.1 ± 3.7	SVR	–	–	–
SG14-5563	C	>20,000 S	90	PU, MV	E−56 (62.7–63.7)	5562.8	5611.5	107.7 ± 3.9	SWJA	Daisen	–	225 W
SG14-5575	C	>20,000 S	70	C, F, V	E−56 (74.7–75.7)	5574.8	5626.4	108.2 ± 3.9	NEJA	Toya, Toya	7.3	950 NE
SG14-5579	V	0.8	40–60	C, MV	G-16 (19.1–20.1)	5578.8	5631.1	108.4 ± 4.0	CVR	Aso	–	525 SW
SG14-5597	C	2400	50	MV	G-16 (37.1–38.1)	5596.8	5649.9	109.0 ± 4.0	Izu-Bonin Arc	Hakone	–	700 NE
SG14-5616	C	18,950	40	MV	G-16 (56.1–57.1)	5615.8	5669.4	109.7 ± 4.1	Kurile Arc	Kutcharo	–	1250 NE
SG14-5648	C	>20,000 S	70–100	MV	E−57 (46.2–47.2)	5648.3	5702.3	110.8 ± 4.2	CVR	Aso	–	525 SW
SG14-5851	C	5400	60–90	C	E−59 (48.4–49.4)	5851.2	5908.0	117.8 ± 4.9	Izu-Bonin Arc	Hakone	–	300 E
SG14-5932	C	650	70	B	F-59 (67.3–68.3)	5932.4	5986.9	120.5 ± 5.1	SVR	Ata	–	650 SW
SG14-5950	C	250	50	PU	E−60 (46.3–47.3)	5950.1	6004.2	121.1 ± 5.2	–	–	–	–

[a] Depth given at the base of the visible tephra or at the identified midpoint of the 1 cm highresolution for the cryptotephra. Previously reported visible tephra deposits are showed in bold with references for correlations to volcanic source and eruptions units being 1. Smith et al. (2013), 2. Albert et al. (2019a). V/C = visible/ cryptotephra. PU= Pumiceous, B=Blocky, C=Cuspate, F=Fluted, V=Vesicular, MV =Microvesicular, MI =Microlite Inclusions. S = samples spiked with lycopodium spores (see methodology). * = depth given at the base of the visible tephra. **$^{40}Ar/^{39}Ar$ age of the Aso-4 eruption deposit (SG06-4963). M = magnitude (see Table 1 for references).

Kirishima complex.

All five of the Kirishima cryptotephras share a geochemical affinity with the more evolved Kr-Iw glass compositions, which is stratigraphically older. SG14-4002 also shows partial overlap with the younger Kr-Aw glasses (Fig. 7B). At the trace element level, the oldest Kirishima cryptotephras (SG14-4496 and SG14-4263) show compositional overlap with the older Kr-Iw tephra, indicating that at least one of these is likely to equate to the Kr-Iw eruption. As both are separated by the widespread DSP tephra in Lake Suigetsu (SG06-4318), this offers a potential means for determining which is the distal equivalent of the Kr-Iw in future research. Whilst the SG14-4053 and SG14-4002 deposits do not chemically overlap with the younger Kr-Aw glasses analysed, they do reside on a trend of elevated Nb content relative to Th consistent with the source area of the Kr-Aw, probably the Hinamoridake edifice (Fig. 7C). Trace element data could not be obtained for the SG14-4010 cryptotephra. The findings of numerous Kirishima ash-fall layers in the SG14 record should prompt further near-source stratigraphic and chemical investigations at Kirishima, to establish more reliably the precise proximal counterparts of the different distal deposits.

6.1.1.2. Aira. The SG14-4598 cryptotephra deposit is preserved between Aso-4 (SG14-4963) and the DSP (SG06-4318) and has a SG age of 73.9 ± 2.3 ka (±1σ). It is correlated to Aira owing to higher Th (~12 ppm) and lower Zr (~117 ppm) contents, which is a distinguishing feature of Aira derived glasses (Fig. 7F). Of the two proximal Aira units in the relevant timeframe (A-Iw and A-Fk), the A-Iw is above the Aso-4 unit (Fig. 2). Whilst the SG14-4598 cryptotephra is in the same stratigraphic position as the A-Iw (Fig. 4), the glasses can be distinguished at both the major and trace element level (Fig. 7D–F). We are therefore currently unable to correlate the SG14-4598 Lake Suigetsu cryptotephra with the Aira tephra.

6.1.1.3. Ata. Two cryptotephras are interpreted as deriving from the Ata caldera: SG14-5469 and SG14-5932 (Table 2). The SG14-5932 glasses have lower SiO_2 and higher CaO content than the overlying SG14-5469 and the proximal and distal Ata deposits (SG06-5353) and are arguably more consistent with glasses erupted from the Kikai caldera at major element level (Fig. 7A–C). Both the SG14-5932 and SG14-5469 glasses are indistinguishable from each other at the trace element level and have Nb contents (~10.5 ppm) which are consistent with glasses erupted from Ata (Albert et al., 2019a, Fig. 7E). We therefore interpret that both these cryptotephra deposits reflect pre-100 ka Ata activity. A potential candidate for one of these cryptotephras is the Ata Maimine eruption unit, however, its distribution is not extensively reported in the near-source setting and no geochemical data are currently available for comparison. Assuming the trace element link between these cryptotephras and Ata is robust, our data extends the compositional range of Ata erupted glasses.

6.1.1.4. Kikai. We have correlated the SG14-4307 cryptotephra dated to 62.3 ± 2.3 ka (±1σ) in SG to an eruption from Kikai. The SG14-4307 glasses show overlap with glasses from near-vent Kikai units in major

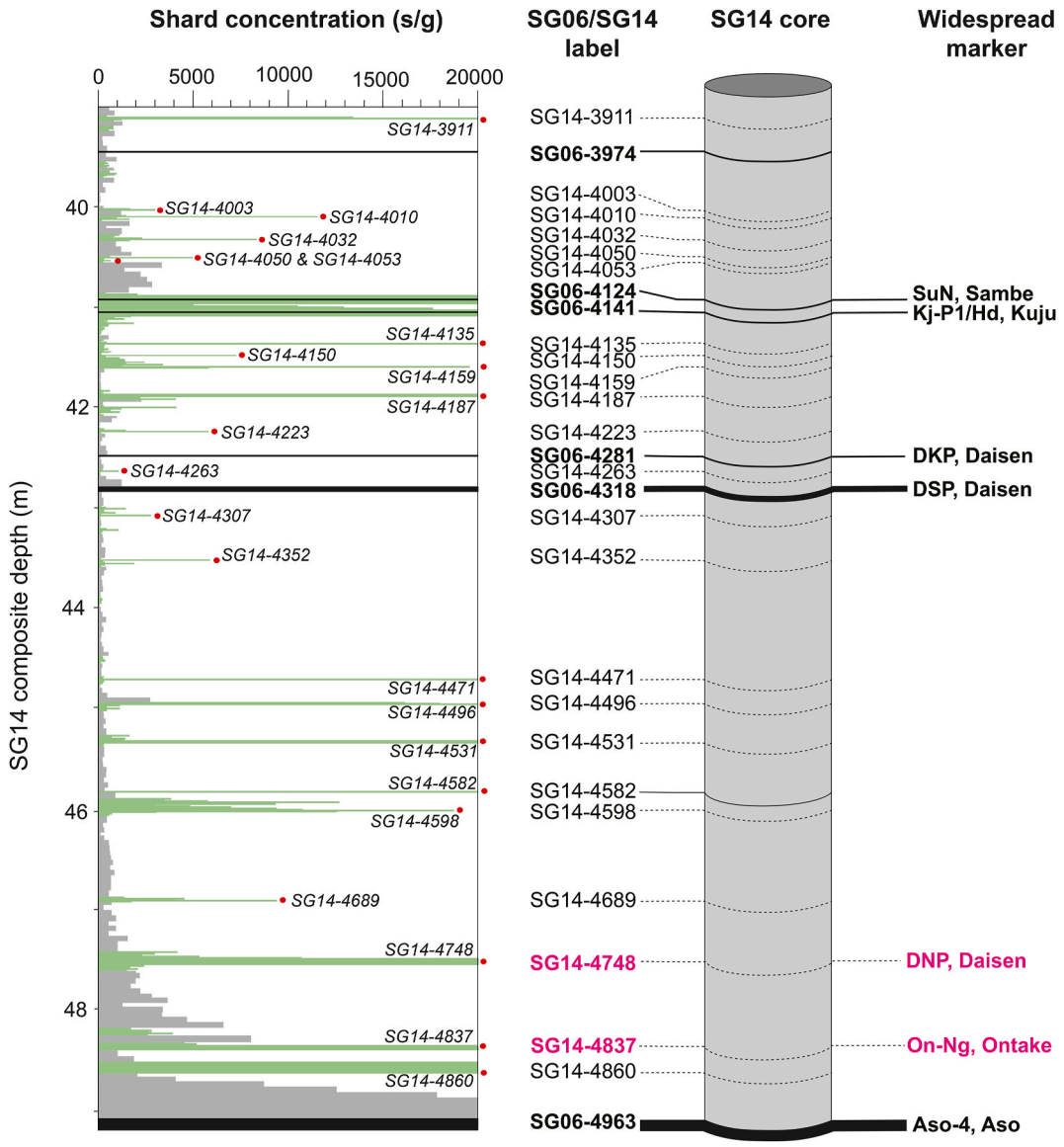

Fig. 4. Glass shard concentrations in the sediments spanning ~120–50 ka of the Lake Suigetsu (SG14) core. These concentrations are capped at 20,000 shards/gram. Concentrations of glass shards in low-resolution (5 cm interval) samples are shown in grey on the LHS panel, whilst high-resolution (1 cm) sample counts are overlain in green. The red dots and labels denote the positions of the isochrons, which were sampled for chemical analysis. The blue dots represent where chemical analysis were conducted but consistent with the K-Tz tephra (i.e. background glass). Previously reported SG06 visible tephras are marked in bold black and new correlations are shown in bold pink.

elements (Fig. 7A–C) and the lower Nb (~5 ppm) content is only consistent with Kikai tephra (Fig. 7E; Albert et al., 2019a). The SG14-4307 is 30 ka younger than the caldera forming K-Tz eruption and has lower SiO_2 (ca. 4 wt%) and Th (ca. 3.5 ppm) contents relative to the K-Tz (SG06-5181; Fig. 7D–F). The only other known Kikai tephra pre-50 ka is preserved beneath the K-Tz (Table 1; Machida and Arai, 2003). Given that SG14-4307 is younger (preserved between the Aso-4 [SG06-4963] and DSP [SG06-4318] tephras; Fig. 4), it provides evidence for an explosive eruption following the K-Tz eruption. The Tane I and Tane II tephras are thought to have erupted from Kikai. They are reported above the K-Tz and are ~65 ka based on their stratigraphic positions (Okuno and Kobayashi, 1994). However, as Kikai is a submerged caldera, there are limited on land exposures near the volcano, with only patchy deposits, such as Tane II, outcropping on small islands. These tephras have not been geochemically characterised so we are unable to establish if SG14-4307 cryptotephra correlates with one of the Tane tephras.

Directly following the 2.8 cm thick visible K-Tz tephra, several cryptotephra peaks (>6000 shards/gram) are identified in the 1.5 m of sediment above (Fig. 4). These have been interpreted as reworked K-Tz deposits due to their similarity in geochemistry and shard characteristics. It is likely that these represent remobilisation of the K-Tz shards in the catchment during periods of high rainfall. Similar peaks in shard concentrations are observed following the deposition of other thick Kikai tephras, for example, following the 3 cm thick K-Ah tephra (ca. 7.3 ka) there are peaks in compositionally and physically similar shards in the 1 m of sediment above the visible unit (McLean et al., 2018).

6.1.1.5. Aso. Eleven crypto/-tephras from Aso have been identified in the studied Lake Suigetsu sediments (Table 2). Six of the cryptotephra deposits are preserved in the 10 m of sediment above the Aso-4 tephra (SG06-4963; Table 2). The other five crypto-/tephras are preserved in the 7 m below: three between Aso-4 and Aso-ABCD (SG06-5287) and two beneath the latter (Table 2). The Aso glasses span the widest

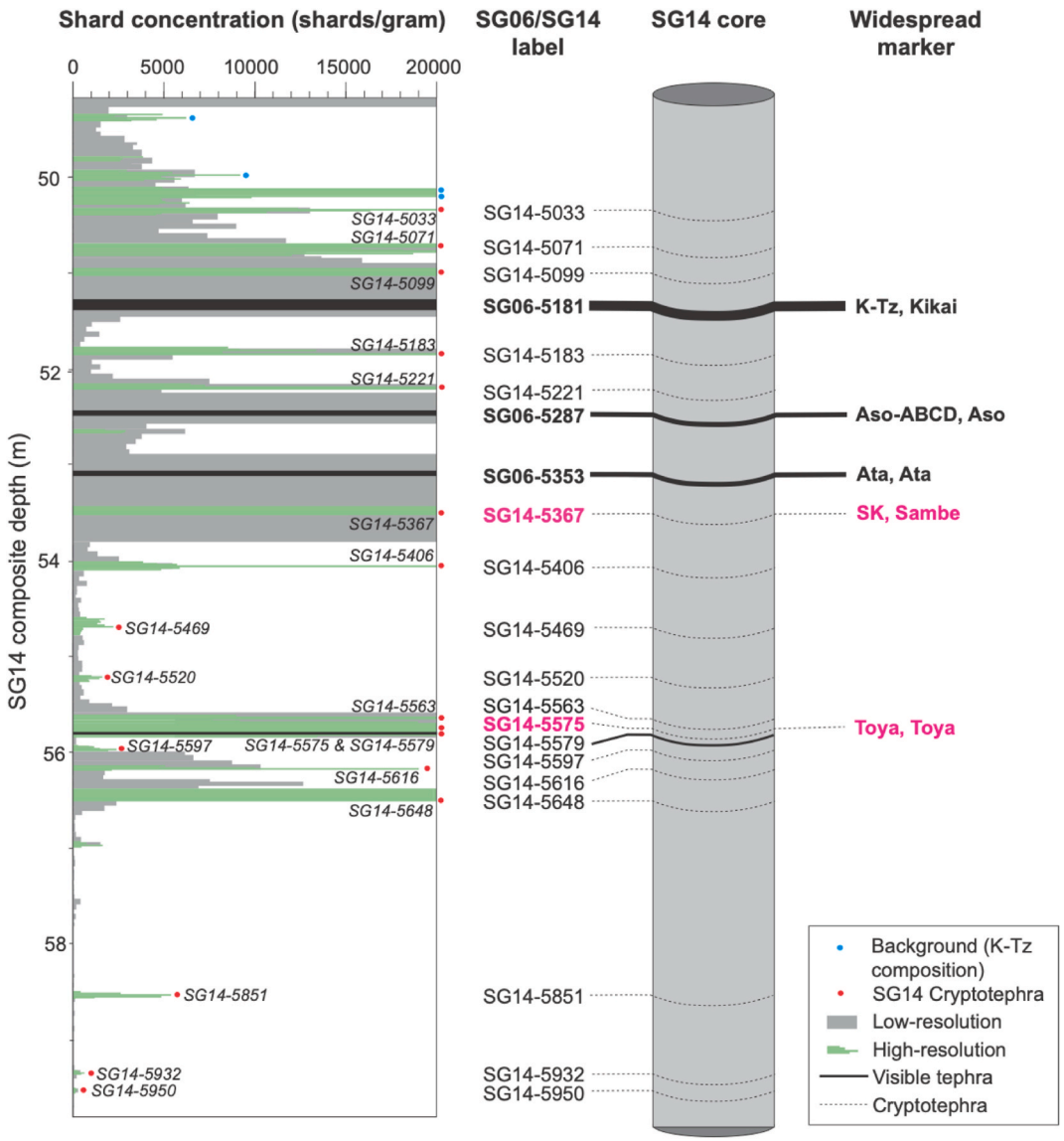

Fig. 4. (*continued*).

compositional range from any volcanic centre reported in this study and range from trachy-andesites through to rhyolites (Fig. 5; Table 3).

The five crypto-/tephras preserved in the 7 m of sediment beneath the Aso-4 layer are compositionally distinct from each other (Fig. 8). The SG14-5648 shows an affinity with Aso-I glasses in major element composition (Fig. 8D). However, many of the units have not been analysed (Aso-H, Aso-J and Aso-L; Hoshizumi et al., 2022) and it is likely that the SG14-5648 will correlate with one of the units preserved between Aso-3 and Aso-ABCD. Of the six post-Aso-4 cryptotephra deposits identified in this study, glasses from the younger SG14-4032 and SG14-3911 deposits form tight compositional clusters, whilst the others show a greater degree of variability, with the SG14-4135 and SG14-4471 spanning the broadest compositional ranges (Fig. 8C). Of the six deposits preserved in Lake Suigetsu between Aso-4 and the ACP-4, only one shows potential correlation based on stratigraphic position and geochemistry: the SG014-3911 with the ACP4 (Fig. 8C). The ACP4 has previously been reported as a 1 mm thick visible tephra in Lake Suigetsu (SG06-3912; Table 2). The two deposits are separated by ~30 cm of sediment. is possible that ACP4 exhibited multiple phases of volcanic activity where magmas of similar composition were erupted, resulting in multiple tephras separated in time. None of the other five newly identified Aso cryptotephra deposits show a geochemical affinity with the Aso units reported for this timeframe (ACP6 and ACP5; Fig. 8C).

6.1.1.6. Kuju. Three cryptotephra deposits have glass compositions that are consistent with Kuju volcano: SG14-4050, SG14-4150 and SG14-5406, which have ages of 52.2 ± 1.1 ka, 56.2 ± 1.8 ka and 102.1 ± 3.3 ka, respectively (Table 2). These deposits demonstrate tightly clustered compositions and overlap with each other on major and trace element compositions (Fig. 8a-d). Two Kuju units (Kj-Mg and Kj-Sm) are reported beneath the widespread Ata, as is the SG14-5406 cryptotephra, whilst the Kj-D is found proximally between the Aso-4 and Kj-Hd tephra and in the same stratigraphic position as the SG14-4150 (Fig. 2; Table 2). Proximally, the Kj-D shows no evidence of being older than Kj-P1/Hd, although we observe 44 cm of sediment (equating to 2.5 kyr) separating the SG14-4150 cryptotephra and the overlaying visible SG06-4124 (Kj-P1/Hd). No prominent Kuju deposits have been reported in near-source sequences in the same stratigraphic position as SG14-4050 (Fig. 2). Given the similar geochemical compositions, the cryptotephras cannot be correlated to eruption units, but this provides the first evidence of at least four eruptions at Kuju which have deposited ash-fall as far away as central Honshu, and are geochemically indistinguishable spanning a 50 kyr period.

Table 3
Average major (EMP) and trace (LA-ICP-MS) element chemistry of the ~120–50 ka Lake Suigetsu crypto-/tephras. Major element glass data has been normalised (water free). <LoD refers to less than limit of detection. Full geochemical datasets are available in the Supplementary Material.

Tephra	SG14-3911		SG14-4002		SG14-4010		SG14-4032		SG14-4050		SG14-4053		SG14-4135 A		SG14-4135 B		SG14-4150		SG14-4159		SG14-4187	
wt.%	Avg.	1 std. dev.	Avg.	1 std. dev.	Avg.	1 std. dev.	Avg.	1 std. dev.	Avg.	1 std. dev.	Avg.	1 std. dev.	Avg.	1 std. dev.	Avg.	1 std. dev.	Avg.	1 std. dev.	Avg.	1 std. dev.	Avg.	1 std. dev.
SiO2	72.24	0.07	66.12	4.22	74.24	0.99	74.43	0.50	79.36	0.94	72.38	1.88	62.24	0.52	67.61	1.95	77.86	0.20	71.58	0.97	66.20	2.75
TiO2	0.42	0.01	1.02	0.26	0.47	0.05	0.34	0.05	0.22	0.09	0.70	0.13	0.99	0.05	0.87	0.12	0.19	0.03	0.60	0.03	0.54	0.24
Al2O3	14.86	0.05	15.43	1.66	13.44	0.49	14.68	0.24	12.28	0.51	13.36	0.65	16.59	0.48	15.24	0.69	12.44	0.08	15.63	0.13	18.47	2.42
FeO	1.63	0.02	4.35	1.17	1.98	0.32	1.36	0.17	0.93	0.20	2.88	0.57	5.66	0.29	3.82	0.81	0.94	0.09	2.39	0.08	2.01	0.83
MnO	0.08	0.01	0.09	0.03	0.05	0.03	0.06	0.02	0.04	0.02	0.07	0.02	0.14	0.03	0.11	0.03	0.04	0.02	0.09	0.02	0.06	0.03
MgO	0.34	0.01	1.26	0.46	0.35	0.11	0.24	0.05	0.16	0.07	0.60	0.27	2.15	0.19	0.88	0.13	0.20	0.03	0.57	0.03	0.65	0.39
CaO	1.10	0.02	4.21	1.68	1.45	0.37	0.74	0.12	0.90	0.29	1.98	0.53	4.99	0.29	2.73	0.83	1.20	0.11	1.79	0.04	5.17	1.40
Na2O	4.52	0.05	3.89	0.19	3.39	0.25	4.42	0.11	3.10	0.23	3.45	0.33	3.86	0.23	4.26	0.16	3.17	0.08	2.93	1.09	4.15	0.51
K2O	4.66	0.04	3.24	0.79	4.46	0.24	4.96	0.13	4.30	0.41	4.35	0.27	3.05	0.20	4.20	0.27	3.77	0.09	4.22	0.07	2.47	0.55
P2O5	0.06	0.02	0.29	0.12	0.06	0.04	0.04	0.03	0.03	0.03	0.13	0.10	0.24	0.02	0.20	0.07	0.02	0.03	0.09	0.04	0.19	0.18
Cl	0.10	0.01	0.11	0.02	0.11	0.02	0.12	0.02	0.11	0.04	0.11	0.03	0.09	0.02	0.09	0.02	0.16	0.02	0.11	0.01	0.08	0.04
(n)	*27*		*9*		*16*		*19*		*28*		*11*		*13*		*6*		*11*		*26*		*9*	
ppm	**Avg.**	**1 std. dev.**	**Avg.**	**1 std. dev.**	**Avg.**	**1 std. dev.**	**Avg.**	**1 std. dev.**	**Avg.**	**1 std. dev.**	**Avg.**	**1 std. dev.**	**Avg.**	**1 std. dev.**	**Avg.**	**1 std. dev.**	**Avg.**	**1 std. dev.**	**Avg.**	**1 std. dev.**	**Avg.**	**1 std. dev.**
Rb	159	3.63	119	36.6	–	–	184	9.89	130	5.45	149	10.9	105	5.89	156	5.22	134	7.06	170	4.21	62.2	5.18
Sr	125	8.03	283	158	–	–	85.8	40.3	156	32.75	235	51.3	362	28.0	194	16.2	174	18.2	219	28.2	861	110
Y	34.5	0.94	24.7	2.70	–	–	36.2	0.90	6.75	1.40	29.4	1.92	27.5	0.97	32.0	0.12	6.82	0.96	32.4	2.43	18.7	1.13
Zr	295	8.14	245	44.7	–	–	305	9.28	94.0	10.0	321	9.35	202	11.0	298	7.16	93.5	8.79	303	20.5	157	6.85
Nb	16.6	0.31	10.7	1.40	–	–	16.9	0.44	11.5	0.39	14.1	0.58	12.61	0.56	17.0	0.39	11.8	0.40	16.1	0.79	21.0	1.57
Ba	820	20.14	651	93.0	–	–	769	38.9	927	78.87	877	18.2	558	27.9	726	12.0	970	33.9	799	29.5	767	42.1
La	32	0.93	27.4	3.78	–	–	34	0.99	23.2	1.27	34.1	0.96	23.9	1.04	29.5	0.64	23.8	1.11	32.4	2.05	29.0	1.75
Ce	70	1.84	58.5	7.90	–	–	74.9	2.27	41.8	3.13	71.7	2.60	54.1	1.94	65.5	0.31	43.8	2.45	69.6	3.42	61.4	3.61
Pr	8.05	0.27	6.62	0.89	–	–	8.62	0.28	3.70	0.41	8.15	0.34	6.46	0.24	7.91	0.03	3.93	0.07	7.90	0.34	6.73	0.43
Nd	33.4	1.16	26.8	3.11	–	–	35.1	2.22	12.2	1.66	32.5	2.22	27.8	1.65	33.4	0.24	12.2	0.57	32.4	1.31	27.5	1.25
Sm	7.43	0.33	5.95	0.58	–	–	7.45	0.66	2.30	0.54	6.92	0.67	6.24	0.63	6.96	0.61	<LOD	<LOD	6.58	0.40	5.15	0.34
Eu	1.27	0.08	1.18	0.34	–	–	1.14	0.13	0.54	0.10	1.22	0.18	1.40	0.09	1.30	0.04	<LOD	<LOD	1.28	0.19	1.51	0.19
Gd	6.12	0.41	4.69	0.54	–	–	6.25	0.57	<LOD	<LOD	5.60	0.65	5.45	0.52	6.16	0.96	<LOD	<LOD	6.03	0.46	4.24	0.46
Dy	5.92	0.29	4.52	0.46	–	–	6.37	0.40	<LOD	<LOD	5.34	0.49	5.11	0.29	5.99	0.50	<LOD	<LOD	5.50	0.72	3.39	0.29
Er	3.68	0.28	2.62	0.34	–	–	4.00	0.23	<LOD	<LOD	3.26	0.27	2.96	0.25	3.42	0.33	<LOD	<LOD	3.39	0.23	2.07	0.26
Yb	3.99	0.25	2.68	0.30	–	–	4.27	0.30	<LOD	<LOD	3.24	0.25	2.92	0.28	4.03	0.05	<LOD	<LOD	3.53	0.49	2.06	0.21
Lu	0.61	0.04	0.39	0.03	–	–	0.63	0.05	<LOD	<LOD	0.49	0.04	0.46	0.04	0.55	0.01	<LOD	<LOD	0.59	0.05	0.31	0.03
Hf	7.88	0.50	6.47	1.24	–	–	8.66	0.52	3.0	0.24	8.66	0.33	5.42	0.51	7.70	0.61	3.12	0.26	7.92	0.76	3.89	0.27
Ta	1.15	0.04	0.63	0.13	–	–	1.20	0.05	1.05	0.05	0.87	0.03	0.84	0.04	1.13	0.07	1.07	0.08	1.11	0.07	1.16	0.07
Pb	22.8	0.60	15.4	2.62	–	–	25.6	1.24	19.2	1.98	19.3	2.73	16.9	0.78	23.3	0.95	17.7	1.24	23.2	1.10	16.2	4.71
Th	14.0	0.62	9.85	2.57	–	–	16.3	0.72	12.8	0.82	13.6	0.68	9.49	0.49	14.0	0.46	12.4	0.73	15.6	0.87	5.78	0.35
U	4.18	0.21	2.16	0.49	–	–	4.80	0.22	2.85	0.14	2.77	0.14	2.75	0.24	4.28	0.13	2.90	0.35	4.34	0.51	1.55	0.11
Tephra	**SG14–4223**		**SG14–4263**		**SG14–4307**		**SG14–4352**		**SG14–4471A**		**SG14–4471B**		**SG14–4496**		**SG14–4531**		**SG14–4582**		**SG14–4598**		**SG14–4689**	
wt.%	**Avg.**	**1 std. dev.**	**Avg.**	**1 std. dev.**	**Avg.**	**1 std. dev.**	**Avg.**	**1 std. dev.**	**Avg.**	**1 std. dev.**	**Avg.**	**1 std. dev.**	**Avg.**	**1 std. dev.**	**Avg.**	**1 std. dev.**	**Avg.**	**1 std. dev.**	**Avg.**	**1 std. dev.**	**Avg.**	**1 std. dev.**
SiO2	59.08	0.39	72.43	0.80	74.27	0.38	65.78	1.12	65.71	1.08	72.86	0.43	72.61	0.78	60.72	0.24	79.44	0.26	78.17	0.32	77.88	2.16
TiO2	0.69	0.08	0.67	0.04	0.57	0.03	0.81	0.07	1.14	0.27	0.42	0.04	0.59	0.05	1.33	0.05	0.19	0.05	0.16	0.03	0.26	0.05
Al2O3	19.72	0.17	13.58	0.23	12.76	0.26	16.62	0.61	15.42	0.37	15.20	0.11	13.84	0.28	16.64	0.10	12.40	0.14	12.37	0.17	13.20	1.50
FeO	3.92	0.14	2.75	0.29	2.72	0.12	4.58	0.50	5.49	0.75	1.48	0.05	2.57	0.29	6.64	0.19	1.04	0.07	1.04	0.09	0.91	0.25
MnO	0.16	0.02	0.05	0.02	0.07	0.02	0.16	0.03	0.13	0.03	0.09	0.01	0.06	0.03	0.17	0.02	0.04	0.02	0.04	0.02	0.03	0.02
MgO	0.73	0.08	0.60	0.10	0.58	0.04	1.29	0.26	1.46	0.32	0.33	0.02	0.57	0.09	2.24	0.07	0.18	0.03	0.16	0.03	0.16	0.10
CaO	2.20	0.22	2.24	0.27	2.38	0.13	3.48	0.50	3.96	0.58	1.07	0.05	2.14	0.27	5.18	0.15	1.18	0.17	1.32	0.15	1.44	0.68
Na2O	6.64	0.16	3.26	0.45	3.90	0.26	4.53	0.20	2.84	0.94	3.99	0.65	3.41	0.49	4.13	0.15	3.30	0.27	3.36	0.12	3.22	0.44
K2O	6.39	0.12	4.20	0.15	2.50	0.06	3.65	0.35	3.43	0.12	4.36	0.12	3.95	0.17	2.35	0.09	2.11	0.12	3.28	0.15	2.83	0.49
P2O5	0.27	0.14	0.10	0.03	0.11	0.04	0.35	0.10	0.33	0.11	0.08	0.02	0.14	0.06	0.51	0.06	0.11	0.03	0.02	0.02	0.06	0.03

(*continued on next page*)

Table 3 (*continued*)

Tephra	SG14-3911		SG14-4002		SG14-4010		SG14-4032		SG14-4050		SG14-4053		SG14-4135 A		SG14-4135 B		SG14-4150		SG14-4159		SG14-4187	
wt.%	Avg.	1 std. dev.	Avg.	1 std. dev.	Avg.	1 std. dev.	Avg.	1 std. dev.	Avg.	1 std. dev.	Avg.	1 std. dev.	Avg.	1 std. dev.	Avg.	1 std. dev.	Avg.	1 std. dev.	Avg.	1 std. dev.	Avg.	1 std. dev.
Cl	0.21	0.02	0.12	0.02	0.12	0.03	0.08	0.02	0.11	0.02	0.12	0.01	0.12	0.01	0.09	0.01	0.01	0.01	0.09	0.01	0.01	0.02
(n)	*36*		*22*		*22*		*28*		*6*		*4*		*30*		*29*		*13*		*24*		*29*	
ppm	**Avg.**	**1 std. dev.**	**Avg.**	**1 std. dev.**	**Avg.**	**1 std. dev.**	**Avg.**	**1 std. dev.**	**Avg.**	**1 std. dev.**	**Avg.**	**1 std. dev.**	**Avg.**	**1 std. dev.**	**Avg.**	**1 std. dev.**	**Avg.**	**1 std. dev.**	**Avg.**	**1 std. dev.**	**Avg.**	**1 std. dev.**
Rb	169	9.71	155	7.54	72.7	2.08	139	16.8	94.3	19.1	157	22.5	147	9.86	69.9	1.36	166	0.32	138	4.97	125	33.0
Sr	345	96.9	155	25.4	128	9.28	378	117	426	67.3	195	67.8	154	24.3	498	12.5	164	2.12	86.7	9.46	257	151.9
Y	26.4	7.27	30.1	1.47	31.1	1.15	31.7	2.41	34.6	5.37	26.4	1.25	30.7	1.73	32.1	0.87	33.0	0.08	13.4	0.67	9.02	1.82
Zr	543	39.8	252	11.5	175	5.36	234	29.7	270	48.2	238	12.5	251	14.5	216	4.54	293	2.44	117	6.68	110	14.0
Nb	167	8.82	9.66	0.32	5.47	0.33	12.6	1.48	13.8	1.50	13.9	0.24	9.74	1.68	11.0	0.26	15.5	0.40	6.68	0.22	10.6	1.32
Ba	543	72.6	598	21.9	403	10.8	694	36.8	817	98.7	814	29.6	597	68.0	531	13.0	827	20.9	559	22.1	784	255
La	106	18.7	24.5	1.34	16.0	0.72	29.4	2.06	32.8	3.66	30.5	0.13	25.0	2.65	26.8	0.73	34.4	0.22	22.0	0.68	24.0	2.49
Ce	183	38.5	54.5	3.54	37.3	1.70	65.9	4.87	73.5	8.21	67.9	5.10	55.4	5.72	61.6	1.35	74.2	0.81	42.1	1.79	43.7	5.43
Pr	16.8	4.59	6.21	0.36	4.42	0.28	7.76	0.58	8.98	1.44	7.31	0.60	6.24	0.71	7.44	0.18	8.80	0.02	3.97	0.21	4.29	0.69
Nd	56.7	17.4	25.7	1.80	19.4	1.21	32.5	2.34	38.3	7.52	29.8	1.11	25.9	2.28	33.7	1.15	35.1	0.10	13.7	0.82	14.7	2.53
Sm	8.26	2.90	5.61	0.63	4.65	0.48	7.10	0.70	6.41	2.64	5.11	1.65	5.77	0.41	7.44	0.42	6.94	0.07	2.58	0.31	2.66	0.65
Eu	1.87	0.55	0.94	0.10	0.95	0.09	1.53	0.23	2.37	0.50	2.06	0.26	0.95	0.17	2.03	0.12	1.29	0.07	0.49	0.06	0.61	0.11
Gd	6.31	2.27	4.78	0.39	4.64	0.49	6.23	0.61	7.63	1.14	6.56	0.61	5.04	0.42	6.62	0.40	6.03	0.19	2.08	0.19	1.88	0.44
Dy	5.18	1.86	5.17	0.62	5.21	0.31	5.75	0.48	6.96	1.30	5.57	0.48	5.19	0.35	6.14	0.30	5.77	0.05	2.19	0.20	1.64	0.31
Er	2.86	0.83	3.48	0.34	3.44	0.36	3.35	0.36	4.28	0.45	3.24	0.07	3.30	0.29	3.51	0.19	3.56	0.07	1.50	0.16	1.00	0.20
Yb	2.74	0.59	3.38	0.34	3.72	0.30	3.46	0.32	4.01	0.81	3.93	0.42	3.49	0.30	3.28	0.23	3.92	0.26	1.79	0.14	1.38	0.23
Lu	0.40	0.08	0.50	0.07	0.56	0.04	0.52	0.06	0.59	0.06	0.61	0.01	0.52	0.04	0.50	0.03	0.60	0.01	0.29	0.03	0.20	0.04
Hf	11.0	1.19	7.01	0.60	4.70	0.33	6.23	0.92	7.77	1.23	7.30	0.24	7.18	0.48	5.64	0.26	7.89	0.51	3.48	0.28	3.38	0.61
Ta	8.54	0.49	0.71	0.04	0.38	0.03	0.91	0.11	0.78	0.09	1.06	0.07	0.74	0.13	0.61	0.01	1.16	0.03	0.64	0.02	0.91	0.11
Pb	13.4	1.14	21.9	1.77	19.3	2.07	20.9	1.94	20.1	4.85	20.5	3.53	22.7	1.07	11.4	0.54	27.2	4.44	19.5	0.85	19.1	3.40
Th	19.9	1.52	13.3	1.13	6.39	0.36	13.1	1.69	7.88	1.50	13.4	0.94	13.0	1.18	5.95	0.19	16.3	0.11	12.1	0.38	10.8	1.31
U	4.18	0.34	3.42	0.16	1.84	0.21	3.87	0.58	1.83	0.36	4.43	0.43	3.31	0.50	1.32	0.06	4.57	0.10	2.75	0.15	2.36	0.34
(n)	*13*		*9*		*13*		*18*		*5*		*2*		*13*		*14*		*4*		*12*		*12*	
Tephra	**SG14–4748**		**SG14–4837**		**SG14–4860**		**SG14–5033**		**SG14–5071**		**SG14–5099**		**SG14–5183**		**SG14–5221**		**SG14–5367**		**SG14–5406**		**SG14–5469**	
wt.%	**Avg.**	**1 std. dev.**	**Avg.**	**1 std. dev.**	**Avg.**	**1 std. dev.**	**Avg.**	**1 std. dev.**	**Avg.**	**1 std. dev.**	**Avg.**	**1 std. dev.**	**Avg.**	**1 std. dev.**	**Avg.**	**1 std. dev.**	**Avg.**	**1 std. dev.**	**Avg.**	**1 std. dev.**	**Avg.**	**1 std. dev.**
SiO2	71.03	0.40	75.16	0.28	76.82	1.20	72.66	0.16	72.71	0.26	68.89	0.81	77.25	0.62	70.33	0.18	76.66	0.16	77.95	0.93	75.07	0.66
TiO2	0.35	0.03	0.26	0.02	0.23	0.02	0.69	0.03	0.35	0.03	0.62	0.10	0.07	0.04	0.62	0.03	0.05	0.03	0.10	0.03	0.61	0.04
Al2O3	15.32	0.31	13.68	0.24	12.93	0.87	13.33	0.17	14.90	0.16	16.61	0.99	13.49	0.49	15.32	0.12	13.95	0.12	12.68	0.67	13.43	0.25
FeO	2.26	0.09	1.39	0.12	1.07	0.22	3.57	0.07	1.33	0.09	2.12	0.52	0.64	0.19	2.24	0.05	0.50	0.05	0.63	0.11	2.44	0.09
MnO	0.06	0.02	0.05	0.02	0.06	0.03	0.13	0.02	0.10	0.02	0.10	0.04	0.07	0.02	0.10	0.02	0.10	0.02	0.08	0.02	0.10	0.02
MgO	0.69	0.07	0.24	0.08	0.20	0.14	0.77	0.06	0.26	0.03	0.54	0.27	0.11	0.04	0.60	0.02	0.12	0.02	0.08	0.05	0.53	0.02
CaO	2.67	0.20	1.62	0.13	1.21	0.41	3.02	0.08	0.96	0.06	2.36	0.49	0.62	0.22	1.78	0.04	0.68	0.06	1.04	0.25	2.04	0.06
Na2O	4.71	0.13	3.67	0.11	3.42	0.37	4.49	0.14	4.54	0.11	4.72	0.21	3.93	0.44	4.44	0.12	3.91	0.22	3.22	0.36	2.88	0.89
K2O	2.41	0.06	3.79	0.21	3.94	0.39	1.07	0.04	4.70	0.09	3.82	0.39	3.67	0.45	4.37	0.08	3.90	0.10	4.08	0.30	2.72	0.05
P2O5	0.11	0.03	0.03	0.02	0.05	0.02	0.14	0.03	0.05	0.03	0.13	0.06	0.06	0.02	0.12	0.04	0.07	0.04	0.05	0.02	0.07	0.02
Cl	0.38	0.03	0.11	0.02	0.09	0.02	0.13	0.03	0.10	0.02	0.08	0.02	0.10	0.05	0.10	0.02	0.07	0.01	0.10	0.02	0.12	0.02
(n)	*11*		*17*		*28*		*14*		*19*		*9*		*7*		*18*		*16*		*10*		*16*	
ppm	**Avg.**	**1 std. dev.**	**Avg.**	**1 std. dev.**	**Avg.**	**1 std. dev.**	**Avg.**	**1 std. dev.**	**Avg.**	**1 std. dev.**	**Avg.**	**1 std. dev.**	**Avg.**	**1 std. dev.**	**Avg.**	**1 std. dev.**	**Avg.**	**1 std. dev.**	**Avg.**	**1 std. dev.**	**Avg.**	**1 std. dev.**
Rb	76.5	1.04	132	6.72	143	5.44	15.9	1.88	13.8	3.99	10.8	1.28	–	–	37.7	1.86	118	5.46	144	14.0	99.3	1.22
Sr	502	17.3	266	21.38	178	36.5	216	35.83	168	15.7	106	29.4	–	–	157	1.74	85.9	32.6	254	90.6	129	5.03
Y	6.63	0.13	16.1	0.42	13.2	0.49	33.9	3.01	151	27.9	59.7	6.21	–	–	239	8.81	8.89	0.35	10.6	0.97	41.8	1.79
Zr	131	3.57	215	4.98	186	4.76	107	9.20	32.5	2.51	26.5	0.44	–	–	32.2	0.88	31.8	1.65	77.0	6.62	224	12.1
Nb	8.30	0.10	10.9	0.22	11.1	0.51	1.84	0.16	281	30.9	146	2.96	–	–	267	6.67	18.6	0.75	11.1	1.40	10.3	0.31
Ba	543	16.1	923	24.62	906	43.7	434	37.00	15.3	1.91	5.89	2.28	–	–	15.2	0.27	958	64.4	809	25.7	451	18.8

(*continued on next page*)

Table 3 (*continued*)

Tephra	SG14-3911		SG14-4002		SG14-4010		SG14-4032		SG14-4050		SG14-4053		SG14-4135 A		SG14-4135 B		SG14-4150		SG14-4159		SG14-4187	
wt.%	Avg.	1 std. dev.	Avg.	1 std. dev.	Avg.	1 std. dev.	Avg.	1 std. dev.	Avg.	1 std. dev.	Avg.	1 std. dev.	Avg.	1 std. dev.	Avg.	1 std. dev.	Avg.	1 std. dev.	Avg.	1 std. dev.	Avg.	1 std. dev.
La	21.2	0.92	31.7	0.80	31.8	1.06	6.45	0.64	761	55.6	452	4.26	–	–	790	17.6	5.96	0.54	27.2	1.09	25.0	0.96
Ce	40.0	1.34	61.4	1.71	61.8	1.71	17.6	1.63	33.3	3.62	16.2	0.26	–	–	32.1	0.97	13.1	1.18	52.2	3.59	56.9	2.23
Pr	3.90	0.21	6.27	0.26	6.17	0.25	2.62	0.24	74.4	7.64	36.5	0.53	–	–	70.7	1.85	1.35	0.18	5.28	0.59	6.60	0.49
Nd	13.4	0.79	23.3	0.90	21.0	0.91	13.9	1.30	8.43	0.95	4.08	0.14	–	–	8.06	0.33	4.72	0.52	17.5	1.00	29.1	1.60
Sm	2.09	0.24	4.00	0.28	3.47	0.30	4.29	0.48	34.5	4.42	16.4	0.98	–	–	34.0	1.23	1.39	0.23	2.94	0.25	6.77	0.50
Eu	0.72	0.01	0.87	0.08	0.68	0.10	1.27	0.08	7.05	0.80	3.80	0.18	–	–	7.24	0.42	0.30	0.03	0.61	0.12	1.33	0.10
Gd	1.43	0.18	3.01	0.34	2.57	0.33	5.02	0.58	1.31	0.17	0.58	0.06	–	–	1.43	0.10	1.31	0.15	2.05	0.18	6.50	0.37
Dy	1.33	0.20	2.83	0.28	2.25	0.24	6.05	0.65	5.76	0.79	3.72	0.35	–	–	5.85	0.24	1.49	0.11	1.85	0.21	7.36	0.18
Er	0.67	0.10	1.71	0.14	1.45	0.17	3.78	0.43	5.84	0.58	4.43	0.41	–	–	5.57	0.51	0.93	0.07	1.09	0.14	4.64	0.36
Yb	0.82	0.06	1.96	0.16	1.63	0.23	3.93	0.43	3.52	0.25	3.00	0.19	–	–	3.41	0.20	1.08	0.13	1.36	0.21	4.86	0.35
Lu	0.13	0.01	0.29	0.02	0.28	0.03	0.59	0.06	4.00	0.35	3.40	0.27	–	–	3.65	0.33	0.14	0.02	0.20	0.03	0.70	0.03
Hf	3.40	0.10	5.56	0.28	4.94	0.51	3.26	0.35	0.57	0.07	0.51	0.02	–	–	0.55	0.04	1.59	0.22	2.53	0.28	6.34	0.15
Ta	0.53	0.01	0.73	0.03	0.79	0.04	0.13	0.01	7.34	0.75	4.40	0.35	–	–	7.18	0.40	1.48	0.07	0.83	0.06	0.71	0.05
Pb	12.0	0.16	18.4	1.03	19.8	0.92	8.08	0.70	1.11	0.15	0.46	0.15	–	–	1.07	0.05	16.2	1.74	20.9	0.59	22.0	0.90
Th	7.20	0.04	12.3	0.50	14.0	0.49	0.92	0.11	24.4	1.23	18.8	1.19	–	–	21.8	0.87	5.05	0.37	13.4	0.75	9.07	1.18
U	2.09	0.07	2.34	0.08	2.65	0.13	0.47	0.06	15.4	1.77	8.03	0.33	–	–	14.2	0.90	3.87	0.19	3.24	0.32	2.38	0.20
(n)	*3*		*22*		*9*		*20*		*18*		*6*		-		*14*		*13*		*8*		*6*	
Tephra	**SG14–5520**		**SG14–5563A**		**SG14–5563B**		**SG14–5575**		**SG14–5579**		**SG14–5597**		**SG14–5616**		**SG14–5648**		**SG14–5851**		**SG14–5932**		**SG14–5950**	
wt.%	**Avg.**	**1 std. dev.**	**Avg.**	**1 std. dev.**	**Avg.**	**1 std. dev.**	**Avg.**	**1 std. dev.**	**Avg.**	**1 std. dev.**	**Avg.**	**1 std. dev.**	**Avg.**	**1 std. dev.**	**Avg.**	**1 std. dev.**	**Avg.**	**1 std. dev.**	**Avg.**	**1 std. dev.**	**Avg.**	**1 std. dev.**
SiO2	74.03	0.19	76.60	0.07	77.96	0.19	78.02	0.28	71.45	0.37	73.09	1.28	76.64	0.27	69.25	0.31	69.31	0.19	71.60	0.34	72.25	0.21
TiO2	0.59	0.04	0.19	0.01	0.23	0.01	0.06	0.02	0.44	0.04	0.47	0.10	0.36	0.03	0.69	0.04	0.71	0.03	0.77	0.04	0.21	0.03
Al2O3	13.20	0.12	13.39	0.17	12.39	0.07	12.76	0.18	15.29	0.18	13.95	0.48	12.71	0.16	15.43	0.13	14.65	0.10	13.68	0.13	14.23	0.11
FeO	2.37	0.08	0.88	0.14	1.07	0.06	0.89	0.04	1.62	0.08	2.95	0.29	1.81	0.09	2.54	0.11	4.05	0.14	3.50	0.14	3.01	0.08
MnO	0.08	0.01	0.03	0.00	0.04	0.03	0.09	0.02	0.09	0.02	0.13	0.03	0.05	0.02	0.10	0.02	0.14	0.02	0.08	0.02	0.08	0.02
MgO	0.54	0.02	0.17	0.08	0.21	0.07	0.03	0.02	0.39	0.05	0.58	0.15	0.40	0.04	0.68	0.05	1.07	0.04	0.83	0.04	0.03	0.02
CaO	2.07	0.05	1.50	0.06	0.96	0.08	0.36	0.03	1.24	0.08	2.71	0.38	2.18	0.09	1.88	0.11	3.88	0.12	2.96	0.17	0.54	0.02
Na2O	4.05	0.04	3.94	0.10	3.59	0.17	4.82	0.20	4.29	0.19	4.84	0.08	3.47	0.15	4.42	0.11	4.95	0.17	3.79	0.13	5.78	0.07
K2O	2.86	0.06	3.07	0.06	3.28	0.04	2.82	0.10	5.04	0.09	1.02	0.09	2.17	0.07	4.72	0.11	0.94	0.02	2.64	0.11	4.98	0.10
P2O5	0.09	0.04	0.08	0.04	0.06	0.01	0.02	0.03	0.06	0.03	0.09	0.04	0.05	0.03	0.20	0.07	0.14	0.03	0.05	0.06	0.01	0.01
Cl	0.11	0.01	0.15	0.01	0.21	0.03	0.12	0.02	0.11	0.01	0.16	0.03	0.14	0.03	0.09	0.01	0.15	0.02	0.10	0.02	0.29	0.01
(n)	*10*		*3*		*4*		*53*		*22*		*13*		*11*		*40*		*11*		*28*		*11*	
ppm	**Avg.**	**1 std. dev.**	**Avg.**	**1 std. dev.**	**Avg.**	**1 std. dev.**	**Avg.**	**1 std. dev.**	**Avg.**	**1 std. dev.**	**Avg.**	**1 std. dev.**	**Avg.**	**1 std. dev.**	**Avg.**	**1 std. dev.**	**Avg.**	**1 std. dev.**	**Avg.**	**1 std. dev.**	**Avg.**	**1 std. dev.**
Rb	–	–	95.0	4.05	85.5	5.33	64.5	3.74	17.1	2.60	16.4	5.55	75.0	1.29	174	5.62	20.3	3.52	97.2	1.88	293	10.4
Sr	–	–	253	27.8	395	123	21.9	10.0	190	14.7	230	46.4	209	4.37	266	46.8	237	8.23	142	3.24	1.58	1.34
Y	–	–	4.86	0.35	5.35	1.03	58.9	4.10	182	12.2	29.0	3.73	21.9	0.84	33.0	1.14	31.3	0.97	42.2	0.99	88.6	2.66
Zr	–	–	124	8.42	125	7.71	79.2	4.72	32.5	1.16	97.0	18.1	175	7.08	292	10.3	100	2.48	235	3.13	861	31.2
Nb	–	–	10.2	0.54	9.26	0.66	5.23	0.27	324	20.2	1.95	0.37	7.37	0.41	16.9	0.67	1.65	0.15	11.1	0.27	225	8.62
Ba	–	–	641	20.8	617	55.7	974	48.7	17.4	1.35	374	53.5	666	27.0	824	51.3	392	19.8	444	9.56	6.96	6.85
La	–	–	23.5	1.26	23.2	0.54	14.9	0.82	818	38.7	6.29	0.94	21.5	1.42	35.2	1.27	6.06	0.15	24.9	0.38	166	4.85
Ce	–	–	43.2	1.85	42.2	0.73	37.7	2.38	36.1	1.24	16.8	2.01	45.5	2.40	77.5	2.59	16.4	1.02	59.2	1.21	315	9.11
Pr	–	–	3.94	0.27	4.03	0.45	4.93	0.33	78.3	3.06	2.48	0.41	4.91	0.41	8.93	0.28	2.46	0.20	6.88	0.23	30.8	1.27
Nd	–	–	13.2	1.11	13.5	1.83	22.4	1.57	8.85	0.47	11.8	1.30	20.3	0.75	35.9	1.24	13.7	1.90	29.7	0.88	114	6.82
Sm	–	–	2.15	0.19	<LOD	<LOD	6.83	0.59	35.4	1.43	3.92	0.67	4.25	0.44	7.57	0.71	<LOD	<LOD	7.08	0.78	21.7	1.07
Eu	–	–	<LOD	<LOD	<LOD	<LOD	0.58	0.16	7.29	0.50	1.22	0.11	0.96	0.10	1.50	0.15	<LOD	<LOD	1.40	0.11	0.30	0.13
Gd	–	–	<LOD	<LOD	<LOD	<LOD	7.78	0.78	1.29	0.09	4.13	0.79	3.99	0.25	6.70	0.47	<LOD	<LOD	6.66	0.72	17.2	1.76
Dy	–	–	<LOD	<LOD	<LOD	<LOD	9.75	1.05	5.88	0.52	5.01	0.28	3.96	0.30	6.31	0.20	<LOD	<LOD	7.50	0.41	17.6	0.97
Er	–	–	<LOD	<LOD	<LOD	<LOD	6.29	0.44	5.77	0.41	3.37	0.53	2.45	0.30	3.47	0.26	<LOD	<LOD	4.69	0.35	8.78	0.55
Yb	–	–	<LOD	<LOD	<LOD	<LOD	7.11	0.53	3.57	0.18	3.06	0.38	2.32	0.26	3.60	0.31	<LOD	<LOD	5.05	0.37	7.73	0.71
Lu	–	–	<LOD	<LOD	<LOD	<LOD	1.03	0.06	3.61	0.16	0.47	0.14	0.36	0.03	0.56	0.06	<LOD	<LOD	0.73	0.03	1.05	0.06

(*continued on next page*)

Table 3 (*continued*)

Tephra	SG14-3911		SG14-4002		SG14-4010		SG14-4032		SG14-4050		SG14-4053		SG14-4135 A		SG14-4135 B		SG14-4150		SG14-4159		SG14-4187	
wt.%	Avg.	1 std. dev.	Avg.	1 std. dev.	Avg.	1 std. dev.	Avg.	1 std. dev.	Avg.	1 std. dev.	Avg.	1 std. dev.	Avg.	1 std. dev.	Avg.	1 std. dev.	Avg.	1 std. dev.	Avg.	1 std. dev.	Avg.	1 std. dev.
Hf	–	–	3.37	0.44	2.85	0.16	3.58	0.34	0.56	0.04	2.97	0.47	4.54	0.41	7.87	0.28	3.48	0.38	6.60	0.50	26.3	1.32
Ta	–	–	0.74	0.03	0.67	0.12	0.37	0.03	8.63	0.51	0.12	0.02	0.47	0.02	1.22	0.05	0.12	0.01	0.71	0.03	12.8	0.85
Pb	–	–	13.4	0.95	13.3	0.64	28.2	1.61	1.28	0.10	6.95	1.07	13.4	0.53	24.4	3.43	7.30	0.49	20.3	0.84	26.0	2.28
Th	–	–	10.5	0.66	9.51	0.87	5.86	0.42	26.1	1.21	0.85	0.23	5.94	0.39	16.5	0.73	1.09	0.12	8.87	0.41	35.4	1.93
U	–	–	2.94	0.27	2.77	0.26	2.49	0.21	18.2	1.61	0.43	0.02	1.30	0.17	4.87	0.16	0.79	0.13	2.32	0.21	7.14	0.45
(*n*)	-		*7*		*2*		*10*		*17*		*4*		*5*		*8*		*6*		*12*		*7*	

6.1.2. Honshu (SWJA, Izu-Bonin Arc and NVZ)

6.1.2.1. Sambe. The SG14-5367 cryptotephra is preserved 47 cm beneath the visible Ata tephra (SG06-5353; Fig. 4) and has a very high shard concentration, with large distinct cuspate and fluted shards containing microvesicles (Table 2; Supplementary Material). These glasses have low Y, Zr, La and Th contents which are typical features of early Sambe activity (Table 3; Albert et al., 2018). The SG14-5367 glasses form a tight compositional cluster and show complete geochemical overlap with those from the SK tephra (Fig. 9). The SK is considered to be the largest eruption from the Sambe volcano erupting 20 km^3 of tephra and has a proposed age of ~100 ka based on: (1) its stratigraphic position beneath the Aso-4 tephra in marine sediments (102 ka; Sagawa et al., 2018) and (2) radiogenic measurements (100 ± 20 ka, Kimura et al., 1999; 110 ± 14 ka, Shitaoka et al., 2009). The Lake Suigetsu age model provides a date of 100.4 ± 3.1 ka (±1σ) for SG14-5367, which is consistent with the age of ~100 ka the SK eruption and has an easterly dispersal, that fits with it being preserved in Lake Suigetsu (Fig. 1; Table 1). Based on the chronostratigraphic position and geochemical compositions, the SG14-5367 is the distal equivalent of the SK eruption. The SK may be a useful marker in terrestrial and marine sequences across Honshu and further afield due to high shard concentrations (Table 2; Fig. 3).

6.1.2.2. Daisen. Two pumiceous cryptotephra deposits have been attributed to Daisen activity: the SG14-4748 which has an age of 79.3 ± 2.0 ka (±1σ); and the SG14-5563 with an age of 107.6 ± 3.9 ka (±1σ) (Table 2). The younger SG14-4748 is clearly from Daisen based on major elements, whilst the more rhyolitic (SiO_2 >76 wt%) SG14-5563 glasses overlap with the Daisen and Sambe compositional fields (Fig. 9A). However, both deposits have >11 Zr/Th ratios, consistent with those from Daisen (Fig. 9B; Albert et al., 2018). The SG14-4748 is in the same chrono-stratigraphic position as the prominent DNP eruption unit (between Aso-4 and DSP; Fig. 2); however, in the absence of near-source glass chemistry (see Albert et al., 2018) we can only tentatively correlate this unit to the Daisen eruption deposit. The SG14-5563 is more challenging to correlate. It is chrono-stratigraphically consistent with two older Daisen tephra units below the Aso-4 and SK marker layers, the DHP and DMP units (Fig. 2). Without fresh proximal deposits to establish their geochemical signature we are precluded from establishing more precise correlations between the Daisen eruption record and Lake Suigetsu.

6.1.2.3. Unknown SWJA tephra. The SG14-4689 cryptotephra forms a discrete peak of colourless pumiceous shards, stratigraphically located between the Aso-4 (SG06-4963) and DSP (SG06-4318) tephras in the Lake Suigetsu sediments (Fig. 4). The high SiO_2 contents (~77.88 wt%) and Zr/Th ratios of 9–11 mean that these data do not plot precisely within the characterised compositional fields for SWJA, but the cryptotephra likely erupted from one of these sources (Fig. 9).

6.1.2.4. Hakone. The tholeiitic cryptotephras, SG14-5033, SG14-5597 and SG14-5851, are all dacite-rhyolites and are easily distinguished from other cryptotephra analysed in this study owing to low K_2O content (~1 wt%) and low Th (<2 ppm) contents, and plot within the Izu-Bonin Arc compositional fields (Figs. 5 and 6). All three deposits show a geochemical affinity with glasses erupted from the Hakone volcano (Fig. 10) and are found beneath the Aso-4 marker layer (SG06-4963) and have ages of 89.8 ± 1.6 ka, 108.9 ± 4.0 ka and 117.7 ± 4.9 ka (±1σ), respectively (Table 2). Whilst it is possible to distinguish the SG14-5851 using major element data, all three Hakone derived cryptotephra deposits are indistinguishable at the trace element level (Fig. 10). Although the SG14-5033 is in the same stratigraphic position as the only previously reported Hakone tephra between the K-Tz and Aso-4 marker tephras (Hk-Da-5; Fig. 2), there are currently no compositional data to

Table 4
Average major element glass compositions of proximal tephra deposits analysed as part of this study to compare to the ~120–50 ka Lake Suigetsu crypto-/tephras. Major element glass data has been normalised. The SK (FLF04-1) tephra sample was collected from the base of Exp.346 U1427A Core 5H Section 7W (62 - 63 cm) and was first teported by Sagawa et al (2018). Full geochemical datasets are available in the Supplementary Material.

Source	Sambe		Sambe		Kirishima		Kirishima		Kirishima		Kirishima	
Tephra	**SK**		**SK**		**Kr-Iw**		**Kr-Iw**		**Kr-Iw**		**Kr-Aw**	
Material	**Pumice**		**Pumice**		**Pumice**		**Pumice**		**Pumice**		**Scoria**	
Deposit type	**Fall**		**Fall**		**Fall**		**Fall**		**Fall**		**Fall**	
Sample	**FLF04–1 (5H-7W-62 cm)**		**FLF133**		**FLF176**		**FLF177**		**FLF178**		**FLF181**	
Location	**IODP-U1427A**		**Kakeyacho Kakeya**		**Umegakubo Quarry**		**Umegakubo Quarry**		**Umegakubo Quarry**		**Umegakubo Quarry**	
wt.%	**Ave.**	**1 σ**	**Ave.**	**1 σ**	**Ave.**	**1 σ**	**Ave.**	**1 σ**	**Ave.**	**1 σ**	**Ave.**	**1 σ**
SiO2	76.60	0.14	76.60	0.14	71.89	3.99	69.50	4.13	72.92	1.94	63.09	0.41
TiO2	0.05	0.02	0.05	0.02	0.52	0.17	0.61	0.09	0.51	0.13	0.86	0.08
Al2O3	13.86	0.10	13.86	0.10	13.96	1.00	14.39	0.81	13.75	0.63	16.12	0.80
FeOt	0.53	0.04	0.53	0.04	2.94	1.46	3.79	1.68	2.44	0.63	6.60	0.61
MnO	0.09	0.02	0.09	0.02	0.07	0.04	0.07	0.03	0.06	0.02	0.18	0.02
MgO	0.12	0.03	0.12	0.03	0.72	0.63	1.23	1.04	0.52	0.20	1.99	0.25
CaO	0.67	0.02	0.67	0.02	2.47	1.23	3.20	1.48	2.09	0.55	5.43	0.38
Na2O	4.18	0.08	4.18	0.08	3.39	0.10	3.39	0.21	3.43	0.18	3.67	0.22
K2O	3.76	0.07	3.76	0.07	3.85	0.64	3.59	0.77	4.09	0.40	1.78	0.17
P2O5	0.06	0.02	0.06	0.02	0.07	0.05	0.10	0.05	0.06	0.03	0.20	0.03
Cl	0.08	0.01	0.08	0.01	0.12	0.03	0.12	0.03	0.13	0.02	0.07	0.02
(n)	*14*		*18*		*9*		*10*		*14*		*11*	
ppm	**Ave.**	**1 σ**	**Ave.**	**1 σ**	**Ave.**	**1 σ**	**Ave.**	**1 σ**	**Ave.**	**1 σ**	**Ave.**	**1 σ**
V	3.03	3.07	2.56	1.42	84.9	45.2	98.7	62.3	77.5	89.8	135	12.0
Rb	112	5.58	102	3.6	140	24.1	116	36.6	123	18.1	60.3	2.4
Sr	118	5.51	109	6.7	198	66.6	293	162.4	180	124.8	330	18.9
Y	8.50	0.45	9.4	1.0	26.2	3.3	24.1	6.1	23.4	4.3	26.2	1.7
Zr	31.5	1.57	33.7	3.7	224	39.7	195	58.3	156	57.0	128	3.7
Nb	18.2	0.83	19.7	2.1	8.5	1.2	7.4	2.1	7.7	0.9	6.2	0.3
Ba	985	30.42	944	58	563	81.8	487	97.0	513	47.5	349	23.4
La	5.75	0.34	6.48	0.93	23.1	3.6	20.2	4.3	22.6	2.7	18.4	1.3
Ce	12.7	0.71	12.5	2.3	50.1	6.5	44.8	10.0	45.8	4.7	39.1	4.6
Pr	1.33	0.09	1.48	0.18	5.61	0.77	5.15	1.13	5.20	0.70	4.84	0.31
Nd	4.28	0.54	4.94	0.92	22.76	2.86	20.89	4.87	20.14	2.76	21.15	1.80
Sm	1.31	0.12	1.40	0.47	5.20	0.61	4.69	1.17	4.37	0.96	5.02	0.28
Eu	0.31	0.03	0.27	0.10	0.88	0.06	0.93	0.14	0.83	0.29	1.30	0.13
Gd	1.15	0.13	1.24	0.18	4.66	0.62	4.08	0.93	3.94	0.58	4.59	0.37
Dy	1.34	0.14	1.48	0.20	4.48	0.57	4.12	0.99	3.90	0.85	4.72	0.37
Er	0.94	0.09	0.85	0.12	2.81	0.35	2.61	0.70	2.54	0.61	2.92	0.24
Yb	0.97	0.12	1.05	0.22	3.07	0.47	2.72	0.70	2.68	0.65	2.79	0.34
Lu	0.14	0.02	0.15	0.03	0.44	0.07	0.40	0.11	0.41	0.08	0.42	0.02
Hf	1.49	0.07	1.7	0.3	6.07	1.33	5.41	1.56	4.59	1.52	3.65	0.22
Ta	1.46	0.03	1.7	0.2	0.62	0.11	0.54	0.16	0.60	0.07	0.41	0.02
Pb	17.5	0.74	18.1	2.7	20.7	2.2	21.2	7.8	19.7	1.8	13.3	1.38
Th	4.8	0.3	5.0	0.4	11.9	2.6	10.2	3.2	10.8	1.5	5.10	0.29
U	3.90	0.16	4.02	0.27	2.99	0.62	2.56	0.78	2.60	0.31	1.21	0.10
(n)	*9*		*14*		*11*		*15*		*6*		*12*	

test this potential correlation. Similarly, there are eleven Hakone tephras preserved beneath Ata in proximal outcrops (Fig. 2) and are likely to correlate with the SG14-5851 and SG14-5597 cryptotephras. The absence of any geochemical characterisation for any pre-50 ka Hakone near-vent units precludes any correlations. However, the glass chemistry of the Lake Suigetsu deposits indicate that the geochemical signatures of successive Hakone eruptions do not vary across at least a 28 kyr period and suggest that proximal glass compositions may not facilitate correlations to particular eruption units.

6.1.2.5. Ontake. The glasses represented by the SG14-4837 and SG14-4860 cryptotephras have Y and Zr contents typical of those produced from the NVZ (Figs. 5 and 6). Both the SG14-4860 and SG14-4837 cryptotephra deposits are preserved within the ~90 cm of sediment above the Aso-4 tephra (SG06-4963; Fig. 4) and have respective ages of 83.0 ± 1.5 ka and 84.1 ± 1.3 ka (Table 2). The cryptotephras have high K_2O contents, which are consistent with eruption deposits from the Ontake volcano, although SG14-4860 marginally extends the known SiO_2 compositional range (Fig. 11B). The two cryptotephras show overlap with those from Ontake at the trace element level, with the younger (SG14-4837) more enriched in Zr (~35 ppm) relative to the older (SG14-4860) (Fig. 11D and E).

We correlate SG14-4837 to the On-Ng eruption of Ontake as the glass compositions and stratigraphic position are in excellent agreement (i.e., located between Aso-4 and DKP; Figs. 2 and 4). This extends the dispersal of this eruption further west than previously reported (see Matsu'ura and Komatsubara, 2024). Using the Lake Suigetsu age model, the age of the On-Ng tephra is now constrained to 83.0 ± 1.5 ka (±1σ). It is not yet possible to correlate SG14-4860 to specific eruption event of Ontake at ~84 ka (~1 ka prior to On-Ng), but we highlight that trace elements are essential to discriminating this event in other sedimentary records.

6.1.3. Honshu/Hokkaido (NEJA and Kurile Arc)

6.1.3.1. Toya. The SG14-5575 cryptotephra deposit is stratigraphically positioned below two key widespread markers (Aso-4 [SG06-4963] and SK [SG14-5367]; Table 2) and has a high shard concentration (Table 2). Despite the generally high background concentrations during this period, the SG14-5575 shards were morphologically distinct (i.e.,

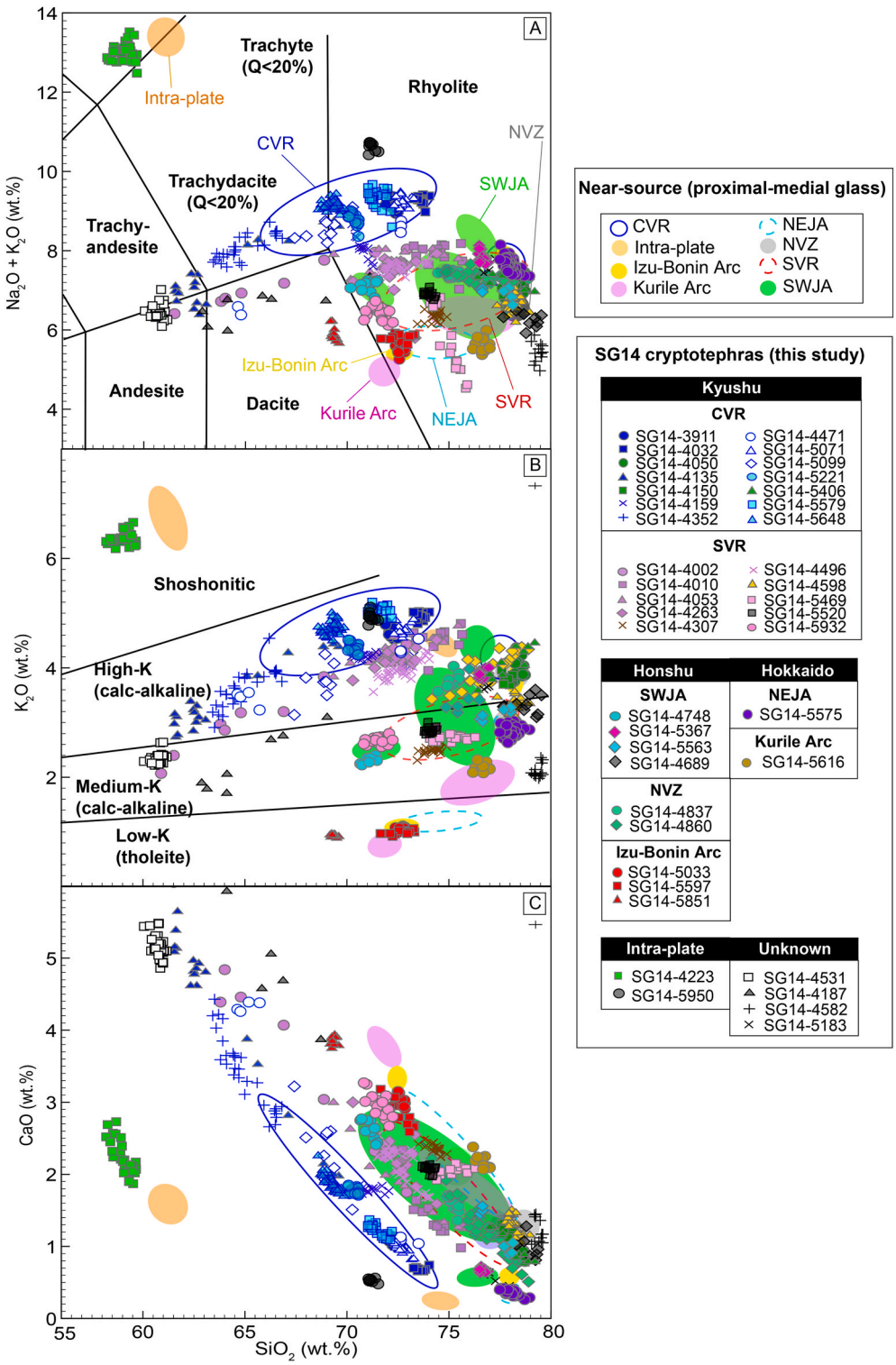

Fig. 5. Major element glass compositions of the crypto-/tephras preserved in the SG14 sediments spanning ~120–50 ka. **(A)** K_2O classification fields follow Peccerillo and Taylor (1976). Glass compositional fields/envelopes for the arcs are labelled in a-c, see Fig. 1 for locations. Compositional fields/envelopes for the following volcanic arcs are from data presented in previous studies for the CVR from Smith et al. (2013) (Aso-A, Aso-D, Aso-4), Albert et al. (2019a) (Aso = ACP-3, ACP-4, ACP-5, ACP-6, Aso-4, Aso-Y, Aso-A, Aso-B, Aso-C, Aso-D Aso-I, Aso-K, Aso-M, Aso-N, Aso-3; Kuju = Kj-Mg, Kj-D, Kj-P1, Kj-Hd); McLean et al. (2020a) (Aso = Aso-Kpfa); Intraplate proximal and Lake Suigetsu tephras for Changbaishan from McLean et al. (2018) (B-Tm) and Ulleungdo from Smith et al. (2011a) (U4/U-Oki); McLean et al. (2018) (U1, U2, U-3); McLean et al. (2020b) (U-Ym); Izu-Bonin Arc from Albert et al. (2019a) (Hakone = Tau8); Albert et al. (2024) (Nijima = Nj-Mt); Kurile Arc from Albert et al. (2019a) (Kutcharo = Kc-Sr, Kc-2/3, Kc-Hb; Mashu = Ma-f); NEJA from Albert et al. (2019a) (Shikotsu = Spfa-1; Towada = To-H; Toya = Toya); NVZ from Albert et al. (2019a) (Ontake = On-Pm1) Albert et al. (2024) (Asama = As-K, As-UG, As-YP) Matsu'ura and Komatsubara (2024) (Ontake = On-Ng, On-Ot, On-In, On-Kt, On-Yb, On-Pm1); SVR from Smith et al. (2011a) (Aira = AT); Smith et al. (2013) (Kikai = K-Ah) Albert et al. (2019a) (Ata = Ata, AT, Ikeda; Aira = A-Iw; Kikai = K-Ah, K-Tz); Albert et al. (2024) (Aira = A-Moeshima, A-Tkn, Kr-Kb; Kirishima = Kr-Kb); McLean et al. (2020a) (Aira = A-Fkm, A-Kn) and SWJA from Albert et al. (2018) (Daisen = DJs, DHg, DSs, DSP; Sambe = Th-pfl, S2-fl, Kr-fa, Uk-fa, Md-fl, U2, U1, Ht-fl, SI, Ikeda, SuN, Sod). Error bars on plots represent reproducibility, and 2 standard deviations of replicate analysis of MPI-DING StHs6/80-G standard.

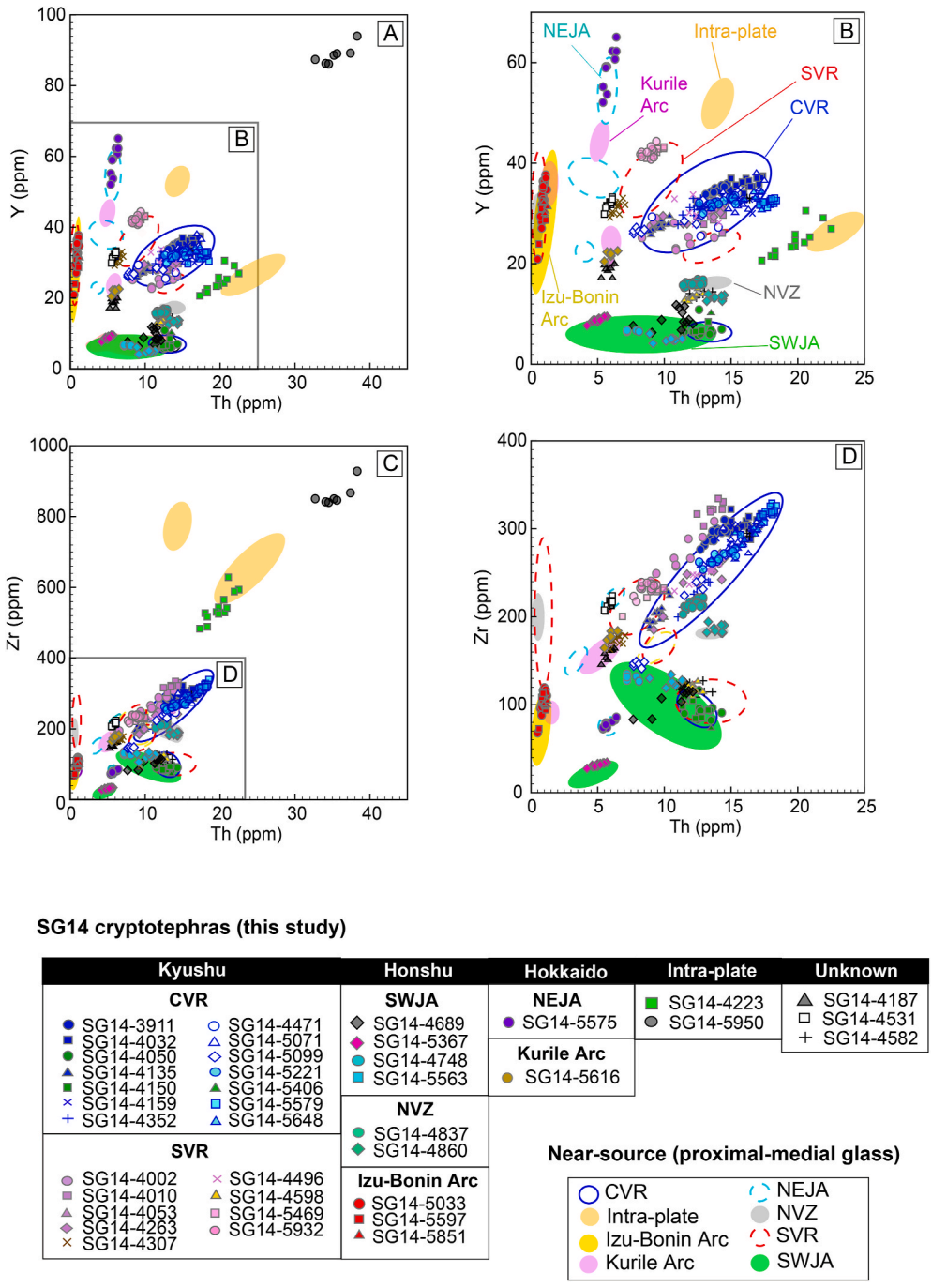

Fig. 6. Trace element glass compositions of the crypto-/tephras preserved in the SG14 sediments spanning ~120 - 50 ka. Glass compositional fields/envelopes for the arcs are labelled in a-c, see Fig. 1 for locations. Compositional fields/envelopes for the following volcanic arcs are from literature data. Data for the CVR is from Albert et al. (2019a) (Aso = ACP-3, ACP-4, Aso-4, Aso-Y, Aso-A, Aso-B, Aso-C, Aso-D Aso-I, Aso-K, Aso-M, Aso-N, Aso-3; Kuju = Kj-Mg, Kj-P1, Kj-Hd) and McLean et al. (2020a) (Aso = Aso-Kpfa); Intraplate proximal and Lake Suigetsu tephras for Changbaishan McLean et al. (2016) (B-Tm) and Ulleungdo from McLean et al. (2018) (U-3) and McLean et al. (2020b) (U-Ym); Izu-Bonin Arc Albert et al., 2019a(Hakone = Tau8) and Albert et al. (2024) (Nijima = Nj-MtG); Kurile Arc from Albert et al. (2019a) (Kutcharo = Kc-Sr, Kc-2/3, Kc-Hb; Mashu = Mashu-f); NEJA from Albert et al. (2019a) (Shikotsu = Spfa-1; Towada = To-H; Toya = Toya); NVZ from Albert et al. (2019a) (Ontake = On-Pm1), Albert et al. (2024) (Asama = As-K, As-UG, As-YP), and Matsu'ura and Komatsubara (2024) (Ontake = On-Ng, On-Ot, On-In, On-Kt, On-Yb, On-Pm1); SVR from Albert et al. (2019a) (Ata = Ata, AT, A-Iw; Kikai = K-Ah, K-Tz), Albert et al. (2024) (Aira = A-Moeshima; Kirishima = Kr-Kb), and McLean et al. (2020a) (Aira = A-Fkm, A-Kn); and SWJA from Albert et al. (2018) (Daisen = DSs and DSP; Sambe = SuN and Sod). Error bars on plots represent reproducibility, and 2 standard deviations of replicate analysis of MPI-DING StHs6/80-G standard.

cuspate and fluted) from the two nearby tephras (both within 16 cm; Fig. 4).

The glass composition of the SG14-5575 deposit fall within the tight compositional field for the proximally characterised Toya deposit, with low FeO, CaO, high Na_2O, and moderate K_2O contents (Fig. 12A; Matsu'ura et al., 2014; Machida and Arai, 2003), but they extend to higher Th and Y contents than previously reported (Fig. 12B). Given the excellent chronostratigraphic position and geochemical agreement, SG14-5575 is correlated to the caldera forming Toya eruption. An age of 108.1 ± 3.9 ka (±1σ) is estimated for the unit based on the Lake Suigetsu age-depth model, which is consistent with previously reported ages for the eruption, yet more precisely constrained (Table 1). This

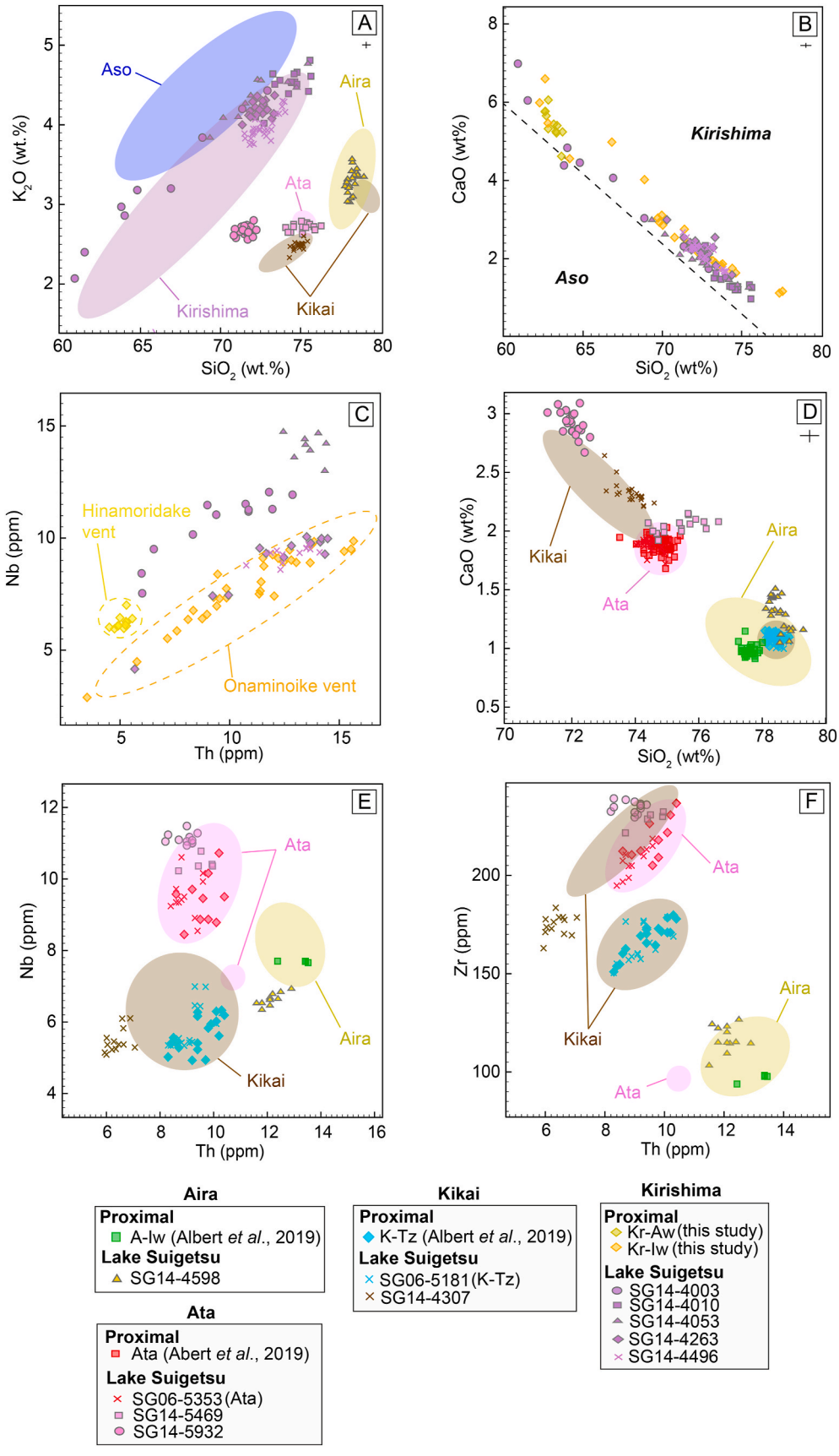

(caption on next page)

Fig. 7. Major and trace element compositions of the SG14 cryptotephras (~120–50 ka) derived from the SVR in comparison for major eruptive SVR centres. Compositional fields/envelopes for the following volcanic centres are from proximal data presented in previous studies. Data for Aira is from Smith et al. (2011a) (AT), McLean et al. (2020a) (A-Fkm, A-Kn), Albert et al. (2019a) (A-Iw), and Albert et al. (2024) (A-Moeshima, A-Tkn); Ata from Albert et al. (2019a) (Ata = Ata, AT, Ikeda); Kikai from Albert et al. (2019a) (K-Ah, K-Tz) and Smith et al., (2013) (K-Ah); Kirishima from Albert et al. (2024) (Kr-Kb) and this study (Kr-Aw, Kr-Iw). Error bars represent 2x standard deviation of repeat analyses of the StHs6/80-G MPI-DING standard glass.

occurrence in Lake Suigetsu is the furthest south that the Toya tephra has been identified and extends the dispersal of this large eruption and allows sedimentary archives to be correlated across a wide geographical range (Fig. 3).

6.1.3.2. Kutcharo. The SG14-5616 cryptotephra is preserved beneath several widespread markers including Aso-4 and Toya (Fig. 4; Table 2). It is characterised as a discrete peak in shard concentration relative to the background (Fig. 4) and is comprised of shards that are small (40 μm in length), colourless and highly vesicular (Supplementary Material). Whilst it is challenging to ascribe a volcanic region based on major elements alone (Fig. 5), the trace concentrations show a clear affinity to those from the Kurile Arc (Th vs. Y; Fig. 6B). The only volcanic centre located along the Kurile Arc known to be active in this timeframe is Kutcharo (Fig. 2). Kutcharo produced at least two large eruptions (≥M6.0) at 120 ka (Kc-Hb/4) and 85 ka (Kc-2/3), which are beneath the Aso-4 unit (Fig. 2; Table 1). The SG14-5616 glasses possess subtly lower FeO content at a given CaO content relative to previously characterised Kutcharo tephras (Fig. 12C). Furthermore, the SG14-5616 glasses are easily discriminated from both the Kc-Hb/4 and Kc-2/3 glasses at the trace element level as the cryptotephra has much lower Y contents (~20 ppm; Fig. 12D) and thus likely represents another Kutcharo eruption at 109.6 ± 4.1 ka. Given the distance to Kutcharo (~1250 km), it is somewhat surprising that the eruption has not been identified in proximal sections, although the eruptive history of Kutcharo is not detailed, and our finding suggests that Kutcharo has had more large eruptions than previously reported.

6.1.4. Intraplate

6.1.4.1. Ulleungdo. The SG14-4223 cryptotephra deposit is stratigraphically preserved between the visible DKP (SG06-4281) and KjP1/Hd (SG06-4141) marker layers in the Lake Suigetsu archive and has a sharp peak in shard concentrations of 5775 shards/gram (Fig. 4). The shards are brown and blocky with microlite inclusions (Table 2; Supplementary Material). The glass chemistry of the SG14-4223 deposit is consistent with compositions erupted from Ulleungdo, but this older deposit has lower SiO_2 (~1 wt%) than the previously reported Ulleungdo deposits (Fig. 12E; McLean et al., 2016, 2018; 2020b; Smith et al., 2013). The age for this deposit, based on the Suigetsu age model, is 59.0 ± 2.1 ka (±1σ). Due to its chronostratigraphic position and age, the SG14-4223 cryptotephra could be associated with the U-Sado/SKP-II tephra that has been previously reported in marine records (Fig. 3). However, the SG14-4223 glasses are compositionally different from those units reported from the Sea of Japan with our data exhibiting much higher MgO content (Derkachev et al., 2019; Chun et al., 2007, Fig. 12E). These two compositionally distinct units indicate that there were at least two eruptions from Ulleungdo at ~60 ka.

6.1.5. Tephra that cannot be attributed to a source

Of the forty-one newly identified deposits, seven cryptotephras could not be correlated to specific arcs or volcanic centres based on their glass chemistry (Table 2). Of note is the lowermost (i.e., oldest) tephra identified in this study (SG14-5950), with an age of 121.0 ± 5.2 ka (±1σ), and with the lowest peak shard concentration (250 shards/gram) of any of the isochrons identified (Table 2). The glasses exhibit a distinct geochemical composition and only overlap with glasses erupted from the CVR in K_2O content (Fig. 5). Nonetheless, the glasses are highly enriched in Nb and Zr, which is indicative of intraplate volcanism (McLean et al., 2020b, Fig. 13B). The compositions are not like those erupted from Changbaishan or Ulleungdo which are, consequently, unlikely to represent the source. Jeju island (location shown in Fig. 1) was active from at least 88 ka based on $^{40}Ar/^{39}Ar$ dating (Brenna et al., 2015); however, no geochemical data are presently available of the eruption deposits for comparison.

6.2. Identifying volcanic sources and eruptions of the Lake Suigetsu tephra

Of all the deposits preserved in Lake Suigetsu between ~120 and 50 ka, twelve (24%) of the layers identified can be correlated to a specific eruption, thirty-one (62%) are correlated to a volcano but not a particular eruption, three (6%) are correlated to a volcanic region only, and there are four (8%) layers for which the source is ambiguous. The reasons behind this difficulty in attribution are largely due to:

1. A lack of chemical data for various volcanoes and eruptions;
2. Poor eruption stratigraphies near the volcanoes due to burial and erosion, which mean that the volcanoes seem less productive than they have been in reality;
3. Successive eruptions from a particular volcano tapping similar melt compositions over long periods of time (as seen elsewhere, e.g., Campi Flegrei, Italy; Vineberg et al., 2023; Smith et al., 2011b) so deposits cannot be reliably correlated to a particular event.

These points are discussed further below.

6.2.1. Limited glass geochemistry for eruption deposits

The major and trace element analyses of the distal Lake Suigetsu crypto-/tephras have been compared to the extensive glass datasets that have been produced for the East Asian volcanic systems, and supplemented by some proximal samples analysed for this study (Table 4). These data show that trace element compositions can help to identify the source of the tephra and reliably correlate the tephra to a particular eruption, especially when the major element compositions overlap. For example, eruption deposits from Ata and Kikai volcanoes share similar major elements but can be easily distinguished using Nb trace element contents (Fig. 7). Despite the availability of trace element data, some crypto-/tephras identified still cannot be correlated to particular sources (e.g., SG14-4582 and SG14-5932) as the glass compositions fall outside the currently known ranges for the arc regions and their volcanoes (Figs. 5 and 6). Until these relatively distinct glass compositions are identified in other studies, no firm correlations can be established for the seven tephra layers that have been identified in Lake Suigetsu in the 120 - 50 ka timeframe.

6.2.2. Incomplete eruption stratigraphies

The identification of a significant Kutcharo deposit that is chemically distinct indicates that there were at least three eruptions from Kutcharo between 125 and 85 ka. Given that the volcano is located 1250 km northeast of Suigetsu, these eruptions are likely to have been much greater than M5. Such large eruptions are almost always preserved in near-vent stratigraphies as the deposits would have been incredibly thick. Nonetheless, only two large eruption deposits have yet been identified near Kutcharo in this time period: Kc-Hb/4 and Kc-2/3 (Hayakawa, 2023; Hasegawa and Nakagawa, 2016; Machida and Arai, 2003). It has been noted elsewhere that some large caldera-forming volcanoes are missing evidence for large magnitude events; e.g., the deposits of the M6.6 Masseria del Monte eruption that is linked to the

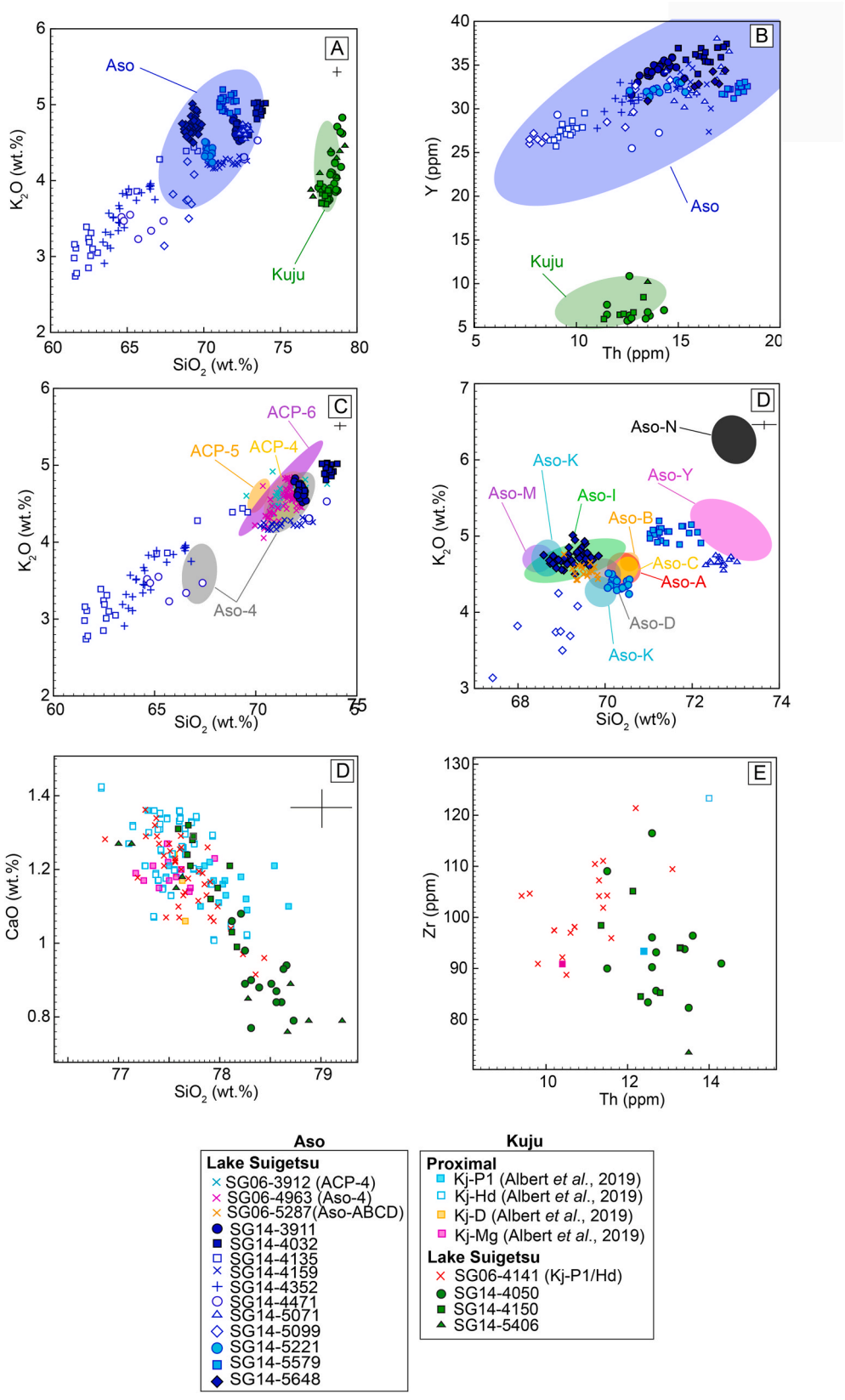

Fig. 8. Major and trace element compositions of the SG14 crypto-/tephras (~120–50 ka) from the CVR. Compositional fields/envelopes for the following volcanic centres are from proximal data presented in previous studies. Data for Aso is from Smith et al. (2013)) (Aso-A, Aso-D, Aso-4), Albert et al. (2019a) (Aso = ACP-3, ACP-4, ACP-5, ACP-6, Aso-4, Aso-Y, Aso-A, Aso-B, Aso-C, Aso-D Aso-I, Aso-K, Aso-M, Aso-N, Aso-3), and McLean et al. (2020a) (Aso = Aso-Kpfa); and Kuju data are from Albert et al. (2019a) (Kj-Mg, Kj-D, Kj-P1, Kj-Hd). Error bars represent 2x standard deviation of repeat analyses of the StHs6/80-G MPI-DING standard glass.

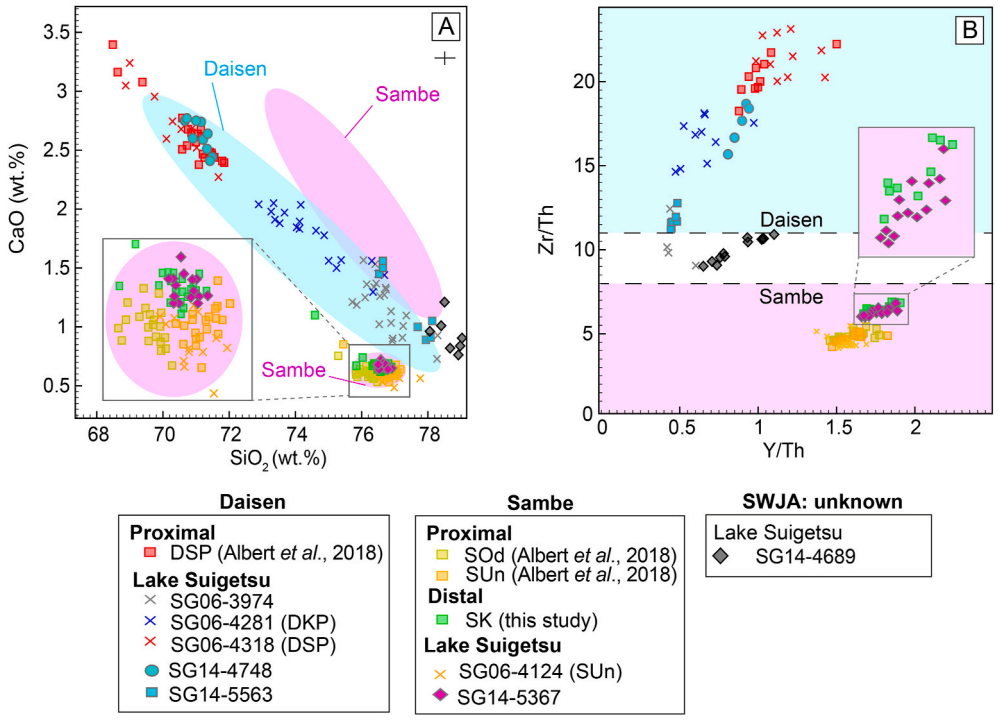

Fig. 9. Major and trace element compositions of the SG14 cryptotephras (~120–50 ka) from the SWJA. Compositional fields/envelopes for the following volcanic centres are from proximal data presented in previous studies. Data for Daisen is from Albert et al. (2018) (DJs, DHg, DSs, DSP); and Sambe data are from Albert et al. (2018) (Th-pfl, S2-fl, Kr-fa, Uk-fa, Md-fl, U2, U1, Ht-fl, SI, Ikeda, SuN, Sod) and this study (SK – sampled from Sagawa et al., 2018). Error bars represent 2x standard deviation of repeat analyses of the StHs6/80-G MPI-DING standard glass.

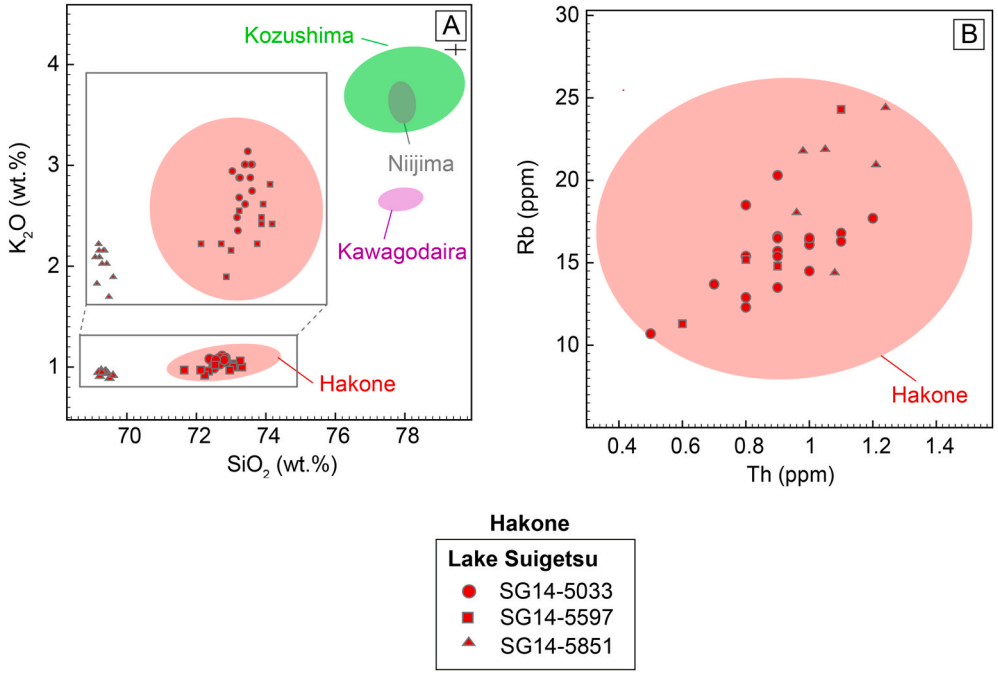

Fig. 10. Major and trace element compositions of the SG14 cryptotephras (~120–50 ka) erupted from the Izu-Bonin Arc compared to those of major eruptive centres located on this arc. Compositional fields/envelopes for the following volcanic centres are from proximal data presented in previous studies. Data for Hakone is from Albert et al. (2019a) (Tau8); Kawagodaira from McLean et al. (2018) (KGP); Kozushima from Suzuki et al. (2016) (Iz-Kt); and Niijima from Albert et al. (2024) (Nj-Mt). Error bars represent 2x standard deviation of repeat analyses of the StHs6/80-G MPI-DING standard glass.

Y-3 tephra, a widespread tephra layer across the central Mediterranean, are not well preserved close to the source volcano, the Campi Flegrei caldera, as subsequent explosive eruptions have destroyed and buried the deposits, and the proximal unit has only recently been identified (Albert et al., 2019b). It is possible that the more recent Kutcharo eruptions have buried or obscured the evidence for this third large Kutcharo eruption in this period. Cryptotephra analysis of high-resolution distal archives such as Lake Suigetsu provide additional

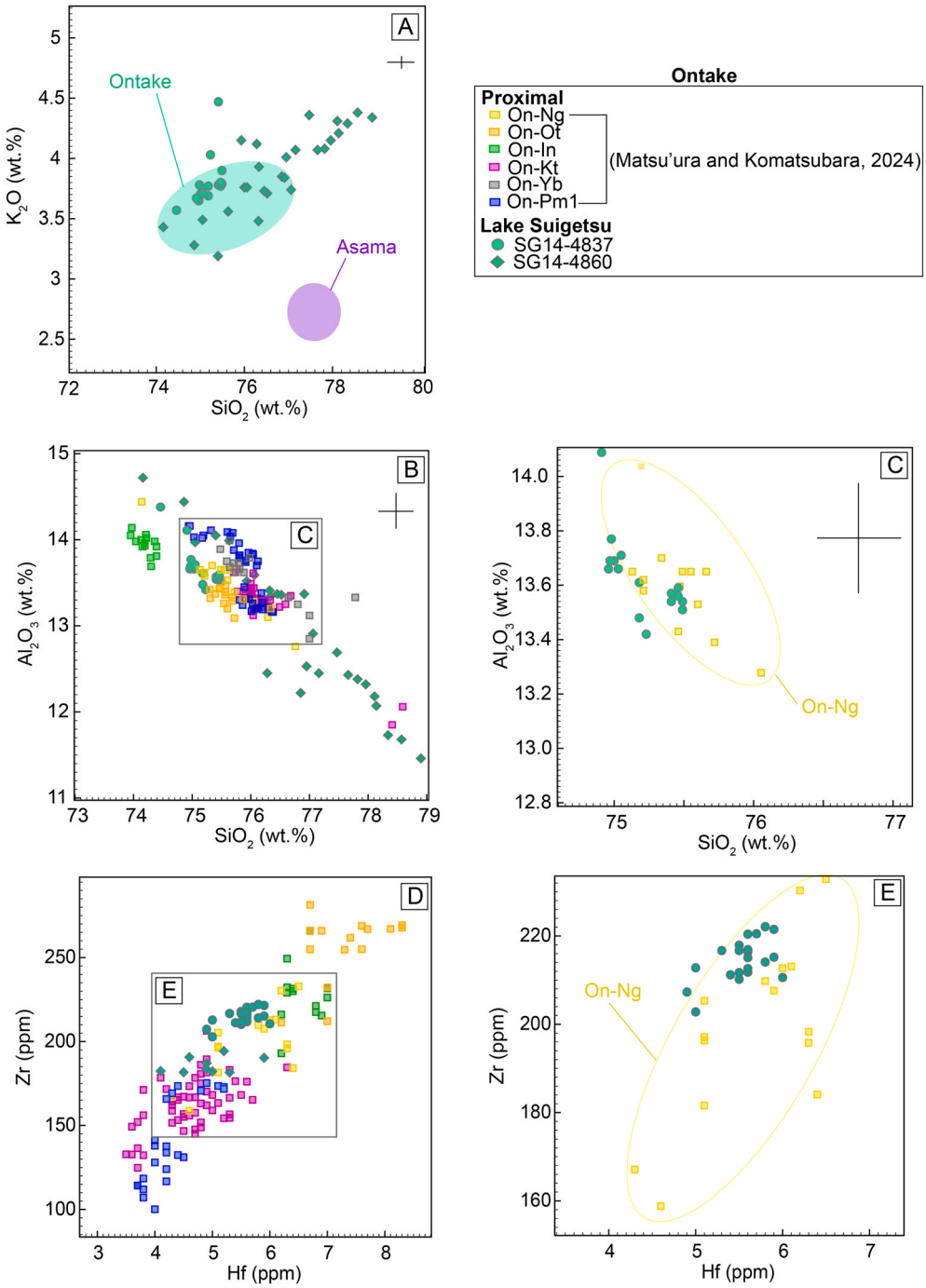

Fig. 11. Major and trace element compositions of the SG14 cryptotephras (~120–50 ka) from the NVZ comparison to those of the major eruptive centres in the region. Compositional fields/envelopes for the following volcanic centres are from proximal data presented in previous studies. Data for Asama is from Albert et al. (2024) (As-K, As-UG, As-YP); and Ontake data are from Albert et al. (2019a) (On-Pm1) and Matsu'ura and Komatsubara (2024) (On-Ng, On-Ot, On-In, On-Kt, On-Yb, On-Pm1). Error bars represent 2x standard deviation of repeat analyses of the StHs6/80-G MPI-DING standard glass.

information on these eruption events that appear to be lacking in the geological record (see Hayakawa, 2023). Further cryptotephra studies on other sediment cores should further constrain the explosive eruption history of volcanoes across Japan.

6.2.3. Similar melt compositions erupted from a volcano over long periods of time

This cryptotephra study further exemplifies that successive eruption deposits from the same volcano over long periods, 50 kyr in the case for Kuju, are frequently geochemically indistinguishable. The repeated chemistry of tephra deposits from Kirishima over a 19 kyr interval means that those of medium to large eruptions may be miscorrelated, particularly those with similar magnitudes and with poor chronological or stratigraphic control. These similar chemistries provide insight into the magmatic system and indicate that similar processes govern melt formation and evolution over prolonged periods of time. It is surprising that these medium to large eruptions do not show variation in trace element composition, which are particularly sensitive to crystallisation of crystals that would be modified by even subtle changes in the upper crustal architecture of the magmatic system. Due to the similar glass

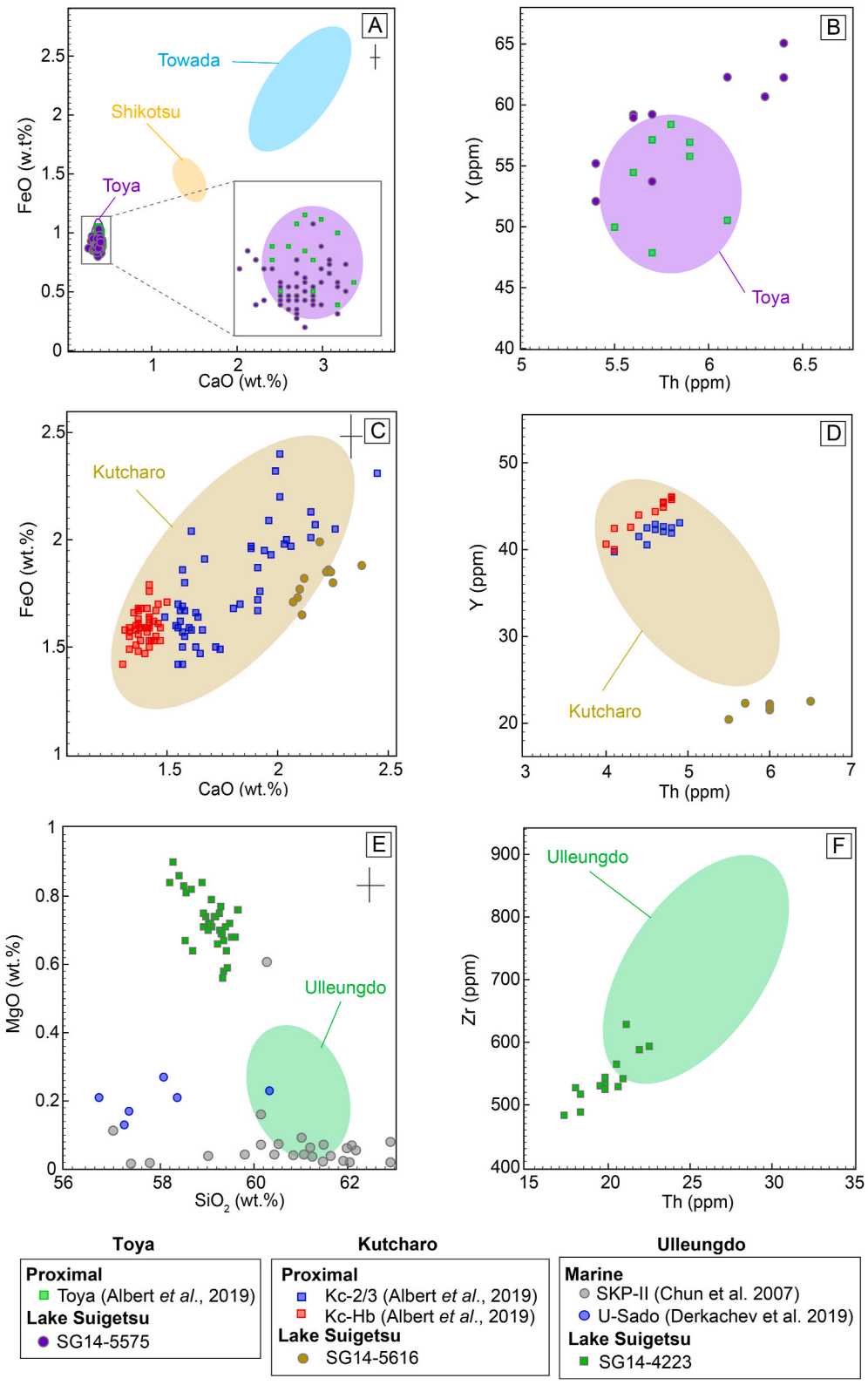

Fig. 12. Major and trace element compositions of the SG14 cryptotephra deposits (~120–50 ka) from the NEJA (A,B), Kurile Arc (C,D) and Intraplate (E,F) volcanoes compared to major eruptive centres located in these regions. Compositional fields/envelopes for the following volcanic centres are from proximal data presented in previous studies. Data for Kutcharo is from Albert et al. (2019a) (Kc-Sr, Kc-2/3, Kc-Hb); Mashu from Albert et al. (2019a) (Ma-f); Shikotsu from Albert et al. (2019a) (Spfa-1); Towada from Albert et al. (2019a) (To-H); Toya from Albert et al. (2019a) (Toya); and Ulleungdo, including other Lake Suigetsu tephras, is from Smith et al. (2011a) (U4/U-Oki), McLean et al. (2018), Smith et al. (2013) (U1, U2, U-3) and McLean et al. (2020b) (U-Ym). Error bars represent 2x standard deviation of repeat analyses of the StHs6/80-G MPI-DING standard glass.

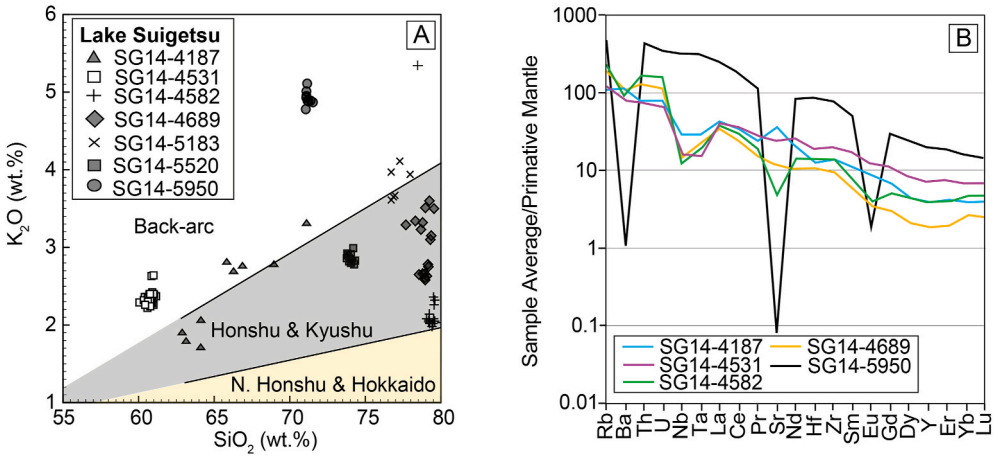

Fig. 13. **(A)** Glass analyses are plotted on the whole-rock K-classification scheme of Peccerillo and Taylor (1976). The back-arc and intraplate volcanism produces high-K (shoshonitic) compositions, which contrast to the eruptive products from northern Honshu and Hokkaido, which have low-K (tholeiite) compositions. Error bars represent 2x standard deviation of repeat analyses of the StHs6/80-G MPI-DING standard glass. **(B)** Sample-averaged Primitive Mantle normalised trace element compositions of five Lake Suigetsu tephras identified within ~120–50 ka sediments which are uncorrelated to specific volcanic sources. Trace element analyses of SG14-5182 and SG14-5520 could not be obtained due to their small shard sizes and/or abundance of microlite inclusions. Primitive mantle values used for normalisation follow Sun and McDonough (1989).

compositions of eruptions, there are periods when the tephra layers cannot be used as isochrons; however, they can still provide chronological constraints, albeit with broad uncertainties.

6.3. Tephra dispersal

The crypto-/tephras identified in Lake Suigetsu between ~120 and 50 ka are from at least twelve volcanoes situated across Japan and from intraplate settings to the west of Japan (Fig. 14). Unsurprisingly, most of the crypto-/tephras preserved in Lake Suigetsu are from volcanoes that are located southwest of Lake Suigetsu and the volcanic ash is carried by the prevailing westerly winds that are experienced across the full range of latitudes occupied by Japan. These volcanoes are also the main sources of cryptotephras in other sections of the core (Albert et al., 2024; McLean et al., 2018). The furthest known sources are 1250 km from Lake Suigetsu and, given that they are so distal, the tephra deposits would have covered extremely large areas, whilst the closest sources are 225 km away and the cryptotephra deposits associated with these eruptions typically represent eruptions that were considerably smaller (Fig. 14). The eruptions that are from sources more than 500 km away are likely to be ≥M5.0, while others from sources in central Honshu could be smaller ≤ M4.0 (Sulpizio et al., 2024). However, this not only depends on the magnitude of the eruption but also on the wind directions and wind strength at the time of the eruption. This shows that eruptions of M4.0 and greater deposited ash over the region, which now hosts the densely populated cities of Tokyo, Osaka and Kyoto, every ~1400 years.

Based on the isopach maps produced by Machida and Arai (2003), the crypto-/tephra preserved in Lake Suigetsu are consistent with recorded thicknesses in the vicinity. In addition, where the identified deposits have not been observed in exposures near Lake Suigetsu, the layers are only present as cryptotephras, highlighting the reliability of the isopachs of Machida and Arai (2003). A great example is the isopach for the SK eruption from Sambe, which shows that dispersal was restricted to a tight ellipse extending northeast of the volcano with visible layers not observed as far east as Lake Suigetsu. In the Lake Suigetsu core, this SK tephra is only preserved as a cryptotephra (Fig. 4). In addition, the large caldera-forming Toya eruption has a broad and roughly circular isopach that testifies to weak winds during the eruption; the visible tephra layer had only been recorded as far south as ODP1150A (370 km SW from Toya) as a cryptotephra (see Matsu'ura and Komatsubara, 2024). The identification of Toya in Lake Suigetsu greatly increases the known dispersal of the eruption.

Key Japanese volcanic events missing from the Lake Suigetsu record include the A-Iw and Kc-2/3. Although eruptions were ≥M6.0, their ash dispersals were away from Lake Suigetsu. The A-Iw was dispersed to the east, whilst the was Kc-2/3 dispersed to the north-northeast (Table 1) and thus, it is unsurprising that no ash is preserved in Lake Suigetsu. Based on Sea of Japan tephra records, there are three eruptions from Changbaishan between around 86 and 50 ka (Lim et al., 2013; Ikehara et al., 2004). None of these eruptions are recorded in Lake Suigetsu, suggesting that the dispersal trajectory did not extend over southern Honshu and possibly lower magnitude than the 946 CE Millennium eruption, which is found as a very thin visible tephra layer in the uppermost metre of Suigetsu sediment (McLean et al., 2016). We surmise that if the isopachs show strong directionality, typically associated with strong winds, and directed away from Suigetsu, it is incredibly unlikely that the tephra will be preserved as even a cryptotephra.

This section of the high resolution Lake Suigetsu record spans three MIS intervals (~70 kyr; Fig. 14) and ideal for investigating relationships between volcanism and climate (Aubry et al., 2022 and references therein). However, no clear relationships in frequency or direction of ash dispersal are observed (Fig. 14). Although this study helps to understand the pacing of explosive volcanism from many volcanoes, its distal location relative to the volcanoes means that it is highly unlikely to have captured all events and, thus does not provide a complete record to interrogate questions related to climate.

6.4. Widespread markers for tephra correlation

The presence of the Toya caldera-forming eruption (SG14-5575) and the SK tephra from Sambe (SG14-5367) expand the geographical limits of ash-fall events and can thus be used over wide areas to synchronise records in MIS5d and MIS5c, respectively. These marker layers could be used for the correlation of paleoenvironmental records, such as the two marine cores in the Pacific (OC9001C and ODP1150A) and the U1427 located in the Sea of Japan which all contain the SK tephras (Fig. 3; Matsu'ura and Komatsubara, 2024; Sagawa et al., 2018). Records that contain both Toya and SK can be used to examine the transition between these two stages, allowing an assessment of whether there is any temporal asynchrony. The Lake Suigetsu age model provides ages of 100.4 ± 3.1 ka (±1σ) and 108.2 ± 3.9 ka (±1σ) for the SK and Toya eruptions, respectively (Table 2). These are consistent with previous estimates.

Twelve key widespread tephra layers have now been documented in Lake Suigetsu between 120 and 50 ka which will be invaluable in the

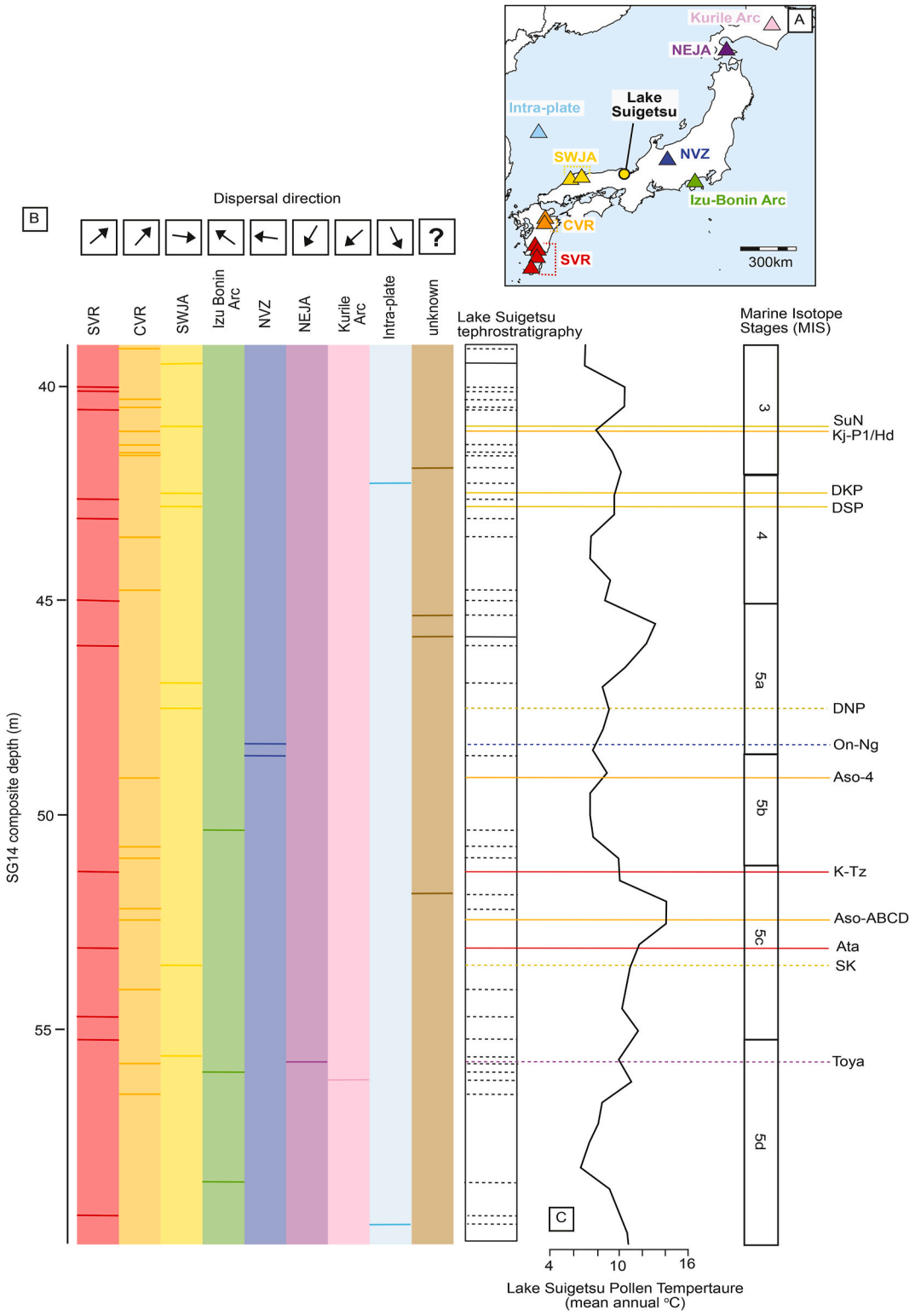

Fig. 14. (A) Summary of the augmented Lake Suigetsu (SG14) tephrostratigraphy (visible and cryptotephra deposits) spanning ~120–50 ka. The distal deposits are correlated, where possible, to their volcanic arcs and specific eruptions using the composition of the volcanic glasses presented in this study. (B) Map showing the location of the eight volcanic regions where deposits have been identified. (C) SG14 tephra layers plotted against the Lake Suigetsu pollen-based, mean 100 yr moving average, annual temperature reconstruction following on from the work of Nakagawa et al. (2021).

correlation of the Lake Suigetsu to others (Fig. 14C).

7. Conclusions

The detailed cryptotephra investigation through the Lake Suigetsu sediments spanning ~120 to 50 ka and the resultant identification of numerous tephra layers provides important insight into the dispersal and tempo of East Asian volcanism. An additional forty-one crypto-/tephra deposits are identified in this timeframe, which is four times as many layers preserved as cryptotephra compared to visible layers. The

geochemistry of the glass shards has enabled most of these distal tephra deposits to be correlated to their volcanic regions/arcs in Japan, and many correlations can be made to a specific volcano and a few to known eruption events. Twenty-seven of the tephras are from eruptive centres southwest of Lake Suigetsu, which is unsurprising given the prevailing westerly winds. The tephra record provides the first evidence for an intense period of explosive activity from Kirishima with five widespread ash dispersals between 69.7 ± 2.4 (±1σ) and 50.5 ± 0.5 ka (±1σ). In addition, the records indicates that tephra from calderas on Hokkaido (~1000 km away) have reached central Honshu (e.g., Kutcharo). Our findings significantly extend the ash dispersal for several known key Pleistocene marker layers, including the Toya ash, which is now identified 950 km from its source, making it one of the most widespread Japanese isochrons. By conducting this detailed cryptotephra investigation we highlight that distal archives can greatly assist in constraining and augmenting the proximal stratigraphies of many of the productive Japanese volcanic centres.

CRediT authorship contribution statement

Sophie O. Vineberg: Conceptualization, Resources, Data Collection, Methodology, Investigation, Formal analysis, Visualization, Writing – original draft, Writing – review & editing, Funding acquisition. **Paul G. Albert:** Conceptualization, Resources, Data Collection, Writing – review & editing, Supervision, Funding acquisition. **Danielle McLean:** Conceptualization, Data Collection, Writing – review & editing, Supervision. **Takehiko Suzuki:** Resources, Writing – review & editing. **Richard A. Staff:** Formal analysis, Writing – review & editing. **Keitaro Yamada:** Data Collection. **Ikuko Kitaba:** Data Collection. **Junko Kitagawa:** Resources. **Christina J. Manning:** Resources. **Hannah M. Buckland:** Data Collection, Resources. **Gwydion Jones:** Resources. **Fumikatsu Nishizawa:** Resources, SG14 Project Members, Resources. **Takeshi Nakagawa:** Resources, Data Collection, Writing – review & editing, Funding acquisition. **Victoria C. Smith:** Conceptualization, Resources, Data Collection, Writing – review & editing, Supervision, Funding acquisition.

Declaration of competing interest

The authors declare that they have no known competing financial interests or personal relationships that could have appeared to influence the work reported in this paper.

Acknowledgments

S.O.V. is funded by NERC as part of the Environmental Research Doctoral Training Programme at the University of Oxford (NERC; NE/S007474/1). VCS and TN acknowledge funding from the Japan Society for the Promotion of Science (JSPS; KAKENHI-15H021443). The SG06 coring campaign was funded by the UK Natural Environmental Research Council (NERC; NE/D000289/1) New Investigators Award to TN. The Fukui-SG14 coring campaign was funded by the Fukui Prefectural government, Japan. P.G.A. H.M.B. and G.J. are funded through a UKRI Future Leader Fellowship award (FLF; MR/S035478/1). TS acknowledges funding from the Japan Society for the Promotion of Science (JSPS; KAKENHI-22H02380). FN acknowledges funding from the Japan Society for the Promotion of Science (JSPS; KAKENHI-JP19K13438.The Lake Suigetsu coring was conducted by the team of Seibushisui Co. Ltd Japan, led by Mr Atsumi Kitamura. This research used samples provided by the International Ocean Discovery Program (IODP), and we thank Dr Yusuke Kubo (IODP) Curator and the KCC (Kochi Core Center) for assistance with the sampling.

Appendix A. Supplementary data

Supplementary data to this article can be found online at https://doi.org/10.1016/j.quascirev.2024.109021.

Data availability

Data is available in the Supplementary Material.

References

Albert, P.G., McLean, D., Buckland, H.M., Suzuki, T., Jones, G., Staff, R.A., Vineberg, S., Kitaba, I., Yamada, K., Moriwaki, H., Ishimura, D., Ikehara, K., Manning, C.J., Nakagawa, T., Smith, V.C., 2024. Cryptotephra preserved in Lake Suigetsu (SG14 core) reveals the eruption timing and distribution of ash fall from Japanese volcanoes during the Late-glacial to early Holocene. Quat. Sci. Rev. 324, 108376. https://doi.org/10.1016/J.QUASCIREV.2023.108376.

Albert, P.G., Smith, V.C., Suzuki, T., McLean, D., Tomlinson, E.L., Miyabuchi, Y., Kitaba, I., Mark, D.F., Moriwaki, H., Nakagawa, T., 2019a. Geochemical characterisation of the Late Quaternary widespread Japanese tephrostratigraphic markers and correlations to the Lake Suigetsu sedimentary archive (SG06 core). Quat. Geochronol. https://doi.org/10.1016/j.quageo.2019.01.005.

Albert, P.G., Smith, V.C., Suzuki, T., Tomlinson, E.L., Nakagawa, T., McLean, D., Yamada, M., Staff, R.A., Schlolaut, G., Takemura, K., 2018. Constraints on the frequency and dispersal of explosive eruptions at Sambe and Daisen volcanoes (South-West Japan Arc) from the distal Lake Suigetsu record (SG06 core). Earth Sci. Rev. 185, 1004–1028. https://doi.org/10.1016/j.earscirev.2018.07.003.

Albert, P.G., Giaccio, B., Isaia, R., Costa, A., Niespolo, E.M., Nomade, S., Pereira, A., Renne, P.R., Hinchliffe, A., Mark, D.F., Brown, R.J., Smith, V.C., 2019b. Evidence for a large-magnitude eruption from Campi Flegrei caldera (Italy) at 29 ka. Geology 47 (7), 595–599. https://doi.org/10.1130/G45805.1.

Aoki, K., 2008. Revised age and distribution of ca. 87 ka Aso-4 tephra based on new evidence from the northwest Pacific Ocean. Quat. Int. 178 (1), 100–118. https://doi.org/10.1016/j.quaint.2007.02.005.

Aubry, T.J., Farquharson, J.I., Rowell, C.R., Watt, S.F., Pinel, V., Beckett, F., Fasullo, J., Hopcroft, P.O., Pyle, D.M., Schmidt, A., Sykes, J.S., 2022. Impact of climate change on volcanic processes: current understanding and future challenges. Bull. Volcanol. 84, 58. https://doi.org/10.1007/s00445-022-01562-8.

Blockley, S.P.E., Pyne-O'Donnell, S.D.F., Lowe, J.J., Matthews, I.P., Stone, A., Pollard, A. M., Turney, C.S.M., Molyneux, E.G., 2005. A new and less destructive laboratory procedure for the physical separation of distal glass tephra shards from sediments. Quat. Sci. Rev. 24 (16–17), 1952–1960. https://doi.org/10.1016/J.QUASCIREV.2004.12.008.

Brenna, M., Cronin, S.J., Kereszturi, G., Sohn, Y.K., Smith, I.E.M., Wijbrans, J., 2015. Intraplate volcanism influenced by distal subduction tectonics at Jeju Island, Republic of Korea. Bull. Volcanol. 77 (1), 1–16. https://doi.org/10.1007/S00445-014-0896-5/METRICS.

Brenna, M., Cronin, S.J., Smith, I.E.M., Sohn, Y.K., Maas, R., 2012. Spatio-temporal evolution of a dispersed magmatic system and its implications for volcano growth, Jeju Island Volcanic Field, Korea. Lithos 148, 337–352. https://doi.org/10.1016/J.LITHOS.2012.06.021.

Bronk Ramsey, C.B., Heaton, T.J., Schlolaut, G., et al., 2020. Reanalysis of the atmospheric radiocarbon calibration record from Lake Suigetsu, Japan. Radiocarbon 62 (4), 989–999. https://doi:10.1017/RDC.2020.18.

Bronk Ramsey, C., Staff, R.A., Bryant, C.L., Brock, F., Kitagawa, H., Van Der Plicht, J., Schlolaut, G., Marshall, M.H., Brauer, A., Lamb, H.F., Payne, R.L., 2012. A complete terrestrial radiocarbon record for 11.2 to 52.8 kyr BP. Science 338 (6105), 370–374. https://doi.org/10.1126/science.1226660.

Bronk Ramsey, C.B., 2008. Deposition models for chronological records. Quat. Sci. Rev. 27 (1–2), 42–60. https://doi.org/10.1016/j.quascirev.2007.01.019.

Brown, S.K., Loughlin, S.C., Sparks, R.S.J., Vye-Brown, C., Barclay, J., Calder, E., Cottrell, E., Jolly, G., Komorowski, J.-C., Mandeville, C., Newhall, C., Palma, J., Potter, S., Valentine, G., 2015. Chapter 2 Global volcanic hazard and risk. https://doi.org/10.1017/CBO9781316276273.004.

Bryant, C.J., Arculus, R.J., Eggins, S.M., 2003. The geochemical evolution of the Izu-Bonin arc system: a perspective from tephras recovered by deep-sea drilling. G-cubed 4 (11).

Chen, X.Y., McLean, D., Blockley, S.P.E., Tarasov, P.E., Xu, Y.G., Menzies, M.A., 2019. Developing a Holocene tephrostratigraphy for northern Japan using the sedimentary record from Lake kushu, rebun island. Quaternary findScience Reviews 215, 272–292. https://doi.org/10.1016/j.quascirev.2019.05.017.

Chun, J.H., Cheong, D., Ikehara, K., Han, S.J., 2007. Age of the SKP-I and SKP-II tephras from the southern East Sea/Japan Sea: implications for interstadial events recorded in sediment from marine isotope stages 3 and 4. Palaeogeogr. Palaeoclimatol. Palaeoecol. 247 (1–2), 100–114. https://doi.org/10.1016/J.PALAEO.2006.11.024.

Cook, E.R., Anchukaitis, K.J., Buckley, B.M., D'Arrigo, R.D., Jacoby, G.C., Wright, W.E., 2010. Asian monsoon failure and megadrought during the last millennium. Science 328 (5977), 486–489. https://doi.org/10.1126/science.1185188.

Crosweller, S.H., Arora, B., Brown, S.K., Cottrell, E., Deligne, N.I., Ortiz Guerrero, N., Hobbs, L., Kiyosugi, K., Loughlin, S.C., Lowndes, J., Nayembil, M., Siebert, L., Stephen, R., Sparks, J., Takarada, S., Venzke, E., 2012. Global database on large magnitude explosive volcanic eruptions (LaMEVE). https://doi.org/10.1186/2191-5040-1-4.

Derkachev, A.N., Utkin, I.V., Nikolaeva, N.A., Gorbarenko, S.A., Malakhova, G.I., Portnyagin, M.V., Sakhno, V.G., Shi, X., Lv, H., 2019. Tephra layers of large explosive eruptions of Baitoushan/Changbaishan Volcano in the Japan Sea

sediments. Quat. Int. 519, 200–214. https://doi.org/10.1016/J.QUAINT.2019.01.043.
Furusawa, A., 2008. Characterizing tephras by major-element analysis of glass inclusions in plagioclase phenocrysts: preliminary results from the DKP tephra of Daisen Volcano, Japan. J. Geol. Soc. Jpn. 114, 618–631.
Ganzawa, Y., Ike, M., 2011. SAR–RTL dating of single grains of volcanic quartz from the late Pleistocene Toya Caldera. Quat. Geochronol. 6 (1), 42–49. https://doi.org/10.1016/j.quageo.2010.07.001.
Hasegawa, T., Nakagawa, M., 2016. Large scale explosive eruptions of Akan volcano, eastern Hokkaido, Japan: a geological and petrological case study for establishing tephro-stratigraphy and -chronology around a caldera cluster. Quat. Int. 397, 39–51. https://doi.org/10.1016/J.QUAINT.2015.07.058.
Hayakawa, Y., 2023. Hayakawa's 2000-year Eruption Database and One Million Year Tephra Database. http://www.hayakawayukio.jp/database (Updated regularly).
Hayakawa, Y., 1985. Pyroclastic geology of Towada volcano. Bull. Earthq. Res. Inst. Univ. Tokyo 60, 507–592.
Hoshizumi, H., Miyabuchi, Y., Miyagi, I., Geshi, N., Takarada, S., 2022. Tephrostratigraphy and eruptive history of Aso-4/3 tephra group, Aso volcano: preparatory process for Aso-4 ignimbrite eruption. Bull Volcanol Soc Japan 67 (1), 91–112.
Ikehara, K., 2015. Marine tephra in the Japan Sea sediments as a tool for paleoceanography and paleoclimatology. Prog. Earth Planet. Sci. 2 (1), 1–14. https://doi.org/10.1186/S40645-015-0068-Z, 2015 2:1.
Ikehara, M., Murayama, M., Tadai, O., Hokanishi, N., Daido, N., Kawahata, H., Yasuda, H., 2006. Late quaternary tephrostratigraphy of two IMAGES cores taken from the off Shikoku in the northwest pacific. The Palaeontological Society of Japan (PSJ) 79, 60–76.
Ikehara, K., Kikkawa, K., Chun, J.-H., 2004. Origin and correlation of three tephras that erupted during oxygen isotope stage 3 found in cores from the Yamato Basin, Central Japan sea. The Quaternary Research (Daiyonki-Kenkyu) 43 (3), 201–212. https://doi.org/10.4116/JAQUA.43.201.
Ito, H., 2014. Zircon U-Th-Pb dating using LA-ICP-MS: simultaneous U-Pb and U-Th dating on the 0.1 Ma Toya tephra. Japan J. Volcanol. Geother. Res. 289, 210–223. https://doi.org/10.1016/J.QUAINT.2017.06.070.
Jochum, K.P., Stoll, B., Herwig, K., Willbold, M., Hofmiann, A.W., Amini, M., Aarburg, S., Abouchami, W., Hellebrand, E., Mocek, B., Raczek, I., Stracke, A., Alard, O., Bouman, C., Becker, S., Dücking, M., Brätz, H., Klemd, R., De Bruin, D., Woodhead, J.D., 2006. MPI-DING reference glasses for in situ microanalysis: new reference values for element concentrations and isotope ratios. G-cubed 7 (2). https://doi.org/10.1029/2005GC001060.
Kamata, H., Danhara, T., Itoh, J., Hoshizumi, H., Kawanabe, Y., 1998. Fission-track ages of zircons in the Miyagi, Shimosakata and Handa pyroclastic-flow deposits erupted from Kuju Volcano in central Kyushu, Japan. Bull. Volcanol. Soc. Jpn 43 (2), 69–73.
Kaneko, K., Inoue, K., Koyaguchi, T., Yoshikawa, M., Shibata, T., Takahashi, T., Furukawa, K., 2015. Magma plumbing system of the Aso-3 large pyroclastic eruption cycle at Aso volcano, Southwest Japan: petrological constraint on the formation of a compositionally stratified magma chamber. J. Volcanol. Geoth. Res. 303, 41–58. https://doi.org/10.1016/J.JVOLGEORES.2015.07.016.
Kawanabe, Y., Hoshizumi, H., Itoh, J., Kamata, H., 1997. Tephra stratigraphy of the Kuju volcano before K-Ah tephra. Programme and Abstracts the Volcanological Society of Japan 2, 105, 1997.
Kimura, J.-I., Okada, S., Nakayama, K., Umeda, K., Kusano, T., Asahara, A., Tateno, M., Danhara, T., 1999. Fission track ages of tephras from Daisen and Sambe volcanoes and their volcanological implications. Quat. Res. 38, 145–155.
Kimura, J.-I., Nagahashi, Y., Satoguchi, Y., Chang, Q., 2015. Origins of felsic magmas in Japanese subduction zone: geochemical characterizations of tephra from caldera-forming eruptions <5 Ma. G-cubed 16 (7), 2147–2174. https://doi.org/10.1002/2015GC005854.
Kiyosugi, K., Connor, C., Sparks, R.S.J., Crosweller, H.S., Brown, S.K., Siebert, L., Wang, T., Takarada, S., 2015. How many explosive eruptions are missing from the geologic record? Analysis of the quaternary record of large magnitude explosive eruptions in Japan. Journal of Applied Volcanology 4 (1), 1–15. https://doi.org/10.1186/S13617-015-0035-9, 2015 4:1.
Kobayashi, M., Koyama, M., 1996. Tephrochronology on the western and southern foots of Hakone volcano, Japan. J. Geogr. 105 (4), 431–447.
Lane, C.S., Cullen, V.L., White, D., Bramham-Law, C.W.F., Smith, V.C., 2014. Cryptotephra as a dating and correlation tool in archaeology. In: Journal of Archaeological Science, vol. 42. Academic Press, pp. 42–50. https://doi.org/10.1016/j.jas.2013.10.033, 1.
Lim, C., Toyoda, K., Ikehara, K., Peate, D.W., 2013. Late quaternary tephrostratigraphy of baegdusan and ulleung volcanoes using marine sediments in the Japan sea/east sea. Quaternary Research 80 (1), 76–87. https://doi.org/10.1016/J.YQRES.2013.04.002.
Machida, H., Arai, F., 2003. Atlas of Tephra in and Around Japan, New Edition (in Japanese).
Machida, H., 1999. Quaternary widespread tephra catalog in and around Japan recent progress. The Quaternary Research (Daiyonki-Kenkyu) 38 (3), 194–201 (in Japanese).
Machida, H., 2002. Volcanoes and tephras in the Japan area. GLOBAL ENVIRONMENTAL RESEARCH-ENGLISH EDITION- 6 (2), 19–28 (in Japanese).
McLean, D., Albert, P.G., Nakagawa, T., Staff, R.A., Suzuki, T., Smith, V.C., 2016. Identification of the Changbaishan 'Millennium'(B-Tm) eruption deposit in the Lake Suigetsu (SG06) sedimentary archive, Japan: synchronisation of hemispheric-wide palaeoclimate archives. Quat. Sci. Rev. 150, 301–307. https://doi.org/10.1016/j.quascirev.2017.12.013.
McLean, D., Albert, P.G., Nakagawa, T., Suzuki, T., Staff, R.A., Yamada, K., Kitaba, I., Haraguchi, T., Kitagawa, J., Smith, V., 2018. Integrating the Holocene tephrostratigraphy for East Asia using a high-resolution cryptotephra study from Lake Suigetsu (SG14 core), central Japan. Quat. Sci. Rev. 183, 36–58. https://doi.org/10.1016/j.quascirev.2017.12.013.
McLean, D., Albert, P.G., Schlolaut, G., Lamb, H.F., Marshall, M.H., Brauer, A., Wade, J., Nakagawa, T., Smith, V.C., 2022. How reliable is μXRF core scanning at detecting tephra layers in sedimentary records? A case study using the Lake Suigetsu archive (central Japan). J. Quat. Sci. 37 (7), 1189–1206. https://doi.org/10.1002/JQS.3432.
McLean, D., Albert, P.G., Suzuki, T., Nakagawa, T., Kimura, J.-I., Chang, Q., MacLeod, A., Blockley, S., Staff, R.A., Yamada, K., 2020a. Refining the eruptive history of Ulleungdo and Changbaishan volcanoes (East Asia) over the last 86 kyrs using distal sedimentary records. J. Volcanol. Geoth. Res. 389, 106669. https://doi.org/10.1016/j.jvolgeores.2019.106669.
McLean, D., Albert, P.G., Suzuki, T., Nakagawa, T., Kimura, J., Chang, Q., Miyabuchi, Y., Manning, C.J., MacLeod, A., Blockley, S.P.E., 2020b. Constraints on the timing of explosive volcanism at Aso and Aira calderas (Japan) between 50 and 30 ka: new insights from the Lake Suigetsu sedimentary record (SG14 core). G-cubed 21 (8). https://doi.org/10.1029/2019GC008874.
Matsu'ura, T., Furusawa, A., Shimogama, K., Goto, N., Komatsubara, J., 2014. Late Quaternary tephrostratigraphy and cryptotephrostratigraphy of deep-sea sequences (Chikyu C9001C cores) as tools for marine terrace chronology in NE Japan. Quat. Geochronol. 23, 63–79. https://doi.org/10.1016/J.QUAGEO.2014.06.001.
Matsu'ura, T., Ikehara, M., Ueno, T., 2021. Late Quaternary tephrostratigraphy and cryptotephrostratigraphy of core MD012422: improving marine tephrostratigraphy of the NW Pacific. Quat. Sci. Rev. 257. https://doi.org/10.1016/j.quascirev.2021.106808.
Matsu'ura, T., Komatsubara, J., 2024. Ontake-Katamachi tephra: marine-terrestrial correlation of a time marker of marine isotopic stage 5b in NE Japan, the Japan Sea, and the NW Pacific. J. Asian Earth Sci. 259, 105876. https://doi.org/10.1016/j.jseaes.2023.105876.
Miyabuchi, Y., 2011. Post-caldera explosive activity inferred from improved 67-30 ka tephrostratigraphy at Aso Volcano, Japan. J. Volcanol. Geotherm. Res. 205 (3–4), 94–113. https://doi.org/10.1016/j.jvolgeores.2011.05.004.
Miyabuchi, Y., 2009. A 90,000-year tephrostratigraphic framework of Aso Volcano, Japan. Sediment. Geol. 220 (3–4), 169–189. https://doi.org/10.1016/J.SEDGEO.2009.04.018.
Nagahashi, Y., Yoshikawa, S., Miyakawa, C., Uchiyama, T., Inouchi, Y., 2004. Stratigraphy and chronology of widespread tephra layersduring the past 430 kyr in the Kinki District and Yatsugatame Mountains: major element composition of the glass shards using EDS analysis. Quat. Res. 43, 15–35.
Nagaoka, S., Okuno, M., Arai, F., 2001. Tephrostratigraphy and eruptive history of the Aira caldera volcano during 100-30 ka, Kyushu, Japan. J. Geol. Soc. Jpn. 107 (7), 432–450.
Nagaoka, S., Okuno, M., 2011. Tephrochronology and eruptive history of Kirishima volcano in southern Japan. Quat. Int. 246 (1–2), 260–269. https://doi.org/10.1016/j.quaint.2011.06.007.
Nakagawa, T., Gotanda, K., Haraguchi, T., Danhara, T., Yonenobu, H., Brauer, A., Yokoyama, Y., Tada, R., Takemura, K., Staff, R.A., Payne, R., Bronk Ramsey, C., Bryant, C., Brock, F., Schlolaut, G., Marshall, M., Tarasov, P., Lamb, H., 2012. SG06, a fully continuous and varved sediment core from Lake Suigetsu, Japan: stratigraphy and potential for improving the radiocarbon calibration model and understanding of late Quaternary climate changes. Quat. Sci. Rev. 36, 164–176. https://doi.org/10.1016/J.QUASCIREV.2010.12.013.
Nakagawa, T., Kitagawa, H., Yasuda, Y., Tarasov, P.E., Gotanda, K., Sawai, Y., 2005. Pollen/event stratigraphy of the varved sediment of Lake Suigetsu, central Japan from 15,701 to 10,217 SG vyr BP (Suigetsu varve years before present): description, interpretation, and correlation with other regions. Quat. Sci. Rev. 24 (14–15), 1691–1701. https://doi.org/10.1016/j.quascirev.2004.06.022.
Nakagawa, T., Tarasov, P., Staff, R., Bronk Ramsey, C., Marshall, M., Schlolaut, G., Bryant, C., Brauer, A., Lamb, H., Haraguchi, T., Gotanda, K., Kitaba, I., Kitagawa, H., van der Plicht, J., Yonenobu, H., Omori, T., Yokoyama, Y., Tada, R., Yasuda, Y., 2021. The spatio-temporal structure of the Lateglacial to early Holocene transition reconstructed from the pollen record of Lake Suigetsu and its precise correlation with other key global archives: implications for palaeoclimatology and archaeology. Global Planet. Change 202, 103493. https://doi.org/10.1016/J.GLOPLACHA.2021.103493.
Newhall, C., Self, S., Robock, A., 2018. Impacts of future VEI 7 eruptions. Geosphere 14 (2). https://doi.org/10.1130/GES01513.1.
Okuno, M., Kobayashi, T., 1994. Late Pleistocene tephra layers distributed on Tane Island, southwest Japan. The Quaternary Research (Daiyonki-Kenkyu) 33 (2), 113–117.
Okuno, M., Nagaoka, S., Saito-Kokubu, Y., Nakamura, T., Kobayashi, T., 2017. AMS radiocarbon dates of pyroclastic-flow deposits on the southern slope of the Kuju volcanic group, Kyushu, Japan. Radiocarbon 59 (2), 483–488. https://doi.org/10.1017/RDC.2016.66.
Oppenheimer, C., 2003. Ice core and palaeoclimatic evidence for the timing and nature of the great mid-13th century volcanic eruption. International Journal of Climatology Int. J. Climatol 23, 417–426. https://doi.org/10.1002/joc.891.
Oppenheimer, C., Wacker, L., Xu, J., Galván, J.D., Stoffel, M., Guillet, S., Corona, C., Sigl, M., Di Cosmo, N., Hajdas, I., Pan, B., 2017. Multi-proxy dating the 'Millennium Eruption' of Changbaishan to late 946 CE. Quaternary Science Reviews 158, 164–171.
Payne, R., Gehrels, M., 2010. The formation of tephra layers in peatlands: an experimental approach. Catena 81 (1), 12–23. https://doi.org/10.1016/J.CATENA.2009.12.001.

Pyle, D.M., 2000. Sizes of volcanic eruptions. In: Sigurdsson, H., Houghton, B.F., McNutt, S.R., Rymer, H., Stix, J. (Eds.), Encyclopedia of Volcanoes. Academic Press, pp. 257–264. https://doi.org/10.1016/B978-0-12-385938-9.00013-4. London 2000.

Peccerillo, A., Taylor, S.R., 1976. Geochemistry of eocene calc-alkaline volcanic rocks from the Kastamonu area, Northern Turkey. Contrib. Mineral. Petrol. 58 (1), 63–81. https://doi.org/10.1007/BF00384745, 1976 58:1.

Reimer, P.J., Bard, E., Bayliss, A., et al., 2013. IntCal13 and Marine13 radiocarbon age calibration curves 0–50,000 Years cal BP. Radiocarbon 55 (4), 1869–1887. https://doi:10.2458/azu_js_rc.55.16947.

Reimer, P.J., Austin, W.E.N., Bard, E., Bayliss, A., Blackwell, P.G., Ramsey, C.B., Butzin, M., Cheng, H., Edwards, R.L., Friedrich, M., Grootes, P.M., Guilderson, T.P., Hajdas, I., Heaton, T.J., Hogg, A.G., Hughen, K.A., Kromer, B., Manning, S.W., Muscheler, R., Talamo, S., 2020. The IntCal20 northern hemisphere radiocarbon age calibration curve (0–55 cal kBP). Radiocarbon 62 (4), 725–757. https://doi.org/10.1017/RDC.2020.41.

Sagawa, T., Nagahashi, Y., Satoguchi, Y., Holbourn, A., Itaki, T., Gallagher, S.J., Saavedra-Pellitero, M., Ikehara, K., Irino, T., Tada, R., 2018. Integrated tephrostratigraphy and stable isotope stratigraphy in the Japan sea and east China sea using IODP sites U1426, U1427, and U1429, expedition 346 asian monsoon. Progress in Earth and Planetary Science 2018 5 (1), 1–24. https://doi.org/10.1186/S40645-018-0168-7, 5(1).

Schlolaut, G., Marshall, M.H., Brauer, A., Nakagawa, T., Lamb, H.F., Staff, R.A., Bronk Ramsey, C., Bryant, C.L., Brock, F., Kossler, A., Tarasov, P.E., Yokoyama, Y., Tada, R., Haraguchi, T., 2012. An automated method for varve interpolation and its application to the Late Glacial chronology from Lake Suigetsu, Japan. Quat. Geochronol. 13, 52–69. https://doi.org/10.1016/j.quageo.2012.07.005.

Schlolaut, G., Staff, R.A., Brauer, A., Lamb, H.F., Marshall, M.H., Bronk Ramsey, C., Nakagawa, T., 2018. An extended and revised Lake Suigetsu varve chronology from ~50 to ~10 ka BP based on detailed sediment micro-facies analyses. Quat. Sci. Rev. 200, 351–366. https://doi.org/10.1016/j.quascirev.2018.09.021.

Shane, P., Nairn, I.A., Martin, S.B., Smith, V.C., 2008. Compositional heterogeneity in tephra deposits resulting from the eruption of multiple magma bodies: implications for tephrochronology. Quat. Int. 178 (1), 44–53.

Shitaoka, Y., Fukuoka, T., Hasegawa, A., Kusano, T., Nagatomo, T., 2009. Thermoluminescence dating of the pyroclastic deposits of the SanbeVolcano. Bull Shimane Nat Mus Mt Sanbe (Sahimel) 7, 15–24.

Sigl, M., Winstrup, M., McConnell, J.R., Welten, K.C., Plunkett, G., Ludlow, F., Büntgen, U., Caffee, M., Chellman, N., Dahl-Jensen, D., Fischer, H., Kipfstuhl, S., Kostick, C., Maselli, O.J., Mekhaldi, F., Mulvaney, R., Muscheler, R., Pasteris, D.R., Pilcher, J.R., et al., 2015. Timing and climate forcing of volcanic eruptions for the past 2,500 years. Nature 523 (7562), 543–549. https://doi.org/10.1038/nature14565.

Smith, V.C., Mark, D.F., Staff, R.A., Blockley, S.P.E., Ramsey, C.B., Bryant, C.L., Nakagawa, T., Han, K.K., Weh, A., Takemura, K., Danhara, T., 2011a. Toward establishing precise 40Ar/39Ar chronologies for Late Pleistocene palaeoclimate archives: an example from the Lake Suigetsu (Japan) sedimentary record. Quat. Sci. Rev. https://doi.org/10.1016/j.quascirev.2011.06.020.

Smith, V.C., Staff, R.A., Blockley, S.P.E., Bronk Ramsey, C., Nakagawa, T., Mark, D.F., Takemura, K., Danhara, T., 2013. Identification and correlation of visible tephras in the Lake Suigetsu SG06 sedimentary archive, Japan: chronostratigraphic markers for synchronising of east Asian/west Pacific palaeoclimatic records across the last 150 ka. Quat. Sci. Rev. https://doi.org/10.1016/j.quascirev.2013.01.026.

Smith, V.C., Isaia, R., Pearce, N.J.G., 2011b. Tephrostratigraphy and glass compositions of post-15 kyr Campi Flegrei eruptions: implications for eruption history and chronostratigraphic markers. Quat. Sci. Rev. 30 (25–26), 3638–3660. https://doi.org/10.1016/j.quascirev.2011.07.012.

Staff, R.A., Ramsey, C.B., Bryant, C.L., Brock, F., Payne, R.L., Schlolaut, G., Marshall, M. H., Brauer, A., Lamb, H.F., Tarasov, P., Yokoyama, Y., Haraguchi, T., Gotanda, K., Yonenobu, H., Nakagawa, T., 2011. New 14C determinations from Lake Suigetsu, Japan: 12,000 to 0 cal BP. Radiocarbon 53 (3), 511–528. https://doi.org/10.1017/S0033822200034627.

Sulpizio, R., Costa, A., Massaro, S., Selva, J., Billotta, E., 2024. Assessing volumes of tephra fallout deposits: a simplified method for data scarcity cases. Bull. Volcanol. 86 (7), 1–14. https://doi.org/10.1007/S00445-024-01753-5/FIGURES/3.

Sun, C., Plunkett, G., Liu, J., Zhao, H., Sigl, M., McConnell, J.R., Pilcher, J.R., Vinther, B., Steffensen, J.P., Hall, V., 2014. Ash from Changbaishan Millennium eruption recorded in Greenland ice: implications for determining the eruption's timing and impact. Geophys. Res. Lett. 41 (2), 694–701. https://doi.org/10.1002/2013GL058642.

Sun, S., McDonough, W.F., 1989. Chemical and isotopic systematics of 630 oceanic basalts: implications for mantle composition and processes. In: Saunders, A.D., Norry, M.J. (Eds.), Magmatism in Ocean Basins, p. 631.

Suzuki, T., Saito, H., Kasahara, A., Kuriyama, E., Imaizumi, T., 2016. Late Quaternary tephrostratigraphy of underground sediments in the middle west part of Aizu Basin, Fukushima, northeast Japan. Quat. Res. 55, 1–16 (In Japanese with English abstract).

Tamura, Y., Tatsumi, Y., 2002. Remelting of an andesitic crust as a possible origin for rhyolitic magma in oceanic arcs: an example from the izu–bonin arc. J. Petrol. 43 (6), 1029–1047. https://doi.org/10.1093/PETROLOGY/43.6.1029.

Tatsumi, Y., Tamura, Y., Nichols, A.R.L., Ishizuka, O., Takahashi, N., Tani, K.-I., 2016. Izu–bonin arc. The Geology of Japan 175–199. https://doi.org/10.1144/GOJ.7.

Tsuji, T., Ikeda, M., Furusawa, A., Nakamura, C., Ichikawa, K., Yanagida, M., Nishizaka, N., Ohnishi, K., Ohno, Y., 2018. High resolution record of Quaternary explosive volcanism recorded in fluvio-lacustrine sediments of the Uwa basin, southwest Japan. Quat. Int. 471, 278–297. https://doi.org/10.1016/j.quaint.2017.10.016.

Tomlinson, E.L., Albert, P.G., Wulf, S., Brown, R.J., Smith, V.C., Keller, J., Orsi, G., Bourne, A.J., Menzies, M.A., 2014. Age and geochemistry of tephra layers from Ischia, Italy: Constraints from proximal-distal correlations with Lago Grande di Monticchio. J. Volcanol. Geoth. Res. 287, 22–39. https://doi.org/10.1016/j.jvolgeores.2014.09.006.

Tomlinson, E.L., Thordarson, T., Müller, W., Thirlwall, M., Menzies, M.A., 2010. Microanalysis of tephra by LA-ICP-MS — strategies, advantages and limitations assessed using the Thorsmörk ignimbrite (Southern Iceland). Chem. Geol. 279 (3–4), 73–89. https://doi.org/10.1016/J.CHEMGEO.2010.09.013.

Turney, C.S.M., 1998. Extraction of rhyolitic component of Vedde microtephra from minerogenic lake sediments. J. Paleolimnol. 19 (2), 199–206. https://doi.org/10.1023/A:1007926322026, 1998 19:2.

Uesawa, S., Toshida, K., Takeuchi, S., Miura, D., 2022. Creating a digital database of tephra fallout distribution and frequency in Japan. Journal of Applied Volcanology 11 (1), 14. https://doi.org/10.1186/s13617-022-00126-x.

Vineberg, S.O., Isaia, R., Albert, P.G., Brown, R.J., Smith, V.C., 2023. Insights into the explosive eruption history of the Campanian volcanoes prior to the Campanian Ignimbrite eruption. J. Volcanol. Geoth. Res. 443. https://doi.org/10.1016/j.jvolgeores.2023.107915.

Wulf, S., Hardiman, M.J., Staff, R.A., Koutsodendris, A., Appelt, O., Blockley, S.P.E., Lowe, J.J., Manning, C.J., Ottolini, L., Schmitt, A.K., Smith, V.C., Tomlinson, E.L., Vakhrameeva, P., Knipping, M., Kotthoff, U., Milner, A.M., Müller, U.C., Christanis, K., Kalaitzidis, S., Pross, J., 2018. The marine isotope stage 1–5 cryptotephra record of Tenaghi Philippon, Greece: towards a detailed tephrostratigraphic framework for the Eastern Mediterranean region. Quat. Sci. Rev. 186, 236–262. https://doi.org/10.1016/J.QUASCIREV.2018.03.011.